National Library of Canada
Acquisitions and Bibliographic Services Branch
395 Wellington Street
Ottawa, Ontario
K1A 0N4

Bibliothèque nationale du Canada
Direction des acquisitions et des services bibliographiques
395, rue Wellington
Ottawa (Ontario)
K1A 0N4

NOTICE

The quality of this microform is heavily dependent upon the quality of the original thesis submitted for microfilming. Every effort has been made to ensure the highest quality of reproduction possible.

If pages are missing, contact the university which granted the degree.

Some pages may have indistinct print especially if the original pages were typed with a poor typewriter ribbon or if the university sent us an inferior photocopy.

Reproduction in full or in part of this microform is governed by the Canadian Copyright Act, R.S.C. 1970, c. C-30, and subsequent amendments.

AVIS

La qualité de cette microforme dépend grandement de la qualité de la thèse soumise au microfilmage. Nous avons tout fait pour assurer une qualité supérieure de reproduction.

S'il manque des pages, veuillez communiquer avec l'université qui a conféré le grade.

La qualité d'impression de certaines pages peut laisser à désirer, surtout si les pages originales ont été dactylographiées à l'aide d'un ruban usé ou si l'université nous a fait parvenir une photocopie de qualité inférieure.

La reproduction, même partielle, de cette microforme est soumise à la Loi canadienne sur le droit d'auteur, SRC 1970, c. C-30, et ses amendements subséquents.

Canada

AN ANALYTICAL STUDY OF RIDE AND HANDLING PERFORMANCE OF AN INTERCONNECTED VEHICLE SUSPENSION

PEIJUN LIU

A Thesis

in

The Department

of

Mechanical Engineering

Presented in Partial Fulfillment of the Requirements

for the Degree of Master of Applied Science at

Concordia University

Montreal, Quebec, Canada

January 1994

© Peijun Liu, 1994

National Library
of Canada

Acquisitions and
Bibliographic Services Branch

395 Wellington Street
Ottawa, Ontario
K1A 0N4

Bibliothèque nationale
du Canada

Direction des acquisitions et
des services bibliographiques

395, rue Wellington
Ottawa (Ontario)
K1A 0N4

Your file Votre référence

Our file Notre référence

The author has granted an irrevocable non-exclusive licence allowing the National Library of Canada to reproduce, loan, distribute or sell copies of his/her thesis by any means and in any form or format, making this thesis available to interested persons.

L'auteur a accordé une licence irrévocable et non exclusive permettant à la Bibliothèque nationale du Canada de reproduire, prêter, distribuer ou vendre des copies de sa thèse de quelque manière et sous quelque forme que ce soit pour mettre des exemplaires de cette thèse à la disposition des personnes intéressées.

The author retains ownership of the copyright in his/her thesis. Neither the thesis nor substantial extracts from it may be printed or otherwise reproduced without his/her permission.

L'auteur conserve la propriété du droit d'auteur qui protège sa thèse. Ni la thèse ni des extraits substantiels de celle-ci ne doivent être imprimés ou autrement reproduits sans son autorisation.

ISBN 0-315-90855-6

Canada

Name PEIJUN LIU

Dissertation Abstracts International is arranged by broad, general subject categories. Please select the one subject which most nearly describes the content of your dissertation. Enter the corresponding four-digit code in the spaces provided.

Architecture

SUBJECT TERM

0	7	2	9

SUBJECT CODE

U·M·I

Subject Categories

THE HUMANITIES AND SOCIAL SCIENCES

COMMUNICATIONS AND THE ARTS

Architecture 0729
Art History 0377
Cinema 0900
Dance 0378
Fine Arts 0357
Information Science 0723
Journalism 0391
Library Science 0399
Mass Communications 0708
Music 0413
Speech Communication 0459
Theater 0465

EDUCATION

General 0515
Administration 0514
Adult and Continuing 0516
Agricultural 0517
Art 0273
Bilingual and Multicultural 0282
Business 0688
Community College 0275
Curriculum and Instruction 0727
Early Childhood 0518
Elementary 0524
Finance 0277
Guidance and Counseling 0519
Health 0680
Higher 0745
History of 0520
Home Economics 0278
Industrial 0521
Language and Literature 0279
Mathematics 0280
Music 0522
Philosophy of 0998
Physical 0523
Psychology 0525
Reading 0535
Religious 0527
Sciences 0714
Secondary 0533
Social Sciences 0534
Sociology of 0340
Special 0529
Teacher Training 0530
Technology 0710
Tests and Measurements 0288
Vocational 0747

LANGUAGE, LITERATURE AND LINGUISTICS

Language
- General 0679
- Ancient 0289
- Linguistics 0290
- Modern 0291

Literature
- General 0401
- Classical 0294
- Comparative 0295
- Medieval 0297
- Modern 0298
- African 0316
- American 0591
- Asian 0305
- Canadian (English) 0352
- Canadian (French) 0355
- English 0593
- Germanic 0311
- Latin American 0312
- Middle Eastern 0315
- Romance 0313
- Slavic and East European 0314

PHILOSOPHY, RELIGION AND THEOLOGY

Philosophy 0422
Religion
- General 0318
- Biblical Studies 0321
- Clergy 0319
- History of 0320
- Philosophy of 0322

Theology 0469

SOCIAL SCIENCES

American Studies 0323
Anthropology
- Archaeology 0324
- Cultural 0326
- Physical 0327

Business Administration
- General 0310
- Accounting 0272
- Banking 0770
- Management 0454
- Marketing 0338

Canadian Studies 0385
Economics
- General 0501
- Agricultural 0503
- Commerce-Business 0505
- Finance 0508
- History 0509
- Labor 0510
- Theory 0511

Folklore 0358
Geography 0366
Gerontology 0351
History
- General 0578
- Ancient 0579
- Medieval 0581
- Modern 0582
- Black 0328
- African 0331
- Asia, Australia and Oceania 0332
- Canadian 0334
- European 0335
- Latin American 0336
- Middle Eastern 0333
- United States 0337

History of Science 0585
Law 0398
Political Science
- General 0615
- International Law and Relations 0616
- Public Administration 0617

Recreation 0814
Social Work 0452
Sociology
- General 0626
- Criminology and Penology 0627
- Demography 0938
- Ethnic and Racial Studies 0631
- Individual and Family Studies 0628
- Industrial and Labor Relations 0629
- Public and Social Welfare 0630
- Social Structure and Development 0700
- Theory and Methods 0344

Transportation 0709
Urban and Regional Planning 0999
Women's Studies 0453

THE SCIENCES AND ENGINEERING

BIOLOGICAL SCIENCES

Agriculture
- General 0473
- Agronomy 0285
- Animal Culture and Nutrition 0475
- Animal Pathology 0476
- Food Science and Technology 0359
- Forestry and Wildlife 0478
- Plant Culture 0479
- Plant Pathology 0480
- Plant Physiology 0817
- Range Management 0777
- Wood Technology 0746

Biology
- General 0306
- Anatomy 0287
- Biostatistics 0308
- Botany 0309
- Cell 0379
- Ecology 0329
- Entomology 0353
- Genetics 0369
- Limnology 0793
- Microbiology 0410
- Molecular 0307
- Neuroscience 0317
- Oceanography 0416
- Physiology 0433
- Radiation 0821
- Veterinary Science 0778
- Zoology 0472

Biophysics
- General 0786
- Medical 0760

EARTH SCIENCES

Biogeochemistry 0425
Geochemistry 0996
Geodesy 0370
Geology 0372
Geophysics 0373
Hydrology 0388
Mineralogy 0411
Paleobotany 0345
Paleoecology 0426
Paleontology 0418
Paleozoology 0985
Palynology 0427
Physical Geography 0368
Physical Oceanography 0415

HEALTH AND ENVIRONMENTAL SCIENCES

Environmental Sciences 0768
Health Sciences
- General 0566
- Audiology 0300
- Chemotherapy 0992
- Dentistry 0567
- Education 0350
- Hospital Management 0769
- Human Development 0758
- Immunology 0982
- Medicine and Surgery 0564
- Mental Health 0347
- Nursing 0569
- Nutrition 0570
- Obstetrics and Gynecology 0380
- Occupational Health and Therapy 0354
- Ophthalmology 0381
- Pathology 0571
- Pharmacology 0419
- Pharmacy 0572
- Physical Therapy 0382
- Public Health 0573
- Radiology 0574
- Recreation 0575
- Speech Pathology 0460
- Toxicology 0383

Home Economics 0386

PHYSICAL SCIENCES

Pure Sciences

Chemistry
- General 0485
- Agricultural 0749
- Analytical 0486
- Biochemistry 0487
- Inorganic 0488
- Nuclear 0738
- Organic 0490
- Pharmaceutical 0491
- Physical 0494
- Polymer 0495
- Radiation 0754

Mathematics 0405
Physics
- General 0605
- Acoustics 0986
- Astronomy and Astrophysics 0606
- Atmospheric Science 0608
- Atomic 0748
- Electronics and Electricity 0607
- Elementary Particles and High Energy 0798
- Fluid and Plasma 0759
- Molecular 0609
- Nuclear 0610
- Optics 0752
- Radiation 0756
- Solid State 0611

Statistics 0463

Applied Sciences

Applied Mechanics 0346
Computer Science 0984
Engineering
- General 0537
- Aerospace 0538
- Agricultural 0539
- Automotive 0540
- Biomedical 0541
- Chemical 0542
- Civil 0543
- Electronics and Electrical 0544
- Heat and Thermodynamics 0348
- Hydraulic 0545
- Industrial 0546
- Marine 0547
- Materials Science 0794
- Mechanical 0548
- Metallurgy 0743
- Mining 0551
- Nuclear 0552
- Packaging 0549
- Petroleum 0765
- Sanitary and Municipal 0554
- System Science 0790

Geotechnology 0428
Operations Research 0796
Plastics Technology 0795
Textile Technology 0994

PSYCHOLOGY

General 0621
Behavioral 0384
Clinical 0622
Developmental 0620
Experimental 0623
Industrial 0624
Personality 0625
Physiological 0989
Psychobiology 0349
Psychometrics 0632
Social 0451

CONCORDIA UNIVERSITY

SCHOOL OF GRADUATE STUDIES

This is to certify that the thesis prepared

By: Peijun LIU

Entitled: An Analytical Study of Ride and Handling Performance of an Interconnected Vehicle Suspension

and submitted in partial fulfillment of the requirements for the degree of

Master of Applied Science

complies with the regulations of this University and meets the accepted standards with respect to originality and quality.

Signed by the Final Examining Committee:

Dr. A.E. Bladh — Chair

Dr. G.H. Yatistas — Examiner

Dr. F.M.L. Amirouche (Univ. of Illinois at Chicago) — External to the Program

Dr. A.K.W. Ahmed — Co-Supervisor

Dr. S. Rakheja — Co-Supervisor

Approved by

Dr. R.B. Bhat, Graduate Program Director
Department of Mechanical Engineering

Dr. D. Taddeo, Dean
Faculty of Engineering & Computer Science

03/02, 19 96

ABSTRACT

AN ANALYTICAL STUDY OF RIDE AND HANDLING PERFORMANCE OF AN INTERCONNECTED VEHICLE SUSPENSION

Peijun Liu

Design of a vehicle suspension involves a difficult compromise among the ride, handling and directional control performance characteristics. While a soft suspension is desired to enhance ride quality, hard suspension springs are required to achieve good handling and directional control performance. Auxiliary roll stiffeners, in conjunction with soft suspension, are frequently used to attain an acceptable compromise between ride and handling performance of a vehicle. Alternatively, an improved compromise between ride and handling can be realized by interconnecting hydro-pneumatic suspension struts in the roll plane. The interconnected suspension can provide soft suspension rate for improved ride quality, and firm roll stiffness and damping for adequate handling and control performance. In this dissertation, a hydro-pneumatic suspension, interconnected in the roll plane, is analytically investigated for its ride and handling performance potentials.

A highway bus equipped with the interconnected hydro-pneumatic suspension system is modeled in the roll plane as a four-degrees-of-freedom dynamical system subject to excitations arising from road irregularities and roll moment caused by directional maneuvers. The static and dynamic properties of the interconnected suspension are derived and discussed in terms of its load-carrying capacity, suspension rate, roll stiffness, and damping forces. The ride and handling performance characteristics of the interconnected suspension are

investigated and compared to those of the conventional suspension systems for deterministic excitations. A passive variable damping mechanism is proposed and investigated to achieve improved vehicle ride quality. The vibration isolation performance characteristics of the interconnected suspension employing the variable damping valves are further investigated for deterministic and random excitations. From the computer simulation results, it is concluded that the interconnected hydro-pneumatic suspension with inherent enhanced anti-roll stiffness and damping characteristics can provide an improved compromise between ride comfort and handling performance of a vehicle.

ACKNOWLEDGMENTS

The author wishes to express his sincere appreciation to his thesis supervisors, Dr. S. Rakheja and Dr. A. K. W. Ahmed for initiating the study topic and providing guidance throughout the course of this investigation.

Thanks are due to the faculty members, staff and other graduate students of CONCAVE Research Center, and the Department of Mechanical Engineering for their help during the course of this work.

The financial support in the form of research assistantships provided by his supervisors, and the International Student Tuition Fee Remission fellowships funded by the Quebec Government, Canada, is gratefully acknowledged.

Finally, the author would like to express his special thanks to his wife, Lingping and other family members for their love, encouragement and support.

TABLE OF CONTENTS

LIST OF FIGURES

LIST OF TABLES

NOMENCLATURE

SYMBOL	DESCRIPTION
a	general orifice damping area
a_ℓ, a_r	orifice damping area of the left and right struts, respectively
a_y	lateral acceleration acting on sprung mass
A_1	general piston rod side area
A_2	general piston head area
A_{1i}	piston rod side area of strut i
A_{2i}	piston head area of strut i
A_m	roll stiffness amplification factor of the interconnected suspension
A_n	roll stiffness amplification factor of the unconnected suspension with anti-roll bar
A_r	piston rod area
c_1	first stage damping coefficient of the multi-stage damper
c_2	third stage damping coefficient of the multi-stage damper
c_c	critical damping coefficient
$c_{t\ell}, c_{tr}$	damping coefficients of the left and right tires, respectively
C_d	discharge coefficient
d	diameter of the anti-roll bar
f_ℓ, f_r	dynamic forces developed by the left and right struts of the unconnected suspension, respectively
f_ℓ', f_r'	dynamic forces developed by the left and right struts of the interconnected suspension, respectively
F_b	vertical elastic force developed by the anti-roll bar
F_ℓ, F_r	generalized suspension forces of unconnected suspensions

F_l', F_r'	generalized suspension forces of the interconnected suspension
g	acceleration due to gravity
G	shear modulus of the anti-roll bar
G_l, G_r	static forces developed by the left and right struts of the interconnected suspension
G_s	static force developed by each of the unconnected strut
h_2	vertical distance from the center of gravity of sprung mass to its roll center
$H(\omega)$	transfer function of the linear filter
I_s	mass moment of inertia of the sprung mass
I_u	mass moment of inertia of the unsprung mass
k_b	spring constant of the anti-roll bar
k_{tl}, k_{tr}	stiffness coefficients of the left and right tires, respectively
k_{vi}	vertical stiffness of a single strut of the interconnected suspension
k_{vu}	vertical stiffness of a single strut of the unconnected suspension
k_θ	auxiliary roll stiffness of the anti-roll bar
k_{vi}^0	vertical stiffness of a single strut of the interconnected suspension at static design position
k_{vu}^0	vertical stiffness of a single strut of the unconnected suspension at static design position
K_{vi}^0	suspension rate of the interconnected suspension at static ride height
K_{vu}^0	suspension rate of the unconnected suspension at static ride height

ℓ	half the suspension strut track
ℓ_b	length of the anti-roll bar across the chassis
ℓ_ℓ, ℓ_r	lateral distances from the left and right suspension struts to the center of gravity of the sprung mass
$\ell_{w\ell}, \ell_{wr}$	lateral distances from the left and right tires to the center of gravity of the unsprung mass
m_s	sprung mass of the vehicle
m_u	unsprung mass of the vehicle
M	restore moment
n	poiytropic exponent
N_u	number of struts used on each side in the roll plane model
$(p_{23})_0$	preset pressure differential of the multi-stage damper
p_{23i}	pressure differential across the damping restriction = $(p_{2i} - p_{3i})$
p_{1i}, p_{2i}, p_{3i}	instantaneous pressures in chambers I, II and III of strut i, respectively
p_{3i0}	static gas pressure of strut i of the interconnected suspension at design ride height
$p_{2\ell 1r}$	pressure differential between chamber II of the left strut (II_ℓ) and chamber I of the right strut (I_r)
$p_{2r1\ell}$	pressure differential between chamber II_r and chamber I_ℓ
p_a	atmospheric pressure
p_c	initial charge pressure
p_ℓ	static pressure in the left strut of the unconnected suspension
p_0	static fluid pressure at design ride position

p_{0i}	static fluid pressure of strut i of the unconnected suspension at design ride position
p_r	static pressure in the right strut of the unconnected suspension
Q_{1i}	volume flow rate in chamber I of strut i
Q_{2i}	volume flow rate in chamber II of strut i
Q_{23i}	volume flow rate from chamber II to chamber III of strut i
Q_{2tIr}	volume flow rate from chamber II_t to chamber I_r
Q_{2rIt}	volume flow rate from chamber II_r to chamber I_t
r	length of the trailing lever of the anti-roll bar
$sgn(\bullet)$	sign function
S_0	power spectral density of the band-limited white noise
$S(\omega)$	power spectral density of road roughness
T_b	torsion couple developed by the anti-roll bar
T_g	external roll moment acting on the sprung mass
v	vehicle velocity
v_{3i}	instantaneous gas volume in chamber III of strut i
v_{3i0}	static gas volume of strut i of the interconnected suspension at design ride height
v_c	initial charge volume of gas in accumulator
v_0	nominal gas volume of a single strut at design ride position
v_{0i}	nominal gas volume of strut i of the unconnected suspension
w_i	static load on suspension strut i
W_i	load-carrying capacity of the interconnected suspension
W_u	load-carrying capacity of the unconnected suspensions
x	vertical displacement of sprung mass

x_0^*	effective static deflection of the strut
x_{il}, x_{ir}	vertical displacement excitations at the left and right tires, respectively
x_s, x_u	general coordinates characterizing vertical displacements of the sprung and unsprung masses, respectively
y	relative vertical motion between the left and right ends of the anti-roll bar
z_l, z_r	relative displacements across the left and right suspension struts, respectively
α	damping parameter
β	piston area ratio ($=A_2/A_1$)
δ	tuning factor of the multi-stage damper
φ	roll angle of sprung mass
γ_1, γ_2	transition velocities of the multi-stage damper
$\eta_0, \ldots, \eta_6$	coefficients characterizing the linear filter
λ_1, λ_2	coefficients characterizing road surface
μ	absolute viscosity of fluid
ϑ_s, ϑ_u	general coordinates characterizing roll angles of the sprung and unsprung masses, respectively
ρ	mass density of the fluid
σ_1^2, σ_2^2	coefficients characterizing road surface
τ	coefficient characterizing road surface
ω	angular velocity

CHAPTER 1

INTRODUCTION AND LITERATURE REVIEW

1.1 GENERAL

The primary functions of a vehicle suspension are to support the vehicle load, protect cargoes and passengers from shock and vibration excitations originating from the tire-road interaction, and provide vehicle guidance with adequate roll and directional stability. The good ride quality and handling performance, however, pose conflicting design requirements for the vehicle suspension. While a lightly damped soft suspension yields good shock attenuation performance, hard suspension with high damping is desirable to achieve good handling. Moreover, lightly damped suspension is detrimental to the vibration isolation effectiveness around the sprung mass resonant frequencies. The design of a vehicle suspension thus involves a compromise between the handling and ride quality performance of the vehicle.

The relative performance characteristics of various passive vehicle suspension designs have been extensively investigated and reported in the literature. It has been established that the relative ride quality analysis of comparable suspensions may be carried out on the base of similar working space [1, 2]. Since the static deflection of a linear suspension spring varies as the inverse square of the natural frequency, the limitations on the permissible working space prohibit the use of soft springs [3]. Nonlinear springs with progressively hardening characteristics, in conjunction with auxiliary roll stiffeners such as anti-roll bars, are thus widely used to achieve good ride quality, high roll stiffness, good handling and directional control performance with reasonable working space. The anti-roll bars, however, affect the vehicle

ride quality in an adverse manner when one of the wheels is subjected to an excitation. Alternatively, an interconnected hydro-pneumatic suspension can provide a soft vertical spring rate and high roll stiffness to achieve an improved compromise between the ride quality and anti-roll performance of the vehicle [4, 5]. The conflicting requirements on suspension damping suggest that a variable damping is extremely vital to achieve improved ride comfort and road holding performance. Although a number of semi-active and active damping mechanisms have been proposed and investigated, the cost and complexity of the realization of semi-active and active variable dampers have limited their general implementation.

In this dissertation, a hydro-pneumatic suspension system interconnected in the roll plane is analytically modeled and analyzed. The static and dynamic properties of the proposed suspension, such as load-carrying capacity, suspension rate, roll stiffness and damping characteristics are evaluated. The shock and vibration isolation performance characteristics of the interconnected suspension system are compared to those of the conventional suspension system, and its potential ride and handling performance benefits are discussed. A passive variable damping mechanism is incorporated to further improve the vibration isolation performance of the interconnected suspension system. The anti-roll performance of the proposed suspension is analyzed for lateral acceleration excitation encountered during a directional maneuver. The ride quality performance is analyzed for deterministic as well as random road excitations.

1.2 REVIEW OF RELEVANT LITERATURE

Numerous passive, semi-active and active vehicle suspensions have been proposed and analyzed using varying analytical and experimental

techniques. The ride, handling and directional control performance characteristics of various suspensions have been extensively investigated and reported in the literature. A review of the relevant literature is carried out and briefly discussed in the following subsections to formulate the scope of this dissertation.

1.2.1 Interconnected Suspension Systems

Although the design, analysis and performance characteristics of passive, semi-active and active suspension systems have been extensively investigated, the studies on interconnected suspensions have been limited. Furthermore, developments in interconnected suspension have primarily evolved from experimental investigations. The roll and pitch properties of a suspension system can be varied considerably by interconnecting the different wheel suspensions of a vehicle. The interconnection among the different wheel suspensions can be realized through either mechanical or fluid couplings.

The ride benefits of a low pitch frequency suspension that may be realized by interconnecting front and rear wheel suspensions have long been established. Mechanically coupled front and rear wheel suspensions, also known as equalizing suspensions, were implemented in Citroen 2CV cars in 1948 [7]. The equalizing suspension, employing a mechanical interconnection between the front and rear wheel suspensions, provided improved ride quality by reducing the pitch frequency [6, 7, 11]. The schematics of three different arrangements of mechanically interconnected suspension are illustrated in Figure 1.1. The influence of mechanical coupling on the pitch and bounce frequency of the suspension can be perhaps better described from the schematic presented in Figure 1.1(a). Under pure vertical motions, the vehicle body D and lever C remain parallel to the ground. The suspension rate thus

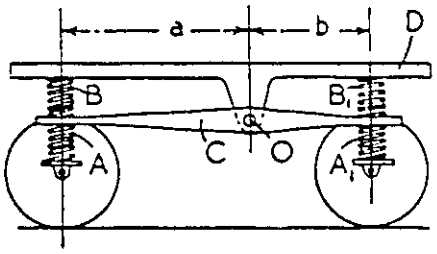

(a)

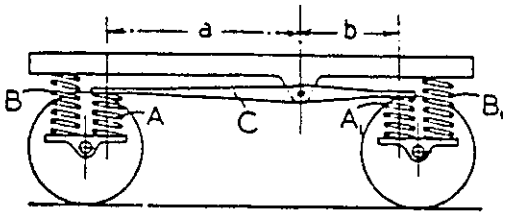

(b)

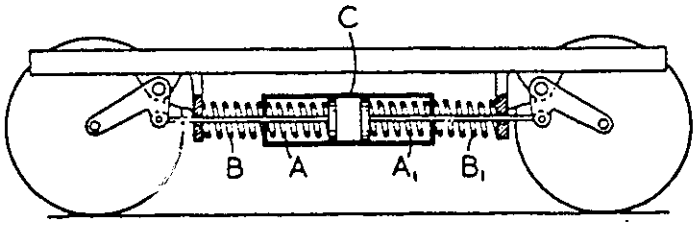

(c)

Figure 1.1 Mechanically interconnected front and rear wheel suspensions [11]

depends on the stiffness of spring A. Under pitch rotation about O, the pitch oscillation frequency of the body, however, depends upon the stiffness of the spring B. The rate of spring A and B can be thus selected to achieve desirable pitch and bounce natural frequencies. Earlier designs employed a soft pitch spring B and a hard bounce spring A to achieve a pitch frequency considerably lower than the bounce frequency. Those suspensions thus resulted in poor anti-pitch performance and low resistance to attitude changes caused by dynamic load transfers.

Moulton [8] developed a coupled rubber suspension using fluid interconnections, frequently refereed to as Hydrolastic. An interconnected 'hydragas' suspension was later realized by replacing the rubber springs by gas springs [9, 10]. The Hydragas suspension consisted of two hermetically sealed spherical containers, as shown in Figure 1.2. The upper container was divided into two chambers separated by an elastic diaphragm. The upper chamber, charged with compressed nitrogen gas, served as the gas spring, and the lower chamber was filled with hydraulic fluid. The lower container comprising an elastic diaphragm was also filled with hydraulic fluid. The underside of the diaphragm was acted upon by a tapered displacer, as shown in Figure 1.2. The damping was achieved from the fluid flows between the upper and lower containers through a damper valve with different bounce and rebound flow characteristics. Figure 1.3 illustrates the interconnection between the front and rear suspensions. In the pitch mode, the fluid flows between the front and rear units, resulting in low pitch rate of each unit. In the bounce and roll modes, however, no fluid flows between the suspensions since both displacers on one side move together. The corresponding spring rates thus remain high. Although the interconnected Moulton suspension resulted in improved ride in the pitch mode, the coupled suspension was far more sensitive to dynamic load transfers

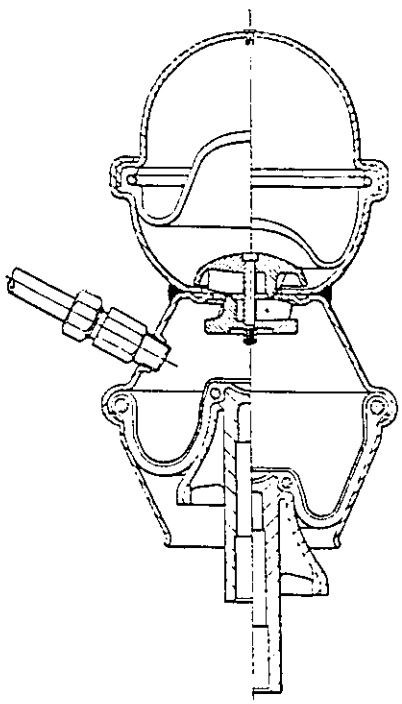

Figure 1.2 Moulton Hydragas suspension unit [10]

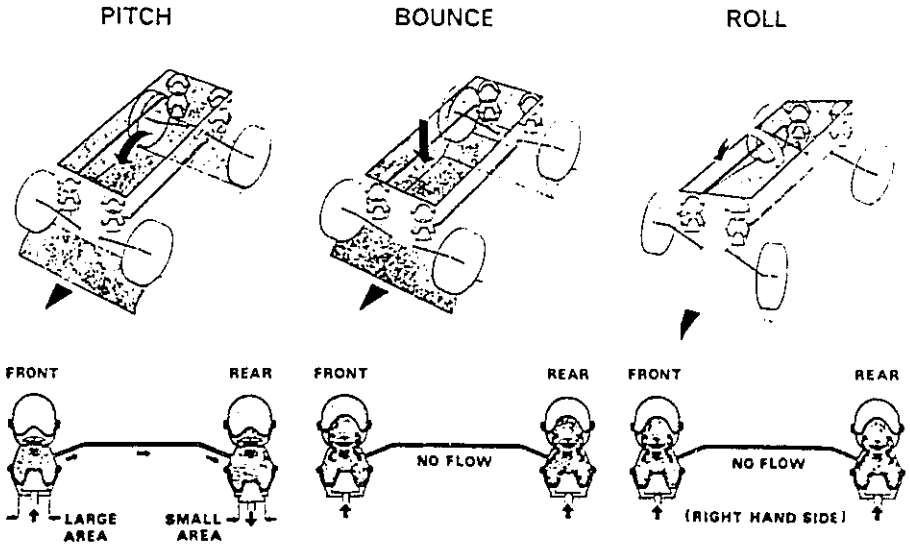

Figure 1.3 Illustration of fluid flows between front and rear wheel suspensions of Moulton Hydragas in the different vibration modes

encountered during accelerating and braking. A modified hydragas system, comprising laterally interconnected rear wheel suspensions, was developed for implementation in the Austin Mini Metro [11]. The results of road tests performed on the modified system, with no interconnection between the front and rear suspensions, demonstrated improved road holding performance.

The interconnection technique used in equalizing and Moulton suspensions resulted in a lower pitch or roll rate. The wheel suspensions can be interconnected in another manner to achieve enhanced roll and/or pitch rates for vehicle attitude control.

Vehicle suspensions with anti-roll bars, which span across the chassis with the ends linking the two road wheels on opposite sides, can be considered as the mechanically interconnected suspensions in the roll plane. This mechanical interconnection tends to improve the anti-roll performance of the vehicle by increasing the suspension roll stiffness.

Passive and active hydro-pneumatic suspension systems interconnected in the roll plane, as illustrated in Figure 1.4, have been analytically modeled by Felez and Vera [13]. The mathematical models, derived using bond graph techniques, were analyzed to evaluate the vehicle response to roll and vertical displacement inputs. The study demonstrated an improved anti-roll characteristics of the interconnected suspensions. Su [4] analyzed a tunable interlinked hydro-pneumatic suspension, similar to that shown in Figure 1.4(a). The tunable interconnected suspension was mathematically modeled as a multi-degrees-of-freedom dynamic system, including the fluid compressibility and valve dynamics. Shock and vibration isolation characteristics of the interlinked suspension were evaluated for deterministic excitations. The study concluded that the ride comfort and handling performance of a vehicle can be significantly improved by interconnecting the suspension in the roll plane. Although the

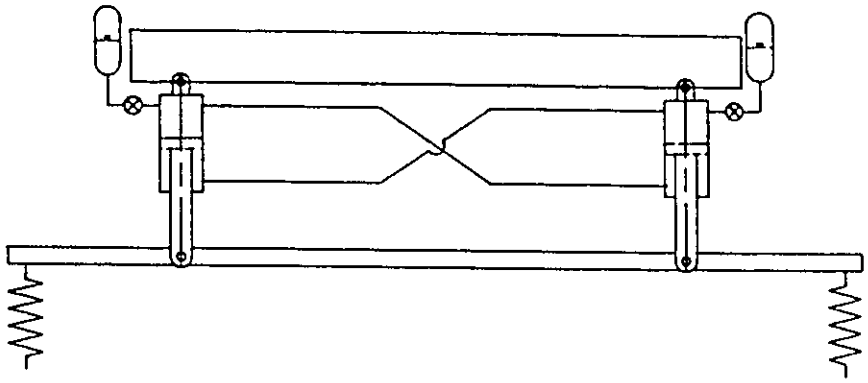

(a)

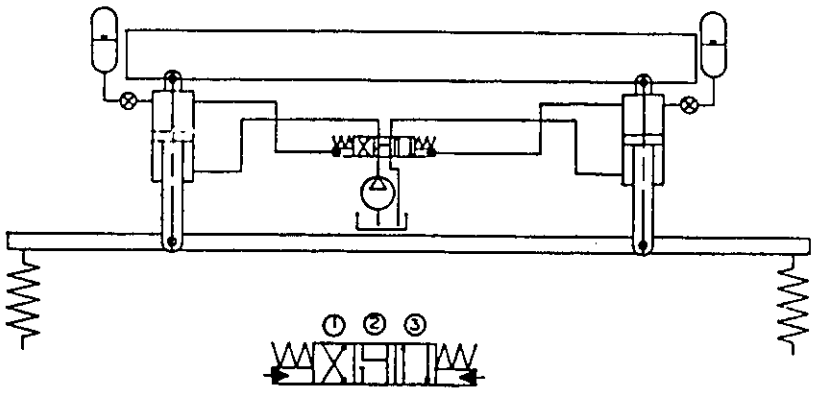

(b)

Figure 1.4 Schematic of interconnected hydro-pneumatic suspension configurations: (a) passive suspension, (b) active suspension [13]

above studies have clearly demonstrated the ride and anti-roll performance benefits of the interconnected suspension, the fundamental static and dynamic properties of interconnected suspension and coupling effects have not been investigated. The ride dynamics of a vehicle with the interconnected suspension subjected to realistic stochastic road irregularities are still remained to be investigated.

Interconnected suspensions can be incorporated with variable damping and self-leveling capacity to achieve enhanced performance of a vehicle. Tanahashi et al. [14] proposed and investigated an interconnected and feedback modulated hydro-pneumatic suspension. The interconnected suspension provided a variable three-stage damping force using an electronic modulation system, depending upon the vehicle running and road conditions. The analytical and experimental studies demonstrated both improved ride comfort and handling characteristics of the vehicle. Mellor [12] investigated the performance of an interconnected hydro-pneumatic suspension with a self-energizing load-dependent internal pump, which was energized by the relative movement between the sprung and unsprung masses of the vehicle. The suspension can provide automatic leveling characteristics of the vehicle.

Upon recognizing the superior anti-roll capacity of a laterally interconnected suspension, the vehicle suspension connected in the pitch plane have been attempted to achieve improved anti-pitch performance [3, 15, 16, 17, 18]. Figure 1.5 illustrates the schematic of a semi-active hydro-pneumatic vehicle suspension interconnected in the pitch and roll planes (frequently refereed as AP suspension), studied by Crolla and Horton [18]. The pitch and roll suspension rates were controlled by diagonally connecting the upper chambers of front suspension struts to the lower chambers of rear suspension struts, and by laterally connecting the upper chambers of the rear suspension

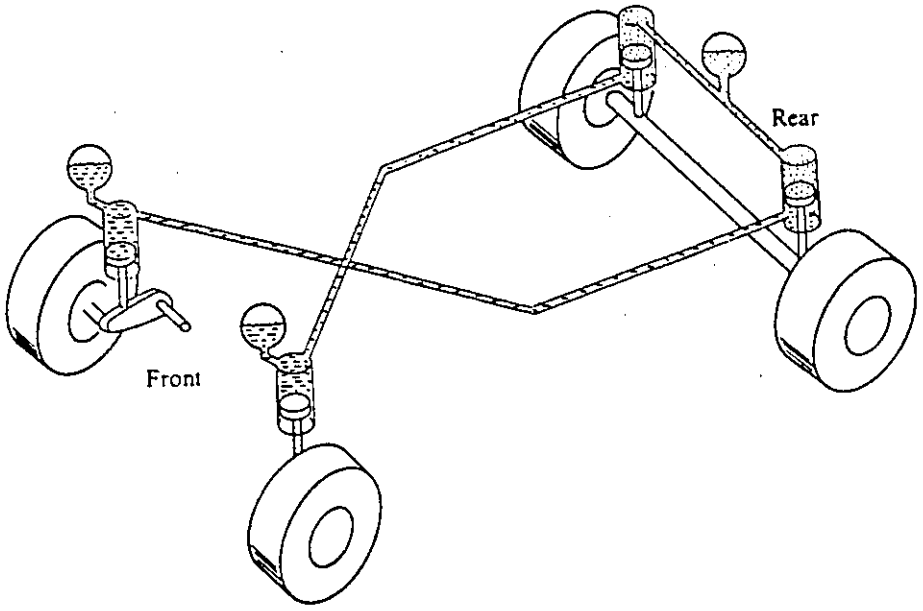

Figure 1.5 Schematic of the AP suspension interconnected in the pitch and roll planes [18]

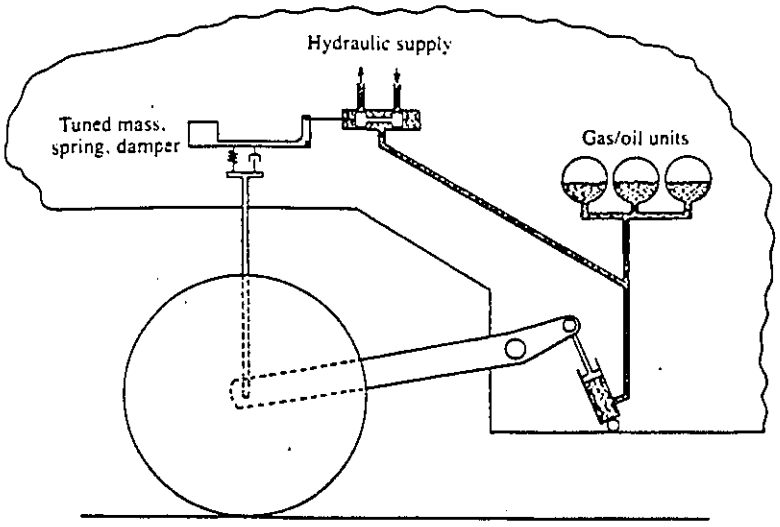

Figure 1.6 Schematic diagram of a single wheel station of the AP suspension [18]

struts. Inertial control valves, as shown in Figure 1.6, were implemented to achieve soft response to road irregularities, and hard response to vehicle maneuvers to attain attitude control and self-leveling. The results of the analytical and experimental study revealed improved ride quality and attitude control of the vehicle. Howard [19] developed a three dimensional model of a vehicle employing an active interconnected suspension system. The results derived from computer simulation demonstrated improved self-leveling, anti-roll and anti-pitch performance characteristics of the active suspension.

1.2.2 Variable Suspension Damping

In view of the inherent performance limitations of constant suspension damping, many multi-stage and variable damping mechanisms have been developed. The analytical models of various multi-stage shock absorbers together with measurement and simulation techniques, damping characteristics and design have been extensively reported in the literature.

Van Vliet [23] developed an analytical model of a hydraulic shock absorber with a fixed relief valve, designed to open during compression to limit the magnitude of maximum compression damping force. Asymmetric damping force-displacement characteristics were established from laboratory testing and computer simulation studies. The damping characteristics of variable orifice dampers have been analyzed by Asami et al [24] and Hundal [25]. Rakheja and Su [26, 71] proposed and analyzed a tunable passive sequential hydraulic damper to achieve variable damping within a vehicle suspension. The sequential damping was realized by introducing compression and rebound pressure relief valves to the fixed orifice hydraulic damper. The analytical model incorporating nonlinearities due to valve dynamics, fluid compressibility and turbulent flows was analyzed for deterministic as well as stochastic road excitations. The results

of the study revealed that the tunable sequential hydraulic damper offered considerable potentials to improve the vehicle ride comfort.

Meller and Fruhauf [27] discussed and compared two kinds of variable damping control systems: external and internal control systems in a pressurized twin-tube shock absorbers. Solenoid pressure control valves are used to achieve three stage damping characteristics. A three-level adjustable shock absorber was developed by Nissan Motor Co., Ltd., which allowed drivers to select the damping force setting from the driver's seat [28]. Toyota Motor Corporation developed a more elaborate suspension with three control modes to be selected by the drivers: normal mode, sport mode, and auto mode [29]. In the normal mode the damping force of the shock absorbers was kept relatively small, while in the sport mode, the damping force was relatively large. In the auto mode, the damping force of the shock absorbers was automatically varied between the normal and the sport modes based upon feedback. Ford Motor Co. [30] developed a Programmed Ride Control (PRC) suspension, which provided drivers selected "firm" or "automatic" ride control using a rock switch. In the automatic mode, the PRC computer adjusts the shock absorber damping to provide a soft ride during normal driving conditions. The damping, however, is changed to firm during hard cornering, braking or acceleration to achieve improved handling. Hennceke [38] discussed and summarized the frequency dependent variable suspension damping.

Active vehicle suspensions, with parameters that change with variations in excitation and response characteristics, provide superior shock and vibration isolation performance, and have also been extensively investigated [41, 42, 43]. However, the requirements of an external energy source and control system with large number of sensors limit the applications of active suspension to cases where performance benefits outweigh the disadvantages associated with costs

and complexities [44, 45]. Semi-active vehicle suspensions offer a compromise between the performance benefits of an active and the simplicity of the passive suspension. A number of semi-active damping mechanisms have been proposed and investigated [31-37]. Since damping force tends to attenuate vibration only in a portion of response cycle, "on-off" semi-active damping has been extensively investigated [31, 39]. Alanoly [40] presented and evaluated six types of semi-active suspension control schemes in terms of peak and RMS acceleration transmissibility. Although hardware implementation of a semi-active suspension is considerably simpler than an active suspension, the realization of semi-active damping requires a comprehensive instrumentation package and control devices [31, 46]. Moreover, semi-active "on-off" control yields a large magnitude of jerk around the discontinuity between the "on" and "off" states [39, 47].

1.2.3 Performance Criteria

Various performance criteria have been proposed to assess the ride comfort and handling performance of different vehicle suspensions. The root mean square of vertical acceleration of vehicle body at passenger/driver location is most commonly used to evaluate the ride performance of ground vehicles. It is now widely accepted that acceleration data should be frequency weighted before rms values are used as objective measures of discomfort [1, 48, 49]. Alternatively, acceleration PSD of body response and vibration transmissibility are also used to assess the relative ride performance of different suspensions [4, 26]. Shock attenuation performance is frequently assessed in terms of peak acceleration response of sprung mass [50]. There are many different methods to evaluate handling performance of a vehicle. Although oversteer and understeer characteristics are commonly used to assess the steady state handling behavior

of vehicles, the response variables, such as wheel load fluctuations, tire slip angles, yaw rate, and vehicle path have been employed to carry out relative performance evaluations of different suspensions. The simplest indicators of handling performance, however, are the roll and pitch angles [51]. While the roll reduction during cornering may represent only one measure of the improved vehicle handling, it is widely established that roll performance of a vehicle is directly related to the transient handling characteristics.

1.3 SCOPE OF PRESENT INVESTIGATION

The analytical and experimental studies, reported in the literature, have clearly demonstrated that an interconnected suspension offers considerable potentials to achieve improved compromise between the roll and ride performance of a vehicle. The modern highway buses and freight vehicles exhibit poor roll stability due to their high center of sprung mass. The implementation of a hydro-pneumatic suspension, interconnected in the roll plane, can enhance the roll stability of these vehicles by providing increased roll stiffness while preserving relatively soft ride. Moreover, the passenger ride quality of highway buses can be further improved by employing dampers with variable suspension damping.

1.3.1 Objective of Present Investigation

The primary objective of this dissertation research is to develop a mathematical model of a laterally interconnected hydro-pneumatic suspension with variable damping in the roll plane, and to evaluate its static and dynamic properties related to ride and handling characteristics of the vehicle. The specific objectives of this thesis are:

(1) To develop roll plane models of vehicles employing unconnected and interconnected hydro-pneumatic suspensions.

(2) To analyze the inherent static and dynamic characteristics of the interconnected suspension in terms of suspension rate, roll stiffness, and damping forces.

(3) To evaluate shock and vibration isolation performance and roll response of the vehicle employing unconnected suspension with and without anti-roll bars, and interconnected suspension for deterministic excitations arising from road irregularities and directional maneuvers.

(4) To integrate multi-stage suspension damping and evaluate the ride performance characteristics for deterministic and stochastic road excitations.

1.3.2 Organization of the Thesis

In chapter 2, three types of hydro-pneumatic suspension systems, namely, interconnected, unconnected, unconnected with anti-roll bars are analytically modeled in the roll plane. The roll plane dynamics of a vehicle is represented by a four-degrees-of-freedom dynamical system under excitations arising from road irregularities and roll moment caused by directional maneuvers. The equations of motion for the vehicle models are derived in terms of generalized suspension forces using Lagrange's energy approach. The generalized suspension forces are derived assuming incompressible fluid in hydraulic struts, turbulent flows through the orifice restrictions, polytropic processes of gas in accumulators, and laminar flows within the interconnecting pipes.

The static and dynamic properties of the three different hydro-pneumatic suspensions are derived and presented in Chapter 3. The suspension properties

are discussed in terms of their load-carrying capacity, suspension rate, roll stiffness and damping forces. Analytical expressions are derived to characterize the force-displacement and force-velocity characteristics of the different suspensions. Five suspension configurations are proposed to further investigate their ride and roll performance potentials.

In chapter 4, the ride and handling performance characteristics of five hydro-pneumatic suspensions are investigated for deterministic excitations using numerical integration approach. The nature of excitations arising from tire-terrain interactions and steering inputs are described. The roll performance characteristics of the suspension systems are evaluated in terms of transient and steady state roll response of the sprung and unsprung masses subject to constant radius turning and lane change maneuvers. The dynamic ride performance characteristics are established in terms of both heave and roll shock isolation characteristics of the suspensions subjected to road excitations. Vibration transmissibility characteristics of different suspension systems are investigated and compared.

In chapter 5, a passive variable damping mechanism is proposed to achieve improved vibration isolation performance of the interconnected hydro-pneumatic suspension. The passive multi-stage damping is realized by modulating the flow through orifices based upon pressure differential across the damper. The vibration isolation performance of the vehicle suspension employing variable damping is further investigated for deterministic and stochastic road excitations. The highlights of the study and the conclusions drawn are summarized in Chapter 6.

CHAPTER 2

DEVELOPMENT OF ROLL PLANE VEHICLE SUSPENSION MODELS

2.1 INTRODUCTION

Design of a passive vehicle suspension involves a compromise among the performance characteristics related to ride comfort, suspension working space, wheel load variations, static and dynamic attitude control, handling and directional control. The primary design considerations, however, include adequate ride comfort and handling and directional control. The attainment of good ride quality necessitates soft spring suspension, while hard springs are necessary to achieve good handling and directional control performance. These conflicting requirements often result in a compromise between handling performance and ride comfort. Auxiliary roll stiffness elements, such as anti-roll bars, are frequently used to achieve good handling and directional control performance. Anti-roll bars, however, deteriorate ride comfort under one-wheel bump. Alternatively, the diagonally interconnected hydro-pneumatic suspension in the roll plane can provide soft vertical spring rate and high roll stiffness to achieve an improved compromise among the ride quality and roll performance of a vehicle. Modern highway buses and fright vehicles exhibit poor roll stability due to their high center of gravity. The interconnected suspension with enhanced roll stiffness can be therefore employed in such cases to improved handling performance and ride comfort.

In this chapter, the roll plane model of a beam axle suspension with laterally interconnected hydraulic struts is developed to investigated its roll and ride characteristics. The roll plane models of conventional suspensions with and without anti-roll bar are developed to carry out relative performance analyses.

2.2 ROLL PLANE MODEL OF AN UNCONNECTED HYDRO-PNEUMATIC SUSPENSION SYSTEM

Vehicle models, varying from simple two-degrees-of-freedom (DOF) quarter-vehicle model to several DOF three-dimensional models, have been developed to analyze the ride, handling and directional control characteristics. While a two-DOF model provides ride performance in the uncoupled vertical mode, a four-DOF roll plane model comprising vertical and roll motions of the sprung and unsprung masses can effectively yield the vertical and roll characteristics of a vehicle. A modern highway bus, equipped with conventional or the laterally interconnected suspensions, is thus characterized by a four-DOF dynamical system in the roll plane to study the vertical and roll characteristics of the interconnected suspension.

2.2.1 Equations of Motion of the Suspension System

The roll plane model of a road vehicle, comprising of beam axle and hydro-pneumatic suspension is presented in Figure 2.1. As illustrated, the vehicle is modeled as a four-degrees-of-freedom dynamical system, comprising vertical and roll motions of the sprung and unsprung masses. Vertical motions of centers of gravity (c.g.) of sprung and unsprung masses are described by x_s and x_u. Roll angles of the sprung and unsprung masses are described by ϑ_s and ϑ_u, respectively, about their respective roll centers. m_s is the sprung mass of the vehicle lumped in the roll plane, and m_u is the mass of axles lumped in the roll plane. The tires are modeled as parallel combinations of linear springs (k_{tl},k_{tr}), and viscous dampers (c_{tl},c_{tr}), assuming point contact between the tire and the road. Excitations to the roll plane model include vertical displacements at the tire-terrain interface (x_{tl},x_{tr}) due to road irregularities, and a roll moment, T_ϑ,

acting on the sprung mass caused by a centrifugal force encountered during a directional maneuver.

As shown in Figure 2.1, the primary vehicle suspension consists of two hydro-pneumatic systems. The forces generated by the left and right suspensions are represented by two primary suspension forces, F_ℓ, F_r, respectively. A detailed schematic of the hydro-pneumatic suspension system is shown in Figure 2.2, and will be discussed later in subsection 2.2.2.

In deriving the equations of motion for the roll plane model, it is assumed that the vibration levels are small, the roll center height of the sprung and unsprung masses remain unchanged. The coupled differential equations of motion for the four-DOF model, derived using Lagrange's energy approach, are presented as follows:

Bounce motion of the sprung mass:

$$m_s\ddot{x}_s - F_\ell - F_r = 0 \tag{2.1}$$

Roll motion of the sprung mass:

$$I_s\ddot{\vartheta}_s - F_r\ell_r + F_\ell\ell_\ell = T_\vartheta \tag{2.2}$$

Bounce motion of the unsprung mass:

$$m_u\ddot{x}_u + (c_{t\ell} + c_{tr})\dot{x}_u + (c_{tr}\ell_{wr} - c_{t\ell}\ell_{w\ell})\dot{\vartheta}_u + (k_{t\ell} + k_{tr})x_u + (k_{tr}\ell_{wr} - k_{t\ell}\ell_{w\ell})\vartheta_u + F_\ell + F_r = c_{t\ell}\dot{x}_{i\ell} + k_{t\ell}x_{i\ell} + c_{tr}\dot{x}_{ir} + k_{tr}x_{ir} \tag{2.3}$$

Roll motion of the unsprung mass:

$$I_u\ddot{\vartheta}_u + (c_{sr}\ell_{wr} - c_{t\ell}\ell_{w\ell})\dot{x}_u + (c_{s\ell}\ell_{w\ell}^2 + c_{sr}\ell_{wr}^2)\dot{\vartheta}_u + (k_{sr}\ell_{wr} - k_{s\ell}\ell_{w\ell})x_u + (k_{s\ell}\ell_{w\ell}^2 + k_{sr}\ell_{wr}^2)\vartheta_u + F_r\ell_r - F_\ell\ell_\ell = c_{sr}\ell_{wr}\dot{x}_{ir} + k_{sr}\ell_{wr}x_{ir} - c_{t\ell}\ell_{w\ell}\dot{x}_{i\ell} - k_{s\ell}\ell_{w\ell}x_{i\ell} \tag{2.4}$$

where I_s is the mass moment of inertia of the sprung mass, and I_u the mass moment of the unsprung mass. ℓ_ℓ, ℓ_r are the lateral distances from left and right suspension struts to the center of gravity of the sprung mass. $\ell_{w\ell}, \ell_{wr}$ are the

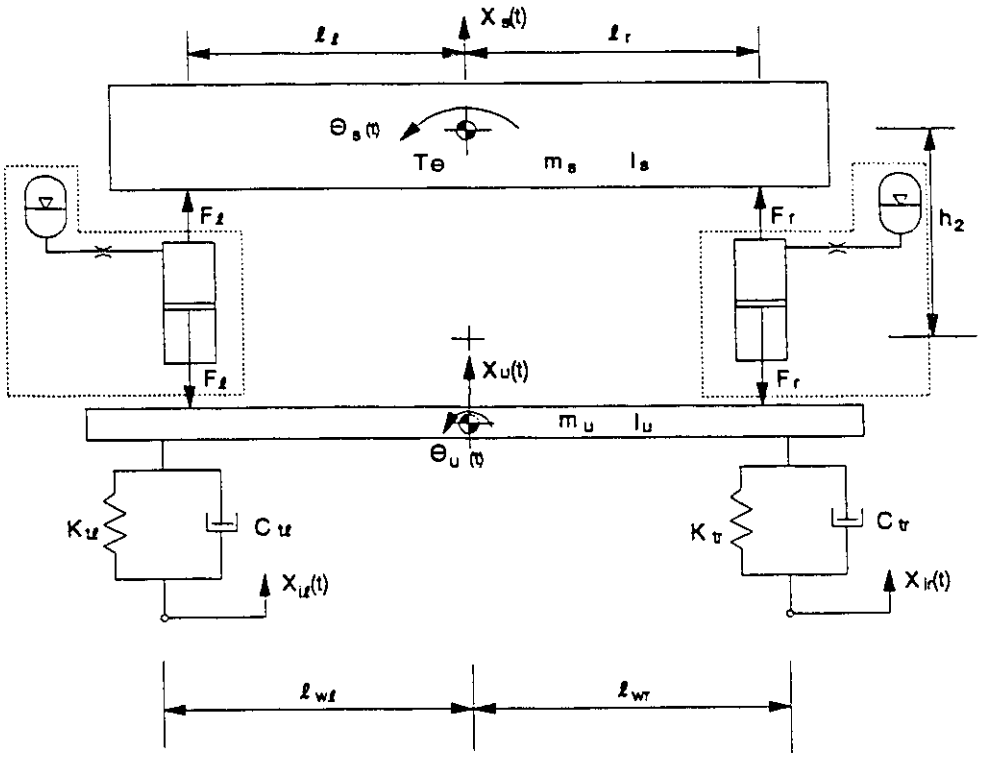

Figure 2.1 Roll plane model of an unconnected hydro-pneumatic suspension system

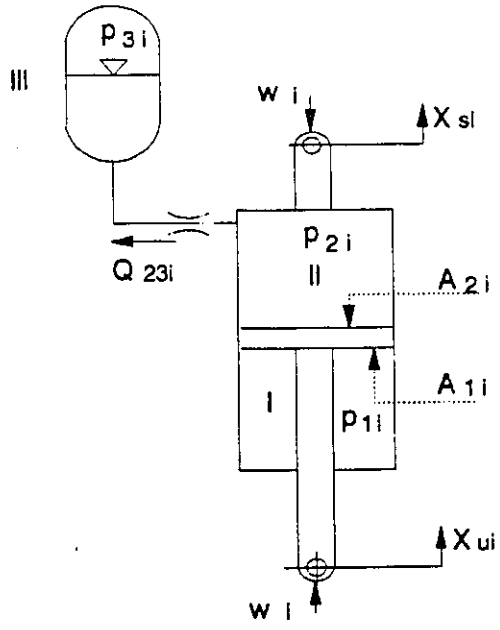

Figure 2.2 Schematic of a hydro-pneumatic suspension strut

lateral distances from the left and right tires to the center of gravity of the unsprung mass.

2.2.2 Generalized Suspension Forces

The hydro-pneumatic suspension, shown in Figure 2.2, comprises a hydraulic strut, an accumulator and a damping restriction. The chamber I of the hydraulic strut is open to atmosphere, while the chamber II contains pressurized hydraulic fluid. Chamber III, the accumulator, contains a separator to prevent the gas from diffusing into the fluid. The dynamic strut forces, F_ℓ and F_r, can be derived assuming incompressible fluid in the struts, turbulent flows through the orifice restrictions, and a polytropic process of the gas in the accumulators.

Static Equilibrium Equation

The pressure of the fluid within each strut under static equilibrium is related to the static load acting on the strut:

$$w_i = (p_{0i} - p_a) A_{2i} \quad , \quad (i = \ell, r) \tag{2.5}$$

where the subscripts ℓ and r refer to the left and right struts; p_{0i} is the absolute internal pressure of suspension strut i under static equilibrium condition; p_a is atmospheric pressure; A_{2i} is the piston head area, and w_i is the static load acting on suspension strut i , given by:

$$w_\ell = \frac{m_s g \ell_r}{N_u(\ell_\ell + \ell_r)} \quad \text{and} \quad w_r = \frac{m_s g \ell_\ell}{N_u(\ell_\ell + \ell_r)} \tag{2.6}$$

where g is the acceleration due to gravity and N_u is the number of struts used on each side in the roll plane model. The fluid pressure under static equilibrium can also be related to the static load in the following manner:

$$p_{0i} = \frac{w_i}{A_{2i}} + p_a \qquad (i = \ell, r) \tag{2.7}$$

Assuming polytropic process, the fluid pressure p_{0i} and the gas volume v_{0i} under static loading can be related to the initial charge pressure, p_{ci}:

$$p_{0i}v_{0i}^{n} = p_{ci}v_{ci}^{n} \quad (i = \ell, r) \tag{2.8}$$

where v_{ci} is the initial charge volume of gas in suspension i, and n is the polytropic exponent.

Fluid Flow Equations

Assuming incompressible fluid flows, the rate of change of fluid volume in chamber *II* of strut i is related to the relative motion across the strut:

$$Q_{2i} = A_{2i}\dot{z}_i \qquad (i = \ell, r) \tag{2.9}$$

where Q_{2i} is the rate of change of fluid volume in chamber *II* of suspension strut i, and $\dot{z}_i$ is the relative velocity across suspension strut i, given by:

$$\begin{aligned} \dot{z}_\ell &= \dot{x}_s - \dot{x}_u - (\dot{\vartheta}_s - \dot{\vartheta}_u)\ell_\ell \\ \dot{z}_r &= \dot{x}_s - \dot{x}_u + (\dot{\vartheta}_s - \dot{\vartheta}_u)\ell_r \end{aligned} \tag{2.10}$$

During compression or rebound strokes, the fluid flows between chambers *II* and *III* through the damping restrictions. Assuming turbulent flow through the damping restriction or the orifice, the flow rate from chamber *II* to *III*, Q_{23i}, can be expressed as

$$Q_{23i} = C_d a_i \sqrt{\frac{2|p_{23i}|}{\rho}} sgn(p_{23i}) \ , \qquad (i = \ell, r) \tag{2.11}$$

where C_d is the discharge coefficient; a_i is the orifice area; ρ is the mass density of the fluid. $p_{23i} = p_{2i} - p_{3i}$ is the pressure differential across the damping restriction, and the *sgn* function describes the direction of fluid flow:

$$sgn(p_{23i}) = \begin{cases} +1; \text{ for } p_{23i} \geq 0 \\ -1; \text{ for } p_{23i} < 0 \end{cases} \qquad (i = \ell, r)$$

For incompressible fluid flows, the rate of change of fluid volume caused by piston movement, Q_{2i}, is related to the orifice flow, Q_{23i}, through the conservation of mass:

$$Q_{2i} = -Q_{23i} \qquad (i = \ell, r) \tag{2.12}$$

Pressure Equations

The pressure differential, p_{23i}, can thus be derived from Equations (2.9), (2.11), and (2.12):

$$p_{23i} = \frac{\rho}{2}\left[\frac{A_{2i}}{C_d a_i}\right]^2 \dot{z}_i^2 sgn(\dot{z}_i) \qquad (i = \ell, r) \tag{2.13}$$

The instantaneous pressure of fluid in chamber *III*, p_{3i}, can be derived assuming polytropic process:

$$p_{3i} = \left(\frac{v_{0i}}{v_{3i}}\right)^n p_{0i} \qquad (i = \ell, r) \tag{2.14}$$

where v_{3i} is the instantaneous volume of gas in chamber *III*, given by:

$$v_{3i} = v_{0i} + A_{2i} z_i; \qquad (i = \ell, r) \tag{2.15}$$

and

$$\begin{aligned} z_\ell &= x_s - x_u - (\vartheta_s - \vartheta_u)\ell_\ell \\ z_r &= x_s - x_u + (\vartheta_s - \vartheta_u)\ell_r \end{aligned} \tag{2.16}$$

Dynamic Forces of the Unconnected Suspension

The dynamic force generated by the suspension strut on each side, f_i, with respect to the static equilibrium position, is established from forces acting upon the piston:

$$f_i = (p_{2i} - p_{0i}) A_{2i} \qquad (i = \ell, r) \tag{2.17}$$

where $p_{2i} = p_{23i} + p_{3i}$, is the instantaneous fluid pressure in chamber *II*. Upon substituting for p_{23i} and p_{3i} from Equations (2.13), (2.14), and (2.15) into (2.17), the dynamic suspension forces generated by strut i can be expressed as:

$$f_i = \frac{\rho A_{2i}^3}{2C_d^2 a_i^2} \dot{z}_i^2 sgn(\dot{z}_i) + p_{0i} A_{2i} \left[\left(\frac{v_{0i}}{v_{0i} + A_{2i} z_i} \right)^n - 1 \right] \quad (i = \ell, r) \tag{2.18}$$

The dynamic force developed by a suspension strut comprises the nonlinear dissipative force due to flows through the damping restrictions and the nonlinear restoring force due to the gas charge in the accumulator. The first term in Equation (2.18) describes the damping force component related to square of the relative velocity across the suspension strut, while the second term describes the nonlinear restoring force due to the gas spring. The generalized suspension forces developed in the roll plane model are related to the total number of suspension units used:

$$F_\ell = N_u f_\ell = \frac{\rho A_{2\ell}^3 N_u}{2C_d^2 a_\ell^2} \dot{z}_\ell^2 sgn(\dot{z}_\ell) + p_{0\ell} A_{2\ell} N_u \left[\left(\frac{v_{0\ell}}{v_{0\ell} + A_{2\ell} z_\ell} \right)^n - 1 \right]$$

$$F_r = N_u f_r = \frac{\rho A_{2r}^3 N_u}{2C_d^2 a_r^2} \dot{z}_r^2 sgn(\dot{z}_r) + p_{0r} A_{2r} N_u \left[\left(\frac{v_{0r}}{v_{0r} + A_{2r} z_r} \right)^n - 1 \right] \tag{2.19}$$

where N_u is the number of suspension units used on each side.

Equations (2.1) to (2.4) and (2.19) describe the vertical and roll dynamics of a vehicle with conventional unconnected suspension subject to excitations arising from roll moment and road irregularities.

2.3 ROLL PLANE MODEL OF AN UNCONNECTED HYDRO-PNEUMATIC SUSPENSION SYSTEM WITH ANTI-ROLL BAR

A road vehicle suspension, in general, is designed with an auxiliary roll stiffness mechanism to enhance its roll stability and directional control performance, and to reduce the vehicle sensitivity to cross-winds. Anti-roll bars are commonly used in road vehicles to achieve enhanced effective roll stiffness.

An anti-roll bar is normally fitted across the chassis with its ends linking the two road wheels on opposite sides, as shown in Figure 2.3. It is bent near the ends to form trailing levers, while the center section is anchored to the spring mass through bushings so that it can be free to rotate. The trailing levers arc up and down with wheel deflections. The relative roll motion of sprung mass against unsprung mass, encountered under a single wheel bump or directional maneuver, cause the bar to twist, and thus provide resistance to bounce travel and body roll. The two ends of the anti-roll bar, however, experience identical motion, when subjected to a pure vertical excitation caused by a bump encountered by both wheels. The anti-roll bar thus simply turns without twisting. Therefore the anti-roll bar has no effect under a two-wheel bump.

2.3.1 Modeling of Anti-roll Bars

The anti-roll bar can be modeled as a torsion spring, as illustrated in Figure 2.4. When one of the wheels lifts a distance with respect to the other wheel under a single wheel bump, an equal and opposite elastic force, F_b, in the vertical direction is generated. Assuming linear property of the anti-roll bar, the spring force acting at each wheel can be expressed as:

$$F_b = k_b y \tag{2.20}$$

where y is the relative vertical motion between left and right end of the bar, and k_b is the spring constant. From the torsion spring shown in Figure 2.4, the vertical spring rate, k_b, can be established as:

$$k_b = \frac{\pi G d^4}{32 \ell_b r^2}. \tag{2.21}$$

where G is the shear modulus of the anti-roll bar; d is the diameter of the bar; r is the length of trailing lever and ℓ_b is the distance between the two ends of the

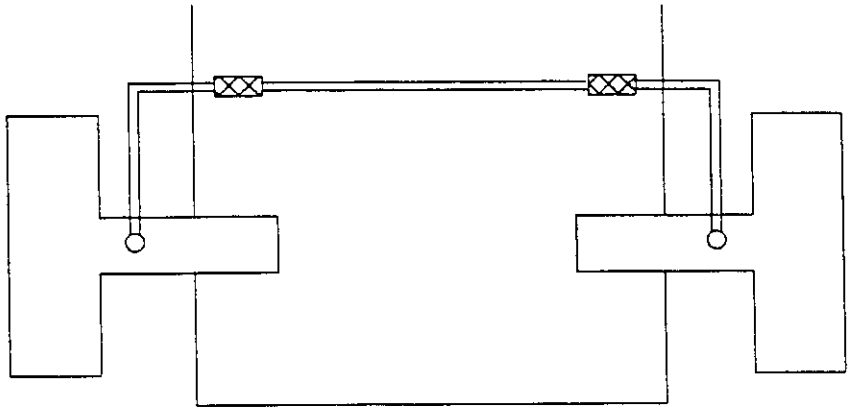

Figure 2.3 Anti-Roll Bar with Pure Roll Stiffness (Top Veiw)

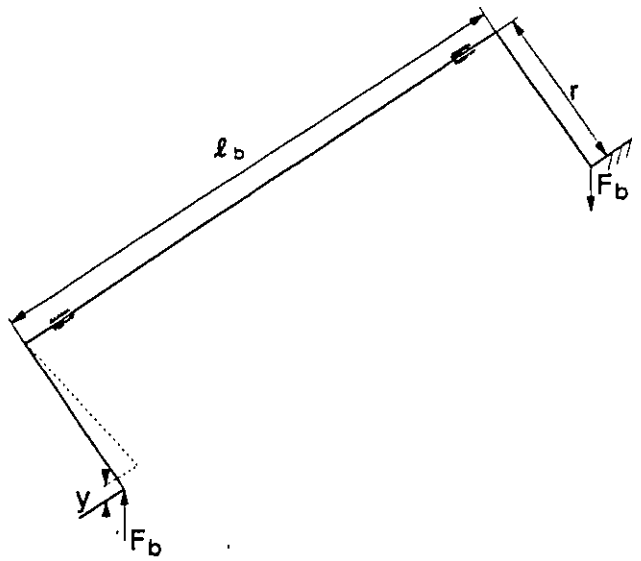

Figure 2.4 Modeling of anti-roll bar

anti-roll bar. The equal and opposite forces developed at the two ends of the anti-roll bar yield a torsion couple acting on the sprung mass, given by :

$$T_b = k_b \ell_b y \tag{2.22}$$

where T_t is the couple acting on the sprung mass. Since the relative vertical motion across the anti-roll bar is related to the roll angle ($\vartheta = x / \ell_b$), the restore roll moment due to the anti-roll bar can be expressed as:

$$T_b = k_\vartheta \vartheta \tag{2.23}$$

where k_ϑ is the auxiliary roll stiffness due to the anti-roll bar, given by:

$$k_\vartheta = \frac{\pi G d^4 \ell_b}{32 r^2} \tag{2.24}$$

A comparison of Equation (2.21) with (2.24) yields:

$$k_\vartheta = k_b \ell_b^2 \tag{2.25}$$

2.3.2 Equations of Motion

The roll plane model of a conventional unconnected hydro-pneumatic suspension with an anti-roll bar is presented in Figure 2.5. The vehicle model is identical to that presented in section 2.2 (Figure 2.1) with the exception of the anti-roll bar, represented by the auxiliary roll stiffness k_ϑ. The equations of motion for the vehicle model are derived in a manner described in section 2.2 and presented below.

Bounce motion of the sprung mass:

$$m_s \ddot{x}_s - F_l - F_r = 0 \tag{2.26}$$

Roll motion of the sprung mass:

$$I_s \ddot{\vartheta}_s - F_r \ell_r + F_l \ell_l + k_\vartheta (\vartheta_s - \vartheta_u) = T_\vartheta \tag{2.27}$$

Bounce motion of the unsprung mass:

$$\begin{aligned} &m_u \ddot{x}_u + (c_{tl} + c_{tr}) \dot{x}_u + (c_{tr} \ell_{wr} - c_{tl} \ell_{wl}) \dot{\vartheta}_u + (k_{tl} + k_{tr}) x_u + (k_{tr} \ell_{wr} - k_{tl} \ell_{wl}) \vartheta_u \\ &+ F_l + F_r = c_{tl} \dot{x}_{il} + k_{tl} x_{il} + c_{tr} \dot{x}_{ir} + k_{tr} x_{ir} \end{aligned} \tag{2.28}$$

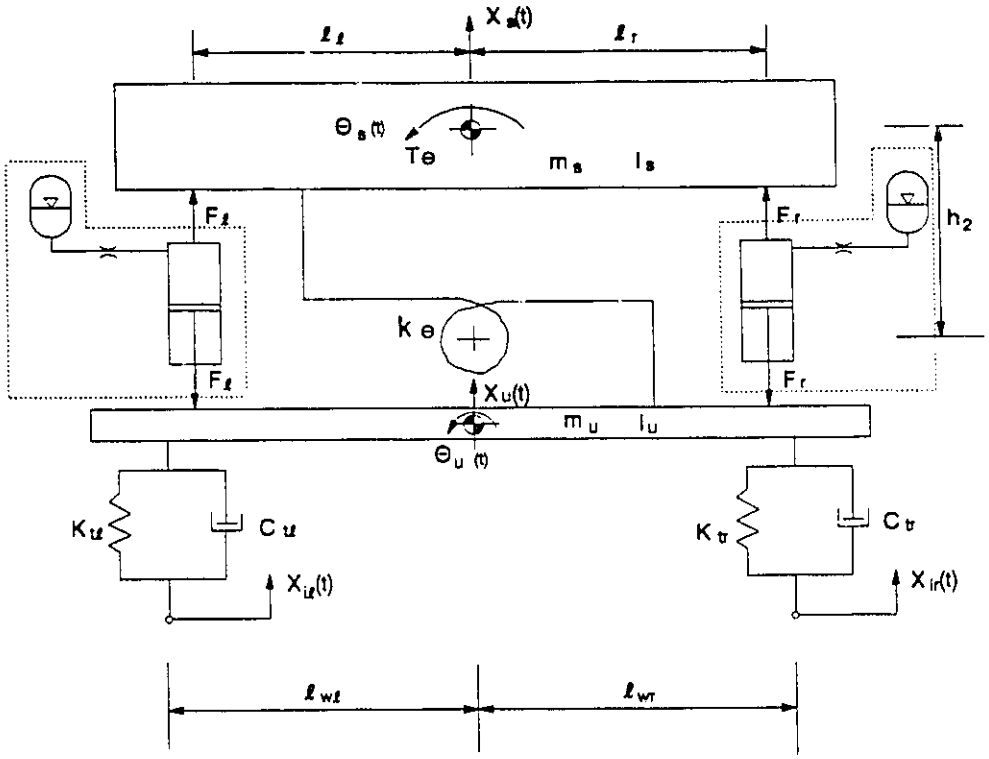

Figure 2.5 Roll plane model of an unconnected hydro-pneumatic suspension system with anti-roll bar

Roll motion of the unsprung mass:

$$I_u\ddot{\vartheta}_u+(c_{tr}\ell_{wr}-c_{tl}\ell_{wl})\dot{x}_u+(c_{tl}\ell_{wl}^2+c_{tr}\ell_{wr}^2)\dot{\vartheta}_u+(k_{tr}\ell_{wr}-k_{tl}\ell_{wl})x_u+(k_{tl}\ell_{wl}^2+k_{tr}\ell_{wr}^2)\vartheta_u$$
$$+F_r\ell_r-F_l\ell_l-k_s(\vartheta_s-\vartheta_u)=c_{tr}\ell_{wr}\dot{x}_{ir}+k_{tr}\ell_{wr}x_{ir}-c_{tl}\ell_{wl}\dot{x}_{il}-k_{tl}\ell_{wl}x_{il} \qquad (2.29)$$

where F_l and F_r have the same expressions as shown in (2.19).

2.4 ROLL PLANE MODEL OF AN INTERCONNECTED HYDRO-PNEUMATIC SUSPENSION SYSTEM

Figure 2.6 illustrates the schematic of a hydro-pneumatic suspension interconnected in the roll plane. The suspension system comprises double-acting hydraulic struts, accumulators, damping restrictions and interconnecting pipes. The upper chamber of the left strut (II_l) is connected to the lower chamber of the right strut (I_r), while the lower chamber of the left strut (I_l) is connected to the upper chamber of the right strut (II_r) This interconnected suspension is different from the well known hydragas suspension which is interconnected between the front and rear struts in order to reduce the pitch stiffness. The primary objective of the proposed interconnected suspension is to increase roll stiffness, while, at the same time, maintain lower bounce and pitch stiffness to achieve good handling and ride qualities.

2.4.1 Equations of Motion

The vehicle, equipped with the proposed interconnected suspension, is modeled in the roll plane as a four-DOF dynamical system, as shown in Figure 2.7. The coupled differential equations of motion of the vehicle model are derived using the techniques and assumptions described in section 2.2. The primary suspension forces due to the left and right struts of the interconnected

suspension are again represented by generalized dynamic forces, F_ℓ' and F_r', respectively. The coupled differential equations of motion are derived using Lagrange's energy approach and presented below.

Bounce motion of the sprung mass:

$$m_s\ddot{x}_s - F_\ell' - F_r' = 0 \tag{2.30}$$

Roll motion of the sprung mass:

$$I_s\ddot{\vartheta}_s - F_r'\ell_r + F_\ell'\ell_\ell = T_\vartheta \tag{2.31}$$

Bounce motion of the unsprung mass:

$$\begin{aligned} &m_u\ddot{x}_u + (c_{u\ell} + c_{ur})\dot{x}_u + (c_{ur}\ell_{wr} - c_{u\ell}\ell_{w\ell})\dot{\vartheta}_u + (k_{u\ell} + k_{ur})x_u + (k_{ur}\ell_{wr} - k_{u\ell}\ell_{w\ell})\vartheta_u \\ &+ F_\ell' + F_r' = c_{u\ell}\dot{x}_{i\ell} + k_{u\ell}x_{i\ell} + c_{ur}\dot{x}_{ir} + k_{ur}x_{ir} \end{aligned} \tag{2.32}$$

Roll motion of the unsprung mass:

$$\begin{aligned} &I_u\ddot{\vartheta}_u + (c_{ur}\ell_{wr} - c_{u\ell}\ell_{w\ell})\dot{x}_u + (c_{u\ell}\ell_{w\ell}^2 + c_{ur}\ell_{wr}^2)\dot{\vartheta}_u + (k_{ur}\ell_{wr} - k_{u\ell}\ell_{w\ell})x_u + (k_{u\ell}\ell_{w\ell}^2 + k_{ur}\ell_{wr}^2)\vartheta_u + F_r'\ell_r - F_\ell'\ell_\ell \\ &= c_{ur}\ell_{wr}\dot{x}_{ir} + k_{ur}\ell_{wr}x_{ir} - c_{u\ell}\ell_{w\ell}\dot{x}_{i\ell} - k_{u\ell}\ell_{w\ell}x_{i\ell} \end{aligned} \tag{2.33}$$

2.4.2 Generalized Suspension Forces

The Generalized forces due to the interconnected suspension, comprising of both elastic and damping forces, can be developed by using static equilibrium, conservation-of-mass, fluid flow equations, and pressure equations.

Static Equilibrium

The static ride height, static deflection and operating pressures in the suspension struts are related to the static loads and the charge pressures. Assuming identical static pressures in the connected chambers ($p_{3\ell 0} = p_{2\ell 0} = p_{1r0}$; and $p_{3r0} = p_{2r0} = p_{1\ell 0}$) and polytropic process, the static pressures can be related to the static loads (w_ℓ and w_r), and initial gas charge pressures in the left and right suspension struts ($p_{\ell c}$ and p_{rc}):

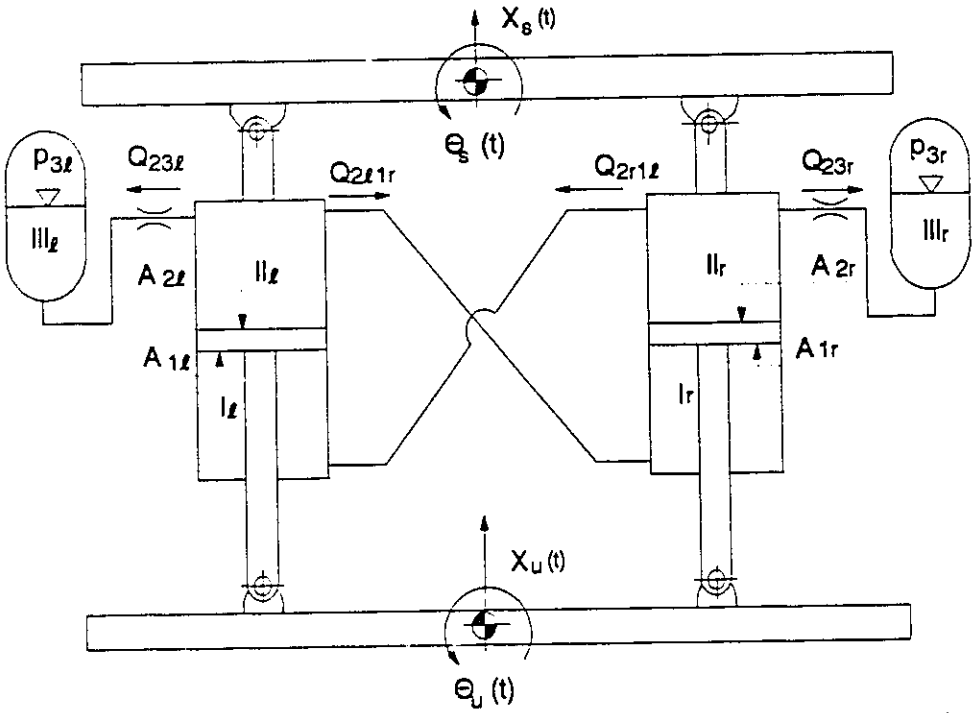

Figure 2.6 Schematic of an interconnected hydro-pneumatic suspension

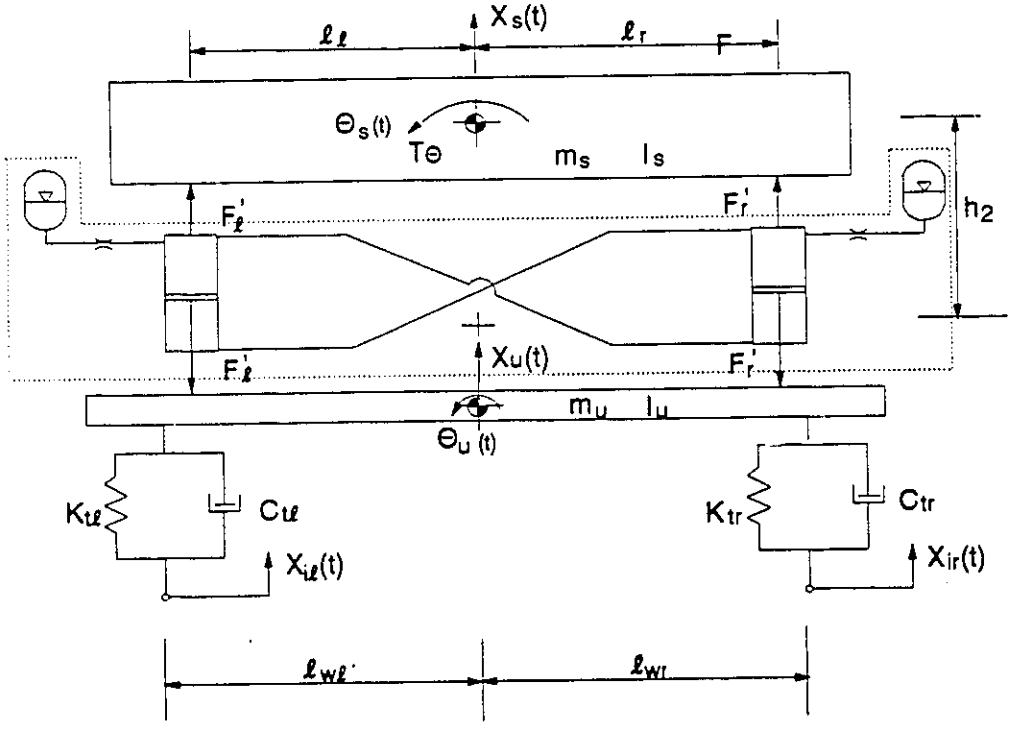

Figure 2.7 Roll plane model of an interconnected hydro-pneumatic suspension system

$$p_{2\ell 0}A_{2\ell} - p_{1\ell 0}A_{1\ell} - p_a(A_{2\ell} - A_{1\ell}) = w_\ell$$
$$p_{2r0}A_{2r} - p_{1r0}A_{1r} - p_a(A_{2r} - A_{1r}) = w_r \qquad (2.34)$$

and

$$p_{3i0}v_{3i0}^n = p_{ic}v_{ic}^n \qquad (i = \ell, r) \qquad (2.35)$$

where p_{3i0} and p_{ic} are the static and initial charge pressures in chamber III of suspension i; v_{3i0} and v_{ic} are the static and initial volumes of gas in the accumulator of suspension i; $p_{1\ell 0}$, $p_{2\ell 0}$ and $p_{3\ell 0}$ are the fluid pressures corresponding to static equilibrium in chambers I, II and III of the left suspension, respectively; p_{1r0}, p_{2r0} and p_{3r0} are the fluid pressures corresponding to static equilibrium in chambers I, II and III of the right suspension, respectively; $A_{1\ell}$ and A_{1r} are the rod side areas of the left and right strut pistons, respectively; $A_{2\ell}$ and A_{2r} are the head side areas of the left and right strut pistons, respectively; w_ℓ and w_r have the same expressions as in Equation (2.6).

The static deflection of suspension struts, $x_{\ell 0}$ and x_{r0}, are derived from the equation of flow continuity under static equilibrium:

$$A_{2\ell}x_{\ell 0} = v_{\ell c} - v_{3\ell 0} + A_{1r}x_{r0}$$
$$A_{2r}x_{r0} = v_{rc} - v_{3r0} + A_{1\ell}x_{\ell 0} \qquad (2.36)$$

Equation (2.36) reveals that the static deflection of the right and left suspension struts are coupled due to interconnections. The simultaneous solution of Equation (2.34) to (2.36) yields the static pressures, volumes and deflections of left and right suspension struts.

Equations of Fluid Flow

The fluid flows within an interconnected suspension include: (i) the flows through orifices and connecting pipes due to piston movement; (ii) the flows due to fluid compressibility. Su [4] investigated the influence of variations in the fluid

bulk modulus on the ride performance characteristics of an interconnected hydraulic suspension. The study demonstrated that the fluid flows due to fluid compressibility were insignificant and thus may be neglected. Assuming turbulent flows through the orifice restrictions between the chambers *II* and *III*, the volume flow rates through the orifices in the left and right suspension units are related to pressure differentials across the orifices, in the following manner:

$$Q_{23i} = C_d a_i \sqrt{\frac{2|p_{23i}|}{\rho}} sgn(p_{23i}); \text{ for } i = \ell, r \tag{2.37}$$

where Q_{23i} is the volume flow rate through the orifice from chamber *II* to *III* of suspension i, and p_{23i} is the instantaneous pressure differential across the orifice, $p_{23i} = p_{2i} - p_{3i}$.

Assuming laminar fluid flows through the interconnecting pipes, and negligible entry and exit losses, the volume flow rates through the pipes linearly relate to the pressure differentials in the following manner:

$$Q_{2\ell 1r} = Kp_{2\ell 1r} \quad \text{and} \quad Q_{2r1\ell} = Kp_{2r1\ell} \tag{2.38}$$

where $K = \pi D^4/128\mu L$; $Q_{2\ell 1r}$ is the volume flow rate from chamber *II* of the left strut to chamber *I* of the right strut; $Q_{2r1\ell}$ is the volume flow rate from chamber *II* of the right strut to chamber *I* of the left strut; $p_{2\ell 1r} = p_{2\ell} - p_{1r}$ is the pressure differential between chamber *II* of the left strut and chamber *I* of the right strut; $p_{2r1\ell} = p_{2r} - p_{1\ell}$ is the pressure differential between chamber *II* of the right strut and chamber *I* of the left strut; D is the diameter of the interconnecting pipe, and L is its length. μ is the absolute viscosity of fluid.

The rate of change of fluid volume in chambers *I* and *II* of struts i is related to the relative velocity across the respective strut:

$$Q_{1i} = A_{1i}\dot{z}_i \quad \text{and} \quad Q_{2i} = A_{2i}\dot{z}_i; \quad \textit{for } i = \ell, r \tag{2.39}$$

where Q_{1i} and Q_{2i} ($i = \ell, r$) are the rates of change of fluid volume in chambers I and II, respectively, due to piston movement. $\dot{z}_i$ ($i = \ell, r$) is the relative velocity across the strut i, given by:

$$\dot{z}_\ell = \dot{x}_s - \dot{x}_u - (\dot{\vartheta}_s - \dot{\vartheta}_u)\ell_\ell$$
$$\dot{z}_r = \dot{x}_s - \dot{x}_u + (\dot{\vartheta}_s - \dot{\vartheta}_u)\ell_r \qquad (2.40)$$

Conservation-of-mass Equations

Assuming incompressible fluid, the flows associated with chambers I of the left and right struts are related by the following fluid continuity equations:

$$Q_{1\ell} = -Q_{2r1\ell}; \quad \text{and} \quad Q_{1r} = -Q_{2\ell 1r} \qquad (2.41)$$

Similarly, the fluid flows associated with chambers II of the left and right struts are expressed by the following continuity equations:

$$Q_{2\ell} + Q_{23\ell} + Q_{2\ell 1r} = 0; \text{ and } \quad Q_{2r} + Q_{23r} + Q_{2r1\ell} = 0 \qquad (2.42)$$

Upon combining Equations (2.39), (2.41) and (2.42), the fluid flows through damping restrictions can be related to the relative velocities across both the struts:

$$Q_{23\ell} = A_{1r}\dot{z}_r - A_{2\ell}\dot{z}_\ell; \quad \text{and} \quad Q_{23r} = A_{1\ell}\dot{z}_\ell - A_{2r}\dot{z}_r \qquad (2.43)$$

Equation (2.43) reveals that the flow rate through the orifice in the left suspension is related to not only the relative velocity across the left strut but also the relative velocity across the right strut, and the same for the flow rate through the orifice in the right suspension.

Pressure Equations

The pressure differentials, p_{23i}, due to orifice flows in the left and right suspension units are obtained from Equation (2.37) as:

$$p_{23i} = \frac{\rho}{2}\left(\frac{Q_{23i}}{C_d a_i}\right)^2 sgn(Q_{23i}); \text{ for } i = \ell, r \qquad (2.44)$$

Upon substituting for Q_{23i} from Equation (2.43), the pressure differentials across the orifices are related to the piston velocities in the following manner:

$$p_{23\ell} = \frac{\rho}{2C_d^2 a_\ell^2}(A_{1r}\dot{z}_r - A_{2\ell}\dot{z}_\ell)^2 sgn(A_{1r}\dot{z}_r - A_{2\ell}\dot{z}_\ell)$$

$$p_{23r} = \frac{\rho}{2C_d^2 a_r^2}(A_{1\ell}\dot{z}_\ell - A_{2r}\dot{z}_r)^2 sgn(A_{1\ell}\dot{z}_\ell - A_{2r}\dot{z}_r) \qquad (2.45)$$

The instantaneous fluid pressure in chambers *III* of the two interconnected struts are derived assuming a polytropic process of the confined gas:

$$p_{3i} = p_{3i0}\left[\frac{v_{3i0}}{v_{3i0} - v_{23i}}\right]^n; \qquad i = \ell, r \qquad (2.46)$$

where v_{23i} is the change of gas volume within the accumulator of suspension i, due to flows between chambers *II* and *III*, given by:

$$v_{23\ell} = \int Q_{23\ell} dt = A_{1r}z_r - A_{2\ell}z_\ell; \text{ and } v_{23r} = \int Q_{23r} dt = A_{1\ell}z_\ell - A_{2r}z_r \qquad (2.47)$$

Upon combining Equations (2.38), (2.39) and (2.41), the pressure differentials due to laminar flows through the interconnected pipes, $p_{2\ell 1r}$ and $p_{2r1\ell}$, can be related to the relative velocity of the struts:

$$p_{2\ell 1r} = -A_{1r}\dot{z}_r / K; \quad \text{and} \quad p_{2r1\ell} = -A_{1\ell}\dot{z}_\ell / K \qquad (2.48)$$

The fluid pressures in chambers *I* and *II* of each strut can be expressed as:

$$p_{1\ell} = p_{2r} - p_{2r1\ell}; \quad \text{and} \quad p_{1r} = p_{2\ell} - p_{2\ell 1r}$$

$$p_{2\ell} = p_{23\ell} + p_{3l}; \quad \text{and} \quad p_{2r} = p_{23r} + p_{3r}$$

From Equations (2.45) to (2.48), the pressures of fluids in different chambers of the interconnected struts can be expressed as:

$$p_{1\ell} = p_{3r0}v_{3r0}^n\left(\frac{1}{v_{3r0} - A_{1\ell}z_\ell + A_{2r}z_r}\right)^n + \frac{\rho}{2C_d^2 a_r^2}(A_{1\ell}\dot{z}_\ell - A_{2r}\dot{z}_r)^2 sgn(A_{1\ell}\dot{z}_\ell - A_{2r}\dot{z}_r) + A_{1\ell}\dot{z}_\ell / K$$

$$p_{1r} = p_{3\ell 0} v_{3\ell 0} \left(\frac{1}{v_{3\ell 0} - A_{1r} z_r + A_{2\ell} z_\ell} \right)^n + \frac{\rho}{2 C_d^2 a_\ell^2} (A_{1r} \dot{z}_r - A_{2\ell} \dot{z}_\ell)^2 \, sgn(A_{1r} \dot{z}_r - A_{2\ell} \dot{z}_\ell) + A_{1r} \dot{z}_r / K \tag{2.49}$$

$$p_{2\ell} = p_{3\ell 0} v_{3\ell 0}^n \left(\frac{1}{v_{3\ell 0} - A_{1r} z_r + A_{2\ell} z_\ell} \right)^n + \frac{\rho}{2 C_d^2 a_\ell^2} (A_{1r} \dot{z}_r - A_{2\ell} \dot{z}_\ell)^2 \, sgn(A_{1r} \dot{z}_r - A_{2\ell} \dot{z}_\ell)$$

$$p_{2r} = p_{3r0} v_{3r0}^n \left(\frac{1}{v_{3r0} - A_{1\ell} z_\ell + A_{2r} z_r} \right)^n + \frac{\rho}{2 C_d^2 a_r^2} (A_{1\ell} \dot{z}_\ell - A_{2r} \dot{z}_r)^2 \, sgn(A_{1\ell} \dot{z}_\ell - A_{2r} \dot{z}_r) \tag{2.50}$$

Dynamic Forces of the Interconnected Suspension

The dynamic forces developed at the right and left strut of the interconnected suspension with respect to the static equilibrium are related to the pressure difference across the piston. The dynamic suspension forces, f_ℓ' and f_r', developed at the left and right struts can be expressed as:

$$\begin{aligned} f_\ell' &= (p_{2\ell} - p_{2\ell 0}) A_{2\ell} - (p_{1\ell} - p_{1\ell 0}) A_{1\ell} \\ f_r' &= (p_{2r} - p_{2r0}) A_{2r} - (p_{1r} - p_{1r0}) A_{1r} \end{aligned} \tag{2.51}$$

Through simple manipulations, the dynamic forces can also be expressed in the following manner:

$$\begin{aligned} f_\ell' &= (p_{3\ell} - p_{3\ell 0} + p_{23\ell}) A_{2\ell} + p_{2r1\ell} A_{1\ell} - (p_{3r} - p_{3r0} + p_{23r}) A_{1\ell} \\ f_r' &= (p_{3r} - p_{3r0} + p_{23r}) A_{2r} + p_{2\ell 1r} A_{1r} - (p_{3\ell} - p_{3\ell 0} + p_{23\ell}) A_{1r} \end{aligned} \tag{2.52}$$

Equation (2.52) reveals that the interconnecting pipes yield feedback or coupling effects within the suspension. The dynamic force generated by an interconnected suspension strut comprises the following three components:

(a) The first terms in Equation (2.52), $(p_{3i} - p_{3i0} + p_{23i}) A_{2i}$; $i = r, \ell$, represent the damping and restoring forces developed due to flows within the same suspension unit i .

(*b*) The terms $p_{2r1\ell}A_{1\ell}$ and $p_{2\ell1r}A_{1r}$, represent the damping forces due to flows through the pipes interconnecting the left and right struts.

(*c*) The last terms in Equation (2.52) represent the negative feedback of damping and restoring forces developed in one suspension strut due to flows within the other strut.

The generalized suspension forces F_ℓ' and F_r', developed by the interconnected suspension, related to the number of axle suspensions of the vehicle:

$$F_\ell' = N_u f_\ell'$$

$$F_r' = N_u f_r'$$

The generalized suspension forces can be expressed as combinations of damping ($F_{\ell c}'$ and F_{rc}') and restoring ($F_{\ell s}'$ and F_{rs}') forces:

$$F_\ell' = F_{\ell c}' + F_{\ell s}'; \text{ and } \quad F_r' = F_{rc}' + F_{rs}' \tag{2.53}$$

For equal static load distributions ($w_\ell = w_r$), identical charge pressures ($p_{\ell c} = p_{rc}$), and identical geometry of the left and right struts ($p_{1\ell 0} = p_{2\ell 0} = p_{1r0} = p_{2r0} = p_0$, $v_{3\ell 0} = v_{3r0} = v_0$, $A_{2\ell} = A_{2r} = A_2$, $A_{1\ell} = A_{1r} = A_1$ and $a_\ell = a_r = a$), the damping and restoring forces of the left and right suspensions can be expressed as follows:

<u>Damping Forces</u>

$$F_{c\ell}' = \frac{\rho A_1^3 N_u}{2C_d^{\,2}a^2}[\beta(\dot{z}_r - \beta\dot{z}_\ell)^2 sgn(\dot{z}_r - \beta\dot{z}_\ell) - (\dot{z}_\ell - \beta\dot{z}_r)^2 sgn(\dot{z}_\ell - \beta\dot{z}_r)] - \frac{128\mu L A_1^2 N_u}{\pi D^4}\dot{z}_\ell$$

$$F_{cr}' = \frac{\rho A_1^3 N_u}{2C_d^{\,2}a^2}[\beta(\dot{z}_\ell - \beta\dot{z}_r)^2 sgn(\dot{z}_\ell - \beta\dot{z}_r) - (\dot{z}_r - \beta\dot{z}_\ell)^2 sgn(\dot{z}_r - \beta\dot{z}_\ell)] - \frac{128\mu L A_1^2 N_u}{\pi D^4}\dot{z}_r \tag{2.54}$$

where $\beta = A_2/A_1$

<u>Restoring Forces</u>

$$F_{s\ell}' = p_0 A_2 N_u[(\frac{v_0}{v_0 - A_1 z_r + A_2 z_\ell})^n - 1] - p_0 A_1 N_u[(\frac{v_0}{v_0 - A_1 z_\ell + A_2 z_r})^n - 1]$$

$$F_{sr}' = p_0 A_2 N_u [(\frac{v_0}{v_0 - A_1 z_\ell + A_2 z_r})^n - 1] - p_0 A_1 N_u [(\frac{v_0}{v_0 - A_1 z_r + A_2 z_\ell})^n - 1] \qquad (2.55)$$

Equations (2.54) and (2.55) reveal that the generalized suspension forces of the interconnected system comprise nonlinear damping and elastic components. The damping and restoring forces are influenced not only by the relative velocity and displacement of the same side struts but also those of opposite side struts. Laminar fluid flows through the interconnected pipes introduce a linear damping component related to the relative velocity across the same side strut.

2.5 SUMMARY

Three hydro-pneumatic suspension systems, namely, unconnected, unconnected with anti-roll bar and interconnected suspensions, are mathematically modeled in the roll plane. The roll plane model of a road vehicle is characterized by four-DOF dynamical system. The analytical model is derived for excitations arising from road irregularities and a roll moment acting on the sprung mass. The generalized suspension forces are derived assuming incompressible fluid, turbulent flows through the orifice restrictions, polytropic process of the confined gas, and laminar flows through the interconnecting pipes. The generalized suspension forces comprise nonlinear damping and restoring forces. Although anti-roll bars have no effect on the generalized suspension forces, they enhance the roll stiffness of the suspension. Unlike the unconnected suspension system, the interconnected suspension system includes internal flows between the left and right struts, which yield feedback effects on the generalized suspension forces.

CHAPTER 3

PROPERTIES OF THE INTERCONNECTED SUSPENSION SYSTEM

3.1 INTRODUCTION

The ride quality, handling and directional control performance of a vehicle is strongly related to the static and dynamic properties of its suspension. Ride and roll dynamic performance of a vehicle in the roll plane is related to suspension properties, such as the load carrying capacity, suspension rate, roll stiffness, damping characteristics. Sharp and Hassan [2, 22] have stated that the performance characteristics of competitive suspensions should be compared on the basis of equal working space.

In this Chapter, properties of three kinds of hydro-pneumatic suspensions, that is, unconnected, unconnected with anti-roll bar and interconnected, are investigated and discussed in terms of their load-carrying capacities, suspension rates, roll stiffness and damping characteristics. Analytical expressions are derived to describe the static and dynamic properties of these suspension systems. The parameters of various suspension systems are selected to achieve comparable static and dynamic properties such that a relative analysis may be carried out to investigate the relative performance characteristics of the interconnected suspension.

3.2 LOAD CARRYING CAPACITY OF HYDRO-PNEUMATIC SUSPENSIONS

The analytical models presented in Chapter 2 demonstrated that a hydro-pneumatic suspension provides restoring characteristics due to the confined gas, and damping forces by forcing the fluid through the restrictions and the interconnecting pipes. The load-carrying capacity of a suspension, defined as

the load supported at the design ride height, is related to its spring characteristics.

3.2.1 Load-Carrying Capacity of Unconnected Suspensions

For symmetric load distribution in the roll plane, anti-roll bars have no effect on the suspension rate. The load-carrying capacity of unconnected suspension with anti-roll bar is thus the same as that of unconnected without anti-roll bar. The load-carrying capacity of the unconnected suspensions can be obtained from Equation (2.5) as:

$$W_u = 2N_u(p_0 - p_a)A_2 \tag{3.1}$$

where N_u is the number of suspension struts used on each side of the vehicle; A_2 is the piston head area; W_u is the load carrying capacity, and p_0 is the nominal gas pressure corresponding to the static equilibrium.

Equation (3.1) reveals that the load-carrying capacity of an unconnected hydro-pneumatic suspension is proportional to the nominal gauge pressure and piston head area. The nominal gas pressure, however, is related to the static deflection of the suspension, which directly influences the working space of the suspension. For a specified static defection, x_0, the normal gas pressure is derived as:

$$p_0 = p_c\left(\frac{v_c}{v_c - A_2 x_0}\right)^n$$

where p_c and v_c are the initial charge pressure and volume of the gas. A high nominal pressure corresponding to the design static deflection implies that smaller hydraulic struts can be adopted. The higher gas pressure, however, poses difficulties associated with the design of seals.

3.2.2 Load-Carrying Capacity of the Interconnected Suspension

Assuming symmetric suspension, the loading capacity can be derived from Equation (2.34) as:

$$W_i = 2N_u(p_0 - p_a)A_r \tag{3.2}$$

where $A_r = A_2 - A_1$ is the piston rod area, which is considerably smaller than the piston head area, A_2. A comparison of Equations (3.1) and (3.2) reveals that the load-carrying capacity of an interconnected suspension is considerably smaller than that of an unconnected suspension, when identical struts and nominal pressures are selected. It is therefore necessary to adjust the nominal pressure or strut configuration of the interconnected suspension in order to achieve the same load-carrying capacity. The nominal pressure of the struts is related to the suspension static deflection in the following manner:

$$p_0 = p_c\left(\frac{v_c}{v_c - A_r x_0}\right)^n \tag{3.3}$$

where x_0 is the static deflection of right and left struts, when identical struts and equal load distribution are considered.

3.3 SUSPENSION RATE

By referring the definition in [72], the suspension rate of a vehicle is considered as the resultant spring rate of all the hydro-pneumatic strut units used in the roll plane model. The characteristic of suspension rate is thus related to the stiffness property of the struts.

3.3.1 Stiffness Characteristics of an Unconnected Hydro-Pneumatic Strut

Figure 3.1 illustrates the schematic of an unconnected hydro-pneumatic strut. The stiffness characteristics of the suspension strut are related to the fluid

pressure corresponding to static equilibrium and strut geometry. Under static equilibrium, the fluid pressures in chambers *II* and *III* are identical. Assuming polytropic process, the gas pressure (p) in chamber *III* can be related to the relative displacement (z) across the strut:

$$p = p_0 v_0^n \frac{1}{(v_0 + A_2 z)^n} \tag{3.4}$$

where v_0 is the volume of the confined gas corresponding to the nominal pressure p_0. The static force G_s developed by the strut can be derived as:

$$G_s = (p - p_a) A_2 = \left[p_0 v_0^n \frac{1}{(v_0 + A_2 z)^n} - p_a \right] A_2 \tag{3.5}$$

The nonlinear stiffness k_{vu} of the suspension strut is thus derived as:

$$k_{vu} = -\frac{dG_s}{dz} = n p_0 v_0^n A_2^2 \frac{1}{(v_0 + A_2 z)^{n+1}} \tag{3.6}$$

Equation (3.6) reveals that the stiffness of the suspension strut increases linearly as a function of the absolute design pressure, and is a nonlinear function of the relative displacement across the strut. The static stiffness corresponding to the static design position ($z = 0$) is obtained as a proportional function of the absolute design pressure, and inversely proportional to the design gas volume v_0:

$$k_{vu}^0 = n A_2^2 \frac{p_0}{v_0} \tag{3.7}$$

The effective static deflection of the strut, x_0^*, can be computed from the static stiffness:

$$x_0^* = \frac{w}{k_{vu}^0} = \frac{w v_0}{n A_2^2 p_0} \tag{3.8}$$

where w is the load supported by one strut at design ride position. Equation (3.8) indicates that the effective static deflection of the suspension strut is

directly proportional to the gas volume v_0 and inversely proportional to the pressure p_0.

3.3.2 Stiffness Characteristics of a Pair of Interconnected Hydro-Pneumatic Struts

A schematic of a pair of hydro-pneumatic struts interconnected in the roll plane is shown in Figure 3.2. Assuming identical geometry of the struts, the gas volume in each strut is related to the relative displacements of struts on both sides in the following manner:

$$\begin{aligned} v_\ell &= v_0 + A_2 z_\ell - A_1 z_r \\ v_r &= v_0 + A_2 z_r - A_1 z_\ell \end{aligned} \tag{3.9}$$

where v_ℓ and v_r are the gas volume in the left and right struts, and v_0 is the gas volume corresponding to the design height. $z_\ell = x_{s\ell} - x_{u\ell}$ and $z_r = x_{sr} - x_{ur}$ are the relative deflections across the left and right struts, respectively. The corresponding gas pressures in the left ($p_{3\ell}$) and right (p_{3r}) struts are computed from the pressure-volume relationship for the polytropic process:

$$p_{3\ell} = p_0 v_0^n \frac{1}{(v_0 + A_2 z_\ell - A_1 z_r)^n}; \text{ and } \quad p_{3r} = p_0 v_0^n \frac{1}{(v_0 + A_2 z_r - A_1 z_\ell)^n} \tag{3.10}$$

Under static equilibrium, the pressures of fluid in the interconnected chambers approach an identical value, such that, $p_{3\ell} = p_{2\ell} = p_{1r}$ and $p_{3r} = p_{2r} = p_{1\ell}$. Therefore, the static forces, G_ℓ and G_r, developed by the left and right struts respectively, can be expressed as:

$$\begin{aligned} G_\ell &= p_{3\ell} A_2 - p_{3r} A_1 - p_a (A_2 - A_1) \\ G_r &= p_{3r} A_2 - p_{3\ell} A_1 - p_a (A_2 - A_1) \end{aligned} \tag{3.11}$$

Upon substituting for absolute pressure, $p_{3\ell}$ and $p_{3\ell}$, from Equation (3.10), Equation (3.11) yields:

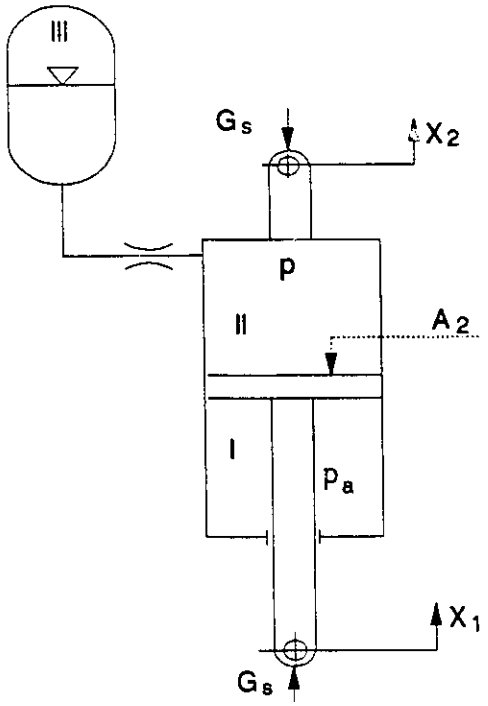

Figure 3.1 Unconnected hydro-pneumatic suspension strut

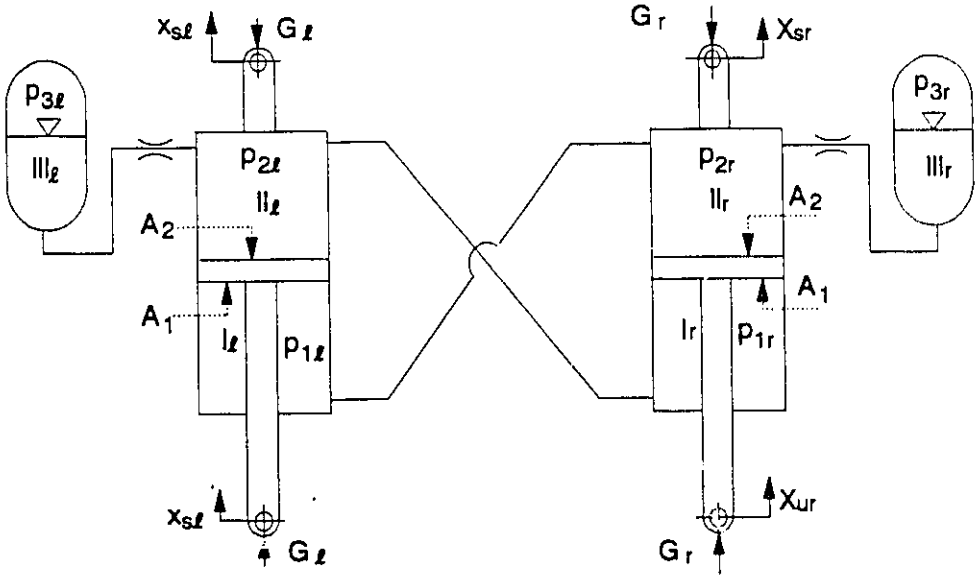

Figure 3.2 Interconnected hydro-pneumatic struts

$$G_\ell = p_0 v_0^n \left[\frac{A_2}{(v_0 + A_2 z_\ell - A_1 z_r)^n} - \frac{A_1}{(v_0 + A_2 z_r - A_1 z_\ell)^n} \right] - p_a (A_2 - A_1)$$

$$G_r = p_0 v_0^n \left[\frac{A_2}{(v_0 + A_2 z_r - A_1 z_\ell)^n} - \frac{A_1}{(v_0 + A_2 z_\ell - A_1 z_r)^n} \right] - p_a (A_2 - A_1) \qquad (3.12)$$

The static stiffness of each hydro-pneumatic strut can then be obtained by taking the first derivative of the static force with respect to the respective relative displacement as:

$$k_{v\ell} = -\frac{dG_\ell}{dz_\ell}; \quad \text{and} \quad k_{vr} = -\frac{dG_r}{dz_r} \qquad (3.13)$$

where $k_{v\ell}, k_{vr}$ are the static stiffness of left and right struts, respectively. The solution of Equation (3.13) yields the static stiffness in the following manner:

$$k_{v\ell} = n p_0 v_0^n \left[\frac{A_2^2 - A_1 A_2 \dfrac{dz_r}{dz_\ell}}{(v_0 + A_2 z_\ell - A_1 z_r)^{n+1}} + \frac{A_1^2 - A_1 A_2 \dfrac{dz_r}{dz_\ell}}{(v_0 + A_2 z_r - A_1 z_\ell)^{n+1}} \right] \qquad (3.14)$$

$$k_{vr} = n p_0 v_0^n \left[\frac{A_2^2 - A_1 A_2 \dfrac{dz_\ell}{dz_r}}{(v_0 + A_2 z_r - A_1 z_\ell)^{n+1}} + \frac{A_1^2 - A_1 A_2 \dfrac{dz_\ell}{dz_r}}{(v_0 + A_2 z_\ell - A_1 z_r)^{n+1}} \right] \qquad (3.15)$$

In pure bounce mode, the relative displacements across the left and right struts are identical, such that $z_\ell = z_r = z$, and $dz_\ell / dz_r = dz_r / dz_\ell = 1$. By letting $k_{v\ell} = k_{vr} = k_{vi}$, and $A_r = A_2 - A_1$, Equations (3.14) and (3.15) are simplified to yield the bounce stiffness of each strut in the interconnected suspension:

$$k_{vi} = n p_0 v_0^n A_r^2 \frac{1}{(v_0 + A_r z)^{n+1}} \qquad (3.16)$$

A comparison of Equation (3.6) with (3.16) reveals that the stiffness of an interconnected strut in the bounce mode has the same form as that of an

unconnected strut. The effective area of an interconnected strut is the piston rod area, while that of an unconnected strut is the piston head area.

The static stiffness of the interconnected suspension corresponding to the design ride height can be obtained by letting $z = 0$:

$$k_{vi}^{0} = nA_r^2 \frac{p_0}{v_0} \tag{3.17}$$

The effective static deflection of an interconnected strut under symmetrical loading is then obtained as:

$$x_0^* = \frac{w}{k_{vi}^{0}} = \frac{wv_0}{nA_r^2 p_0} \tag{3.18}$$

where $w = w_l = w_r$ is the static load carried by each strut corresponding to the design position.

Assuming identical struts on each axle, the bounce mode suspension rates of the unconnected and interconnected suspensions in the roll plane is derived from Equations (3.6) and (3.16):

$$K_{vu} = 2N_u k_{vu} = 2N_u n p_0 v_0^n A_2^2 \frac{1}{(v_0 + A_2 z)^{n+1}} \tag{3.19}$$

$$K_{vi} = 2N_u k_{vi} = 2N_u n p_0 v_0^n A_r^2 \frac{1}{(v_0 + A_r z)^{n+1}} \tag{3.20}$$

where K_{vu} is the suspension rate of the unconnected suspension, and K_{vi} is the suspension rate of the interconnected suspension. The suspension rates corresponding to the static ride height of the vehicle can be derived by letting $z = 0$ in Equations (3.19) and (3.20):

$$K_{vu}^{0} = 2N_u n \frac{p_0}{v_0} A_2^2 \tag{3.21}$$

$$K_{vi}^{0} = 2N_u n \frac{p_0}{v_0} A_r^2 \tag{3.22}$$

Equations (3.21) and (3.22) further reveal that the suspension rates of unconnected and interconnected suspensions differ by their respective effective working areas, A_2 and A_r.

3.4 SUSPENSION ROLL STIFFNESS

Suspension roll is defined as the rotation of vehicle sprung mass about a fore-aft axis with respect to a transverse line joining a pair of wheel centers [72]. In the roll plane, it is the roll motion of sprung mass about the suspension roll center. Suspension roll stiffness can be derived from the restoring moment developed by the suspension subject to a static roll angle. During roll motions, the left and right struts develop unequal forces leading to certain heave motion of the sprung mass.

3.4.1 Roll Stiffness of the Unconnected Suspension

The vehicle sprung mass will experience a roll angle φ and a displacement x with respect to the unsprung mass, when subjected to a roll moment, as shown in Figure 3.3. The static roll deflections of the sprung mass cause unequal gas pressures in the left and right struts, which may be derived from Equation (3.4):

$$p_\ell = p_0 v_0^n \frac{1}{(v_0 + A_2 z_\ell)^n}; \qquad \text{and} \qquad p_r = p_0 v_0^n \frac{1}{(v_0 + A_2 z_r)^n} \tag{3.23}$$

where p_ℓ and p_r are the pressures of the gas in left and right struts, respectively; z_ℓ and z_r are the relative vertical motions across the left and right struts. Assuming small roll motion, the relative displacements can be expressed as:

$$z_\ell = x - \ell\varphi; \quad \text{and} \quad z_r = x + \ell\varphi \tag{3.24}$$

where ℓ is half the suspension strut track. The restore moment developed due to suspension forces can then be expressed as:

$$M = (p_\ell - p_r)A_2 \ell N_u = p_0 v_0^n A_2 \ell N_u \left\{ \frac{1}{[v_0 + (x - \ell\varphi)A_2]^n} - \frac{1}{[v_0 + (x + \ell\varphi)A_2]^n} \right\} \qquad (3.25)$$

The suspension roll stiffness is the rate of change of the roll moment M with respect to the relative roll angle φ, and reflects the resistance of the vehicle body to roll about its roll center. The roll stiffness of an unconnected suspension $K_{\varphi u}$ is thus derived as:

$$K_{\varphi u} = \frac{dM}{d\varphi} = np_0 v_0^n A_2^2 \ell^2 N_u \left\{ \frac{1 - \frac{dx}{d\varphi}/\ell}{[v_0 + (x - \ell\varphi)A_2]^{n+1}} + \frac{1 + \frac{dx}{d\varphi}/\ell}{[v_0 + (x + \ell\varphi)A_2]^{n+1}} \right\} \qquad (3.26)$$

where $dx/d\varphi$ is due to the non-linear property of gas springs. $dx/d\varphi$ can be computed from the static equilibrium equation:

$$(p_\ell - p_0)A_2 + (p_r - p_0)A_2 = 0 \qquad (3.27)$$

Upon substituting for p_ℓ and p_r from Equation (3.23), the equation of static equilibrium can be expressed as:

$$g(x, \varphi) = \frac{1}{[v_0 + (x - \ell\varphi)A_2]^n} + \frac{1}{[v_0 + (x + \ell\varphi)A_2]^n} - \frac{2}{v_0^n} = 0 \qquad (3.28)$$

and

$$\frac{dx}{d\varphi} = -\frac{\partial g / \partial \varphi}{\partial g / \partial x} = \ell \left\{ \frac{[v_0 + A_2(x + \ell\varphi)]^{n+1} - [v_0 + A_2(x - \ell\varphi)]^{n+1}}{[v_0 + A_2(x + \ell\varphi)]^{n+1} + [v_0 + A_2(x - \ell\varphi)]^{n+1}} \right\} \qquad (3.29)$$

For a given roll angle φ, Equation (3.28) is solved to yield x. Equation (3.29) is then solved for $dx/d\varphi$ to determine the roll stiffness of the unconnected suspension from Equation (3.26). In the absence of roll motion ($\varphi = 0$), the solution of Equations (3.28) and (3.29) yields $x = 0$ and $dx/d\varphi = 0$. The static roll stiffness corresponding to the static ride position is thus computed as:

$$K_{\varphi u}^0 = K_{vu}^0 \ell^2 \qquad (3.30)$$

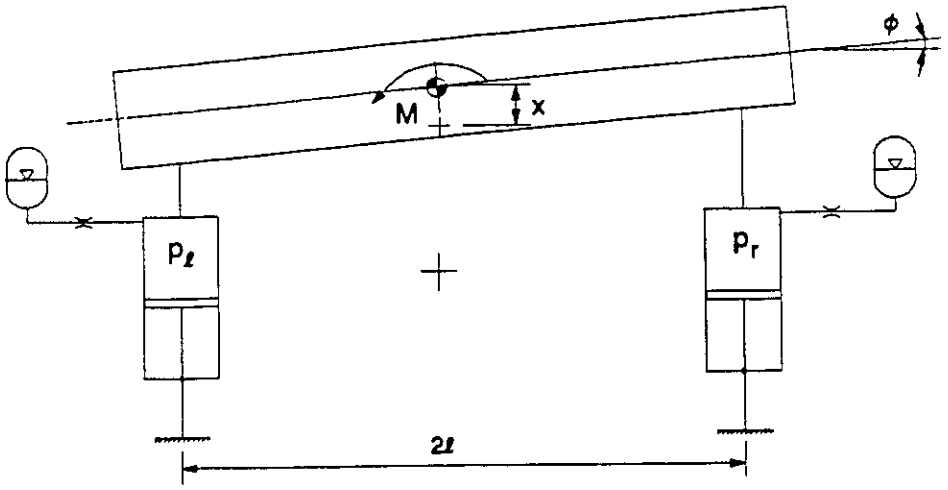

Figure 3.3 Unconnected hydro-pneumatic suspension in a rolled position

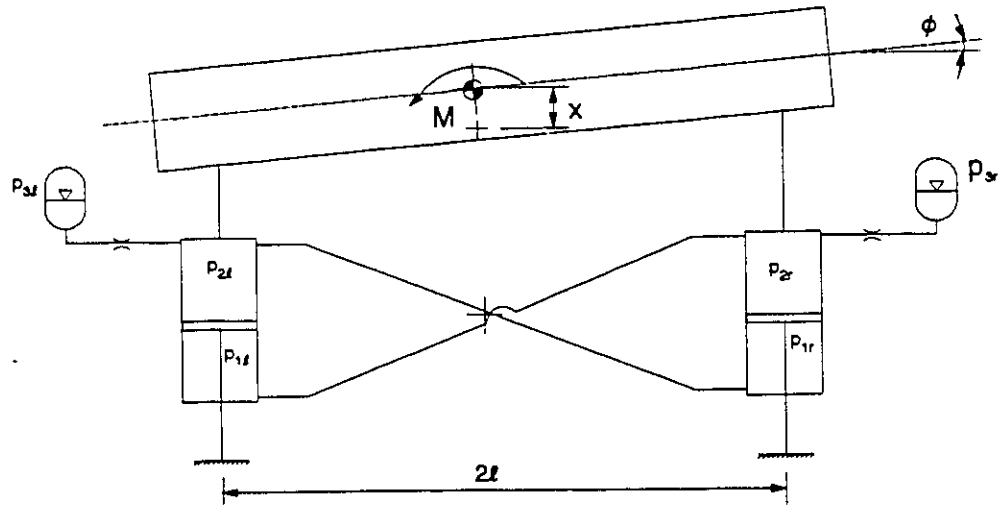

Figure 3.4 Interconnected hydro-pneumatic suspension in a rolled position

where K_{vu}^{0} is the suspension rate of the unconnected suspension at design ride position as derived in Equation (3.21).

3.4.2 Roll Stiffness of the Unconnected Suspension with Anti-Roll Bar

As discussed earlier in Chapter 2, the anti-roll bar adds auxiliary roll stiffness to the vehicle suspension. The total roll stiffness is the sum of the auxiliary roll stiffness and the roll stiffness arising from the hydro-pneumatic struts, as described by Equation (3.26). The total roll stiffness of the unconnected suspension with anti-roll bar can be expressed as:

$$K_{\varphi b} = K_{\varphi u} + k_{\vartheta} \tag{3.31}$$

where $K_{\varphi b}$ is the total roll stiffness of the unconnected with anti-roll bar; k_{ϑ} is the auxiliary roll stiffness due to anti-roll bar. At static ride height, the roll stiffness of the suspension with anti-roll bar can be related to the vertical suspension rate in the following manner:

$$K_{\varphi b}^{0} = K_{vu}^{0} \ell^{2} A_{n} \tag{3.32}$$

where $A_{n} = 1 + k_{\vartheta} / K_{vu}^{0} \ell^{2}$ is termed as the roll stiffness amplification factor of the anti-roll bar.

3.4.3 Roll Stiffness of the Interconnected Suspension

The sprung mass of a vehicle equipped with an interconnected suspension experiences a roll motion about its roll center when subjected to a roll moment. The roll motion is also accompanied by corresponding vertical displacement due to the nonlinear property of the gas springs, as shown in Figure 3.4. When the sprung mass is subjected to roll rotation, the corresponding pressures in the left and right struts ($p_{3\ell}$ and p_{3r}) are related to the relative vertical displacements across the struts, as described earlier in Equation (3.10):

$$p_{3\ell} = p_0 v_0^n \frac{1}{(v_0 + A_2 z_\ell - A_1 z_r)^n}; \text{ and } \quad p_{3r} = p_0 v_0^n \frac{1}{(v_0 + A_2 z_r - A_1 z_\ell)^n} \tag{3.33}$$

where $z_\ell = x - \ell\varphi$ and $z_r = x + \ell\varphi$. x is the vertical displacement of the sprung mass with respect to the unsprung mass, and φ is the roll angle of the sprung mass around its roll center. Under static conditions, the pressures of fluid in interconnected chambers approach the same values ($p_{3\ell} = p_{2\ell} = p_{1r}$ and $p_{3r} = p_{2r} = p_{1\ell}$). The restore roll moment is thus derived as:

$$M = \ell(A_1 + A_2)(p_{3\ell} - p_{3r}) \tag{3.34}$$

Substituting for $p_{3\ell}$ and p_{3r} from Equation (3.33) yields:

$$M = p_0 v_0^n (A_1 + A_2)\ell N_u \left\{ \frac{1}{[v_0 + A_2(x - \ell\varphi) - A_1(x + \ell\varphi)]^n} - \frac{1}{[v_0 + A_2(x + \ell\varphi) - A_1(x - \ell\varphi)]^n} \right\} \tag{3.35}$$

Roll stiffness, which is defined as the rate of change of roll moment with respect to roll angle, is derived as:

$$K_\varphi = n p_0 v_0^n (A_1 + A_2)\ell N_u \left\{ \frac{(A_2 + A_1)\ell - (A_2 - A_1)\frac{dx}{d\varphi}}{[v_0 + A_2(x - \ell\varphi) - A_1(x + \ell\varphi)]^{n+1}} + \frac{(A_2 + A_1)\ell + (A_2 - A_1)\frac{dx}{d\varphi}}{[v_0 + A_2(x + \ell\varphi) - A_1(x - \ell\varphi)]^{n+1}} \right\} \tag{3.36}$$

$dx/d\varphi$ is again computed from the corresponding static equilibrium equation:

$$(p_{3\ell} + p_{3r} - 2p_0)(A_2 - A_1) = 0 \tag{3.37}$$

Substituting for $p_{3\ell}$ and p_{3r} from (3.33) into above equation results in:

$$f(x, \varphi) = \frac{1}{[v_0 + A_2(x - \ell\varphi) - A_1(x + \ell\varphi)]^n} + \frac{1}{[v_0 + A_2(x + \ell\varphi) - A_1(x - \ell\varphi)]^n} - \frac{2}{v_0^n} = 0 \tag{3.38}$$

$dx/d\varphi$ is thus derived from Equation (3.38) as:

$$\frac{dx}{d\varphi} = \frac{(A_2 + A_1)\ell}{A_2 - A_1} \left\{ \frac{[v_0 + A_2(x + \ell\varphi) - A_1(x - \ell\varphi)]^{n+1} - [v_0 + A_2(x - \ell\varphi) - A_1(x + \ell\varphi)]^{n+1}}{[v_0 + A_2(x + \ell\varphi) - A_1(x - \ell\varphi)]^{n+1} + [v_0 + A_2(x - \ell\varphi) - A_1(x + \ell\varphi)]^{n+1}} \right\}$$

(3.39)

For a given sprung mass roll angel φ, Equations (3.38) and (3.39) are solved to determine x and $dx/d\varphi$, respectively. Equation (3.36) is thus solved to yield the roll stiffness characteristic of the interconnected suspension. In the absence of sprung mass roll ($\varphi = 0$), Equations (3.38) and (3.39) yield: $x = 0$, and $dx/d\varphi = 0$. The roll stiffness corresponding to the design ride height is then computed as:

$$K_{\varphi i}^{0} = 2N_u n \frac{p_0}{v_0}(A_2 + A_1)^2 \ell^2 \tag{3.40}$$

Using Equation (3.22) and noticing $A_r = A_2 - A_1$, the static roll stiffness can be expressed in terms of the suspension rate:

$$K_{\varphi i}^{0} = K_{vi}^{0} \ell^2 \left(\frac{\beta + 1}{\beta - 1}\right)^2 \tag{3.41}$$

where $\beta = A_2/A_1$ is the piston area ratio of the interconnected struts, which is always greater than one. Equation (3.41) reveals that the static roll stiffness of the interconnected suspension can be effectively enhanced by selecting smaller piston area ratios. A roll stiffness amplification factor A_m can thus be defined as:

$$A_m = \left(\frac{\beta + 1}{\beta - 1}\right)^2 \tag{3.42}$$

A comparison of Equations (3.30) and (3.41) clearly reveals that the roll stiffness of the interconnected suspension corresponding to the design ride height is larger than that of the unconnected suspension when both suspension struts are selected to yield identical suspension rates. The amplification factor A_m is determined by strut configuration. This inherent anti-roll property of an interconnected suspension offers considerable potentials to achieve a better compromise between the ride and handling qualities without the aid of anti-roll bars.

3.5 DAMPING PROPERTIES OF HYDRO-PNEUMATIC SUSPENSIONS

The vehicle ride and roll performance characteristics are related to the damping properties of its suspension. The hydro-pneumatic suspension interconnected in the roll plane yields additional damping due to fluid flow through the interconnecting pipes, and due to the coupling effects. Since anti-roll bars do not contribute to suspension damping, the damping properties of the unconnected suspension with anti-roll bar are thus identical to those of the suspension without anti-roll bar.

3.5.1 Damping Property of the Unconnected Suspension

Assuming turbulent flows through constant area orifices, the damping force developed by an unconnected hydro-pneumatic strut, derived in Chapter 2, is expressed as:

$$f_{ci} = \frac{\rho A_2^3}{2C_d a^2} \dot{z}_i^2 sgn(\dot{z}_i), \qquad (i = \ell, r) \tag{3.43}$$

In the bounce mode, since $\dot{z}_\ell = \dot{z}_r = \dot{z}$, the damping force developed by a single unconnected hydro-pneumatic strut can be expressed as:

$$f_c = \frac{\rho A_2^3}{2C_d a^2} \dot{z}^2 sgn(\dot{z}) \tag{3.44}$$

In roll mode, since $\dot{z}_\ell = -\dot{z}_r$, the damping forces developed by the left and right struts are equal in magnitudes but opposite in directions. Since there are no coupling effects between the left and right struts of the unconnected suspension, the damping force developed by a single strut in the roll mode possesses the same expression as that in the bounce mode.

3.5.2 Damping Property of the Interconnected Suspension

Damping forces developed by the left and right struts of an interconnected suspension have been derived in Chapter 2. The damping force due to left and right struts, as shown in Figure 3.2, is expressed as:

$$f_{cl}' = \frac{\rho A_1^3}{2C_d^2 a^2}[(\dot{z}_l - \beta\dot{z}_r)^2 sgn(\dot{z}_l - \beta\dot{z}_r) - \beta(\dot{z}_r - \beta\dot{z}_l)^2 sgn(\dot{z}_r - \beta\dot{z}_l)] + \frac{128\mu L A_1^2}{\pi D^4}\dot{z}_l$$

$$f_{cr}' = \frac{\rho A_1^3}{2C_d^2 a^2}[(\dot{z}_r - \beta\dot{z}_l)^2 sgn(\dot{z}_r - \beta\dot{z}_l) - \beta(\dot{z}_l - \beta\dot{z}_r)^2 sgn(\dot{z}_l - \beta\dot{z}_r)] + \frac{128\mu L A_1^2}{\pi D^4}\dot{z}_r \quad (3.45)$$

Equation (3.45) reveals that the damping force developed by one strut comprises a nonlinear component due to orifice flows and a linear component due to laminar flows through the pipes. Further the damping force developed by one strut is related to relative velocities across both struts. A dominant linear damping property can be thus achieved by selecting large orifice area a and small diameter interconnecting pipes. Alternatively, a dominant quadratic form of damping force may be obtained by using small orifice area and large interconnecting pipes. In the bounce mode, since $\dot{z}_l = \dot{z}_r = \dot{z}$ and $\beta = A_2/A_1 > 1$, the velocity squared terms in Equation (3.45) can be simplified as:

$$(\dot{z}_l - \beta\dot{z}_r)^2 = (\dot{z}_r - \beta\dot{z}_l)^2 = (1-\beta)^2\dot{z}^2; \text{ and}$$

$$sgn(\dot{z}_l - \beta\dot{z}_r) = sgn(\dot{z}_r - \beta\dot{z}_l) = -sgn(\dot{z}) \quad (3.46)$$

The damping force developed by each interconnected strut can thus be expressed as:

$$f_{cV}' = \frac{\rho A_1^3}{2C_d^2 a^2}(\beta-1)^3\dot{z}^2 sgn(\dot{z}) + \frac{128\mu L A_1^2}{\pi D^4}\dot{z} \quad (3.47)$$

In the roll mode, $\dot{z}_l$ and $\dot{z}_r$ are related to the roll velocity of the sprung mass with respect to the unsprung mass and possess opposite directions. The damping forces developed by the left and right struts, derived from Equation (3.45), are thus equal in magnitudes but opposite in directions. The damping force developed by one strut in the roll mode can be simplified as:

$$f'_{aR} = \frac{\rho A_1^3}{2C_d^2 a^2}(\beta+1)^3 \dot{z}^2 sgn(\dot{z}) + \frac{128\mu L A_1^2}{\pi D^4}\dot{z} \tag{3.48}$$

where $\dot{z}$ is the relative velocity across the strut. A comparison of Equation (3.47) and (3.48) reveals that the damping force developed by one strut in the roll mode is always larger than that in the bounce mode due to the coupling effects of the left and right struts of the interconnected suspension.

3.6 SIMULATION PARAMETERS

In order to investigate the stiffness and damping properties of an interconnected hydro-pneumatic suspension, five different configurations of vehicle suspensions are considered, which include: (i) unconnected without anti-roll bar; (ii) unconnected with anti-roll bar; (iii) interconnected *I* (IC-1); (iv) interconnected *II* (IC-2); and (v) interconnected *III* (IC-3). The parameters of different suspension are selected to achieve identical load-carrying capacities and static suspension rates at the design position (except interlinked IC-3, which is selected to realized lower suspension rate). The vehicle model parameters are selected for a modern high-decker highway bus [73], while the parameters of different suspension configurations are selected to realize their stiffness properties similar to those of the currently used suspension system. Table 3.1 lists the common simulation parameters for the five suspension configurations, while Table 3.2 illustrates the specific simulation parameters for different configurations.

TABLE 3.1

Simulation parameters of the vehicle model [73]

SYMBOLS	*DESCRIPTION*	*PARAMETER VALUES*
m_s	Sprung mass	14110 kg
m_u	Unsprung mass	3616 kg
I_s	Moment of inertia of sprung mass	19300 kgm^2
I_u	Moment of inertia of unsprung mass	3819.9 kgm^2
k_{tl}, k_{tr}	Stiffness coefficients of left and right tires	3574.8 kN/m
c_{tl}, c_{tr}	Damping coefficients of left and right tires	9500 Ns/m
ℓ_l, ℓ_r	Lateral distances from left and right struts to sprung mass c.g.	0.7 m
ℓ_{wl}, ℓ_{wr}	Lateral distances from left and right tires to unsprung mass c.g.	1.03 m
h_2	Vertical distance between sprung mass c.g. and its roll center	0.62 m
h_1	Vertical distance between unsprung mass c.g. and its roll center	0 m
μ	Dynamic viscosity of fluid	0.6 Ns/m^2
ρ	Mass density of fluid	797 kg/m^3
C_d	Discharge coefficient	0.7
n	Polytropic coefficient	1.38
N_u	Number of struts used on each side	4
p_a	Atmospheric pressure	101300 Pa

TABLE 3.2

Simulation parameters of different hydro-pneumatic suspensions

Parameters	*Unconnected without anti-roll bar*	*Unconnected with anti-roll bar*	*Interconnected IC-1*	*Interconnected IC-2*	*Interconnected IC-3*
Nominal gas volume v_0 (m^3)	*0.00672*	*0.00672*	*0.00672*	*0.00427*	*0.00672*
Nominal gas pressure p_0 (Pa)	7×10^5	7×10^5	7×10^5	10^6	10^6
Piston head area A_2 (m^2)	*0.0289*	*0.0289*	*0.03251*	*0.02166*	*0.02473*
Piston rod side area A_1 [or rod area A_r] (m^2)			*0.00361 [0.0289]*	*0.0024 [0.01926]*	*0.00547 [0.01926]*
Piston area ration β			*9*	*9*	*4.52*
Orifice area a (m^2)	3×10^{-4}	3×10^{-4}	3×10^{-4}	3×10^{-4}	3×10^{-4}
Length of connecting pipes L (m)	-	-	*1.5*	*1.5*	*1.5*
Diameter of connecting pipes D (m)	-	-	*0.03*	*0.03*	*0.03*
Roll stiffness of anti-roll bar (kNm/rad)	-	*264.6*	-	-	-

3.7 COMPARISON OF PROPERTIES OF DIFFERENT SUSPENSIONS

The static properties of different suspension configurations at design ride position are computed and compared, as shown in Table 3.3. The unconnected, unconnected with anti-roll bar, and interconnected suspensions are configured to achieve identical load carrying capacity, static deflection and vertical suspension rate. The parameters of the unconnected suspension with anti-roll bar and the interconnected suspension are selected to achieve identical roll stiffness of the two suspensions. The properties of three different interconnected suspension configurations, termed as IC-1, IC-2 and IC-3, are investigated and compared to those of the conventional suspensions. While the IC-1 and IC-2 are configured to yield static properties identical to those of the unconnected suspension with anti-roll bar, the IC-3 suspension with low bounce rate and high roll stiffness is configured to achieve improved ride and handling performance. The auxiliary roll stiffness of ant-roll bar is chosen such that the roll stiffness amplification factor of that kind of suspension is the same as that of the interconnected suspensions.

The static properties of the five suspension systems are further evaluated and compared as functions of the vertical and roll displacements of the sprung mass with respect to the unsprung mass. Figure 3.5 illustrates the vertical suspension rates of the five suspension configurations as a function of the relative displacement across the struts. As can be seen, all the suspensions exhibit progressively hardening properties due to the force-deflection characteristics of the gas springs. Unconnected, IC-1 and IC-2 suspensions yield almost identical vertical rates over the defection range of ± 0.03 m, whereas the IC-3 suspension yields lower vertical rate

TABLE 3.3

Comparison of static properties of hydro-pneumatic suspensions

Static properties at design position	*Unconnected without anti-roll bar*	*Unconnected with anti-roll bar*	*Interconnected IC-1*	*Interconnected IC-2*	*Interconnected IC-3*
Load-carrying capacity *(kg)*	*14110*	*14110*	*14110*	*14110*	*14110*
Suspension rate *(kN/m)*	*960*	*960*	*960*	*960*	*610*
Effective static deflection *(m)*	*0.144*	*0.144*	*0.144*	*0.144*	*0.227*
Roll stiffness *(kNm/rad)*	*470.4*	*735*	*735*	*735*	*735*
Roll stiffness amplification factor	*1*	*1.56*	*1.56*	*1.56*	*2.46*

Figure 3.6 presents a comparison of static roll stiffness of the five suspensions as a function of the sprung mass roll angle with respect to the unsprung mass. The roll stiffness rates of all the interconnected suspensions are considerably larger than that of the unconnected suspension, due to the coupling effects of the interconnected struts. The roll stiffness of unconnected suspension with anti-roll bar is considerably enhanced by the auxiliary roll stiffener. The roll stiffness of all the suspension configurations tends to decrease with an increase in the sprung mass roll angle, although the relative reductions in the roll stiffness differ for various configurations. The static roll stiffness of all the three interconnected suspensions, corresponding to zero degree relative roll

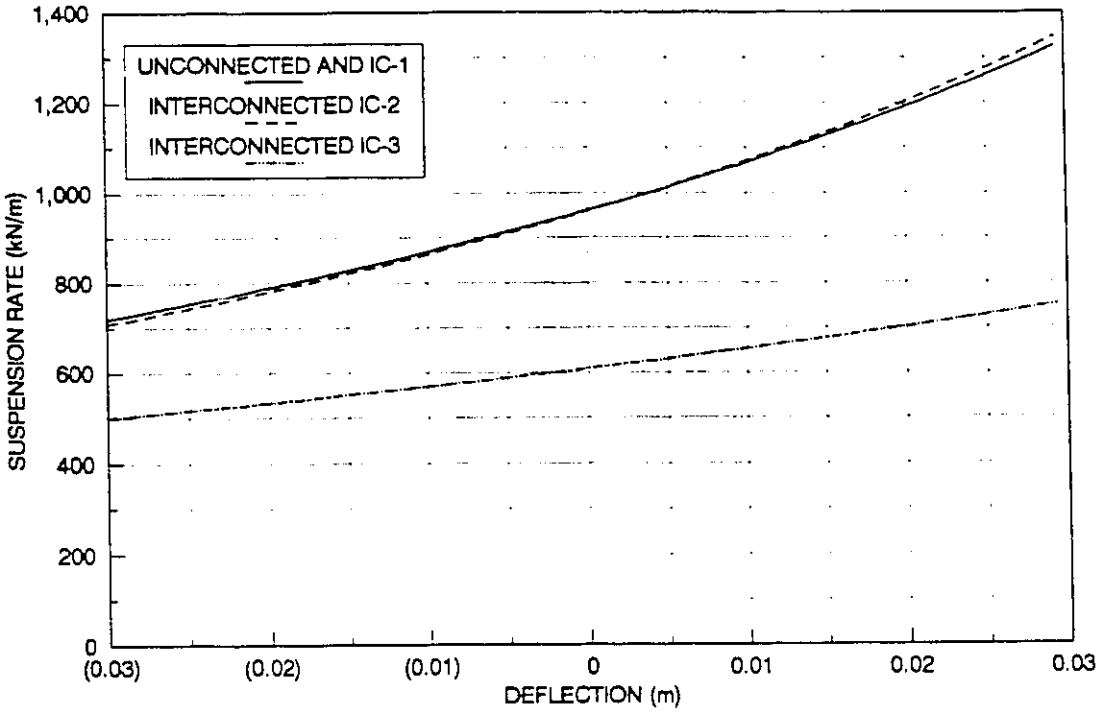

Figure 3.5 Suspension rate of different suspension systems

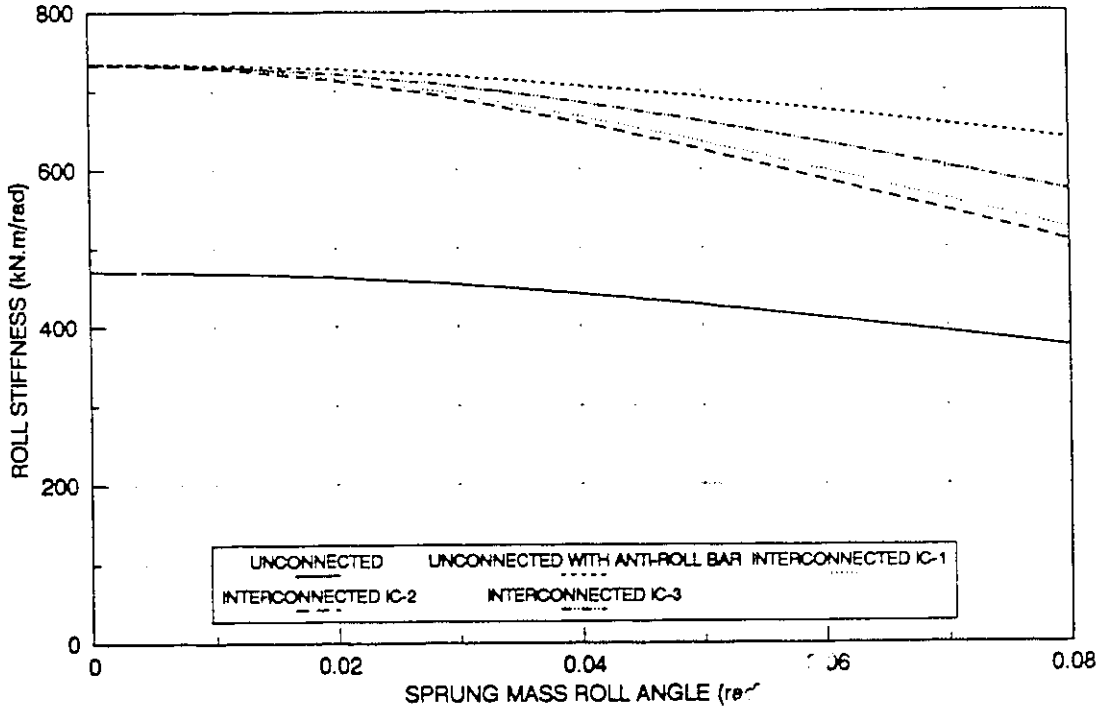

Figure 3.6 Roll stiffness of different suspension systems

displacement, is identical to that of the unconnected suspension with anti-roll bar. The static roll stiffness of the suspension employing unconnected struts, however, is 36% lower than those of the other configurations. While the anti-roll bar suspension exhibits the largest roll stiffness in the entire range of roll displacement considered, the roll stiffness of interconnected suspensions tends to decrease relatively rapidly with an increase in the roll angle. The IC-3 suspension, with lower bounce rate, yields larger roll stiffness than the IC-1 and IC-2 suspensions.

The ride and handling properties of a vehicle are strongly related to the damping properties of its suspension. The relative vertical and roll damping properties of the suspension configurations are thus evaluated assuming constant area damping orifices. The assumption of laminar flows within the interconnecting pipes is valid, since the maximum Reynolds number in the pipes is much smaller than the transition number (R_e=2200). Figure 3.7 and 3.8 illustrate the damping forces of a single strut under the bounce and roll modes of deflections, respectively. The damping force of a single strut in the bounce mode is computed under identical vertical deflections of the right and left wheels, while the damping force in the roll mode is computing by subjecting the right and left wheels to out-of-phase vertical deflections. Although the suspension systems are configured with identical orifice areas, the resulting damping properties of the various suspension systems are considerably different as illustrated in the Figures. Since anti-roll bars do not contribute to the damping properties of a suspension, the damping properties of the two unconnected suspensions are identical. Figure 3.7 demonstrates that the bounce mode damping force of an IC-1 suspension strut is similar to that of the unconnected suspension, while the damping forces of IC-2 and IC-3 struts are similar. These results are mainly due to the effective working area of the respective struts in the bounce mode. As

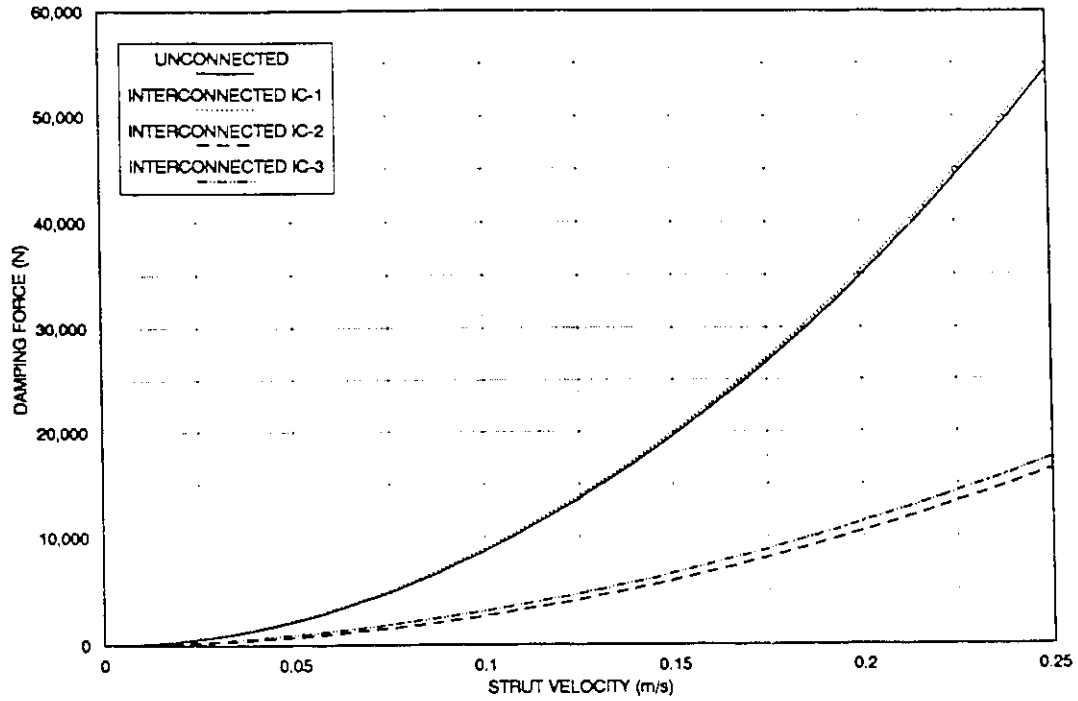

FIGURE 3.7 Damping force developed by a single strut in the bounce mode

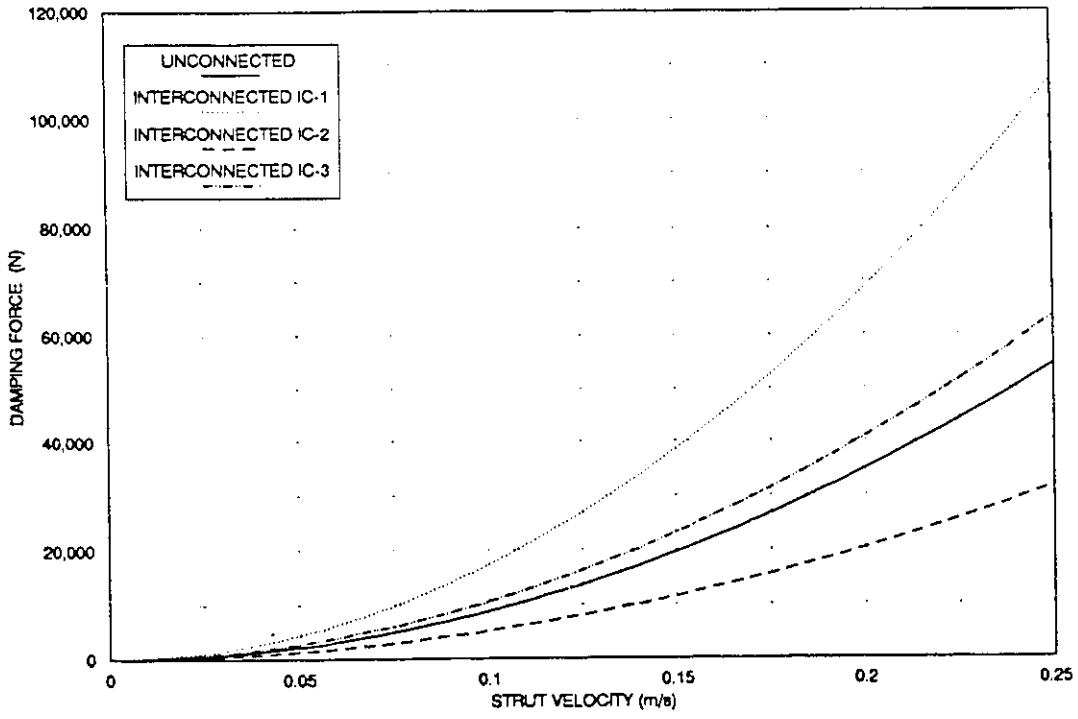

FIGURE 3.8 Damping force developed by a single strut in the roll mode

illustrated in Table 3.2, the piston rod area of IC-1 strut and the piston head area of the unconnected suspension are identical, while the piston rod area of IC-2 strut is the same as that of IC-3 strut.

The damping force of an unconnected suspension strut in the roll mode is identical to that in the bounce mode. The roll mode damping forces due to the interconnected struts in all the configurations, however, increase considerably due to feedback effects, as described in Equation (3.48). The roll mode damping forces of IC-1 and IC-2 struts approach values nearly twice as large as those in the bounce mode. The roll mode damping force of the IC-3 suspension strut, however, approaches a value that is more than three times the bounce mode damping. This relative high roll mode damping of the IC-3 suspension can be attributed to the smaller piston area ratio β.

3.8 SUMMARY

Stiffness and damping properties of different hydro-pneumatic suspensions are investigated and discussed in terms of load-carrying capacity, suspension rate, roll stiffness and damping characteristics. Five different suspension systems, including unconnected, unconnected with anti-roll bar, IC-1, IC-2, and IC-3 are configured such that their load carrying capacities and static deflections (except IC-3) are identical. The IC-3 suspension is configured to achieve low suspension rate but high roll stiffness. The unconnected suspension system provides considerably low roll stiffness, and identical damping properties in the roll and bounce modes. While anti-roll bars do not influence the suspension rate, they enhance the suspension roll stiffness considerably. The interconnected suspensions exhibit an inherent anti-roll property and thus yield high roll stiffness. All the suspension configurations exhibit progressively hardening suspension rates, while their roll stiffness rates

tend to decrease with an increase in the sprung mass roll angle. The interconnected suspensions with constant area damping orifices yield considerably large damping in the roll mode due to coupling effects.

CHAPTER 4

DYNAMIC RESPONSES OF THE INTERCONNECTED SUSPENSION WITH FIXED ORIFICE DAMPING

4.1 INTRODUCTION

The ride and handling characteristics of a vehicle are related to its tire and suspension characteristics etc. The ride quality of a vehicle may be assessed in terms of the acceleration perceived by the passenger/driver or the acceleration response of the sprung mass to road excitations. The handling response of the vehicle may be related to the roll and lateral response of the sprung and unsprung masses when the vehicle is subjected to a directional maneuver. In this section, the roll plane model of a highway bus equipped with different configurations of unconnected and interconnected suspension, are analyzed to determine the relative vertical and roll response of the vehicle subject to road irregularities and centrifugal forces arising from a directional maneuver. The natures of excitations arising from tire-terrain interactions and steering inputs are described. The roll performance characteristics of the suspension systems are evaluated in terms of the transient and steady state roll responses of sprung and unsprung masses during constant radius turning and lane changing maneuvers. The dynamic ride performances are established in terms of both heave and roll shock isolation characteristics of the suspensions subjected to road excitations. Vibration transmissibility characteristics of different suspensions are also investigated by using harmonic excitations arising from the tire-terrain interactions.

4.2 DESCRIPTION OF EXCITATIONS

The analysis of ride quality and handling performance characteristics of vehicle models requires input data. The input data should be representative of typical excitations arising from steering maneuvers and tire-terrain interfaces. The input data due to steering maneuvers can be expressed in terms of transient lateral acceleration experienced by sprung and unsprung masses. The excitations arising from tire-terrain interactions are characterized as half-sine displacement bumps and a rounded step displacement excitation.

4.2.1 Lateral Acceleration Excitations

The mobility of a vehicle is related to its ease of handling and directional response. Although vehicles spend around 80% of their travel time during straight driving, their anti-roll capabilities are very important for road safety during cornering and emergency highway maneuvers. The sprung and unsprung masses of a vehicle are subjected to centrifugal acceleration during a directional maneuver. The acceleration causes a roll moment, which results in roll motion of sprung and unsprung masses. The handling quality of a vehicle is primarily related to vehicle's ability to counteract the overturning moment caused by the centrifugal or lateral acceleration. Various studies have concluded that rollover threshold of heavy vehicles, which is the maximum value of lateral acceleration that a vehicle can withstand during a steady turn, lies in the range of 0.3 g - 0.5 g [75].

The lateral acceleration encountered during a steady turn maneuver is approximated as in Figure 4.1. The magnitude of lateral acceleration is considered to be 2.5 m/s^2, which is slightly lower than the rollover threshold of typical heavy vehicles.

The heavy vehicles experience large magnitude oscillatory lateral acceleration during high speed lane change maneuvers. Field tests performed

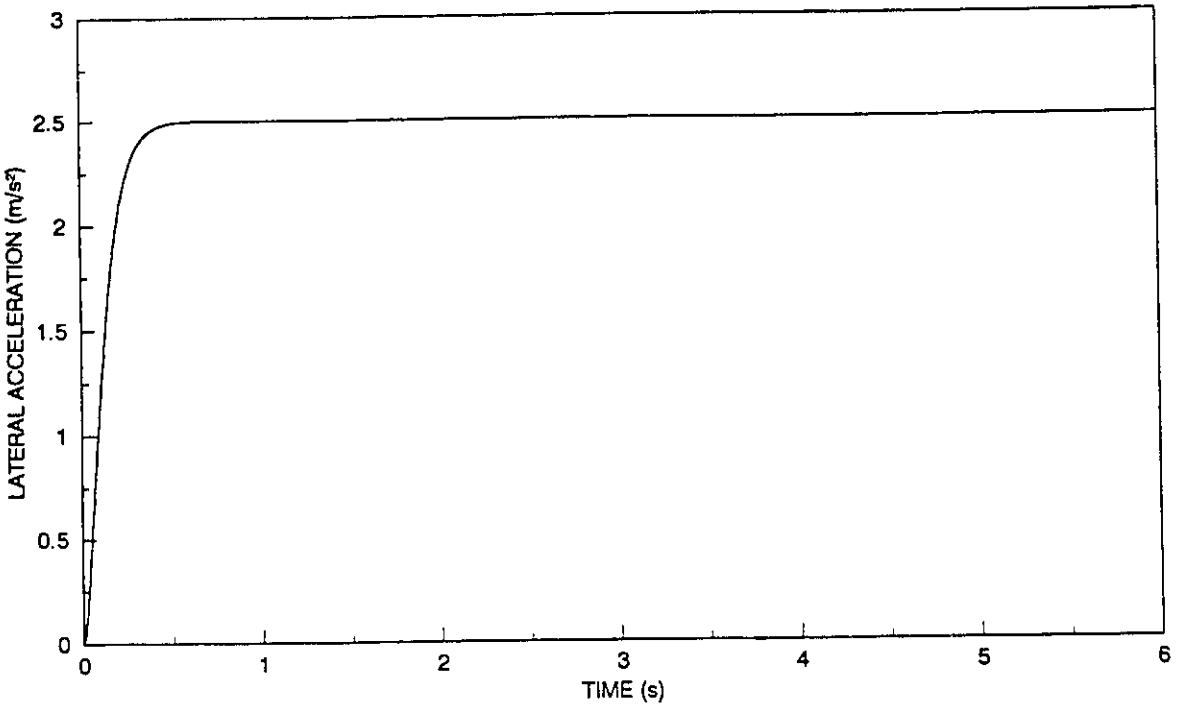

Figure 4.1 A rounded step lateral acceleration acting on vehicle during steady turning

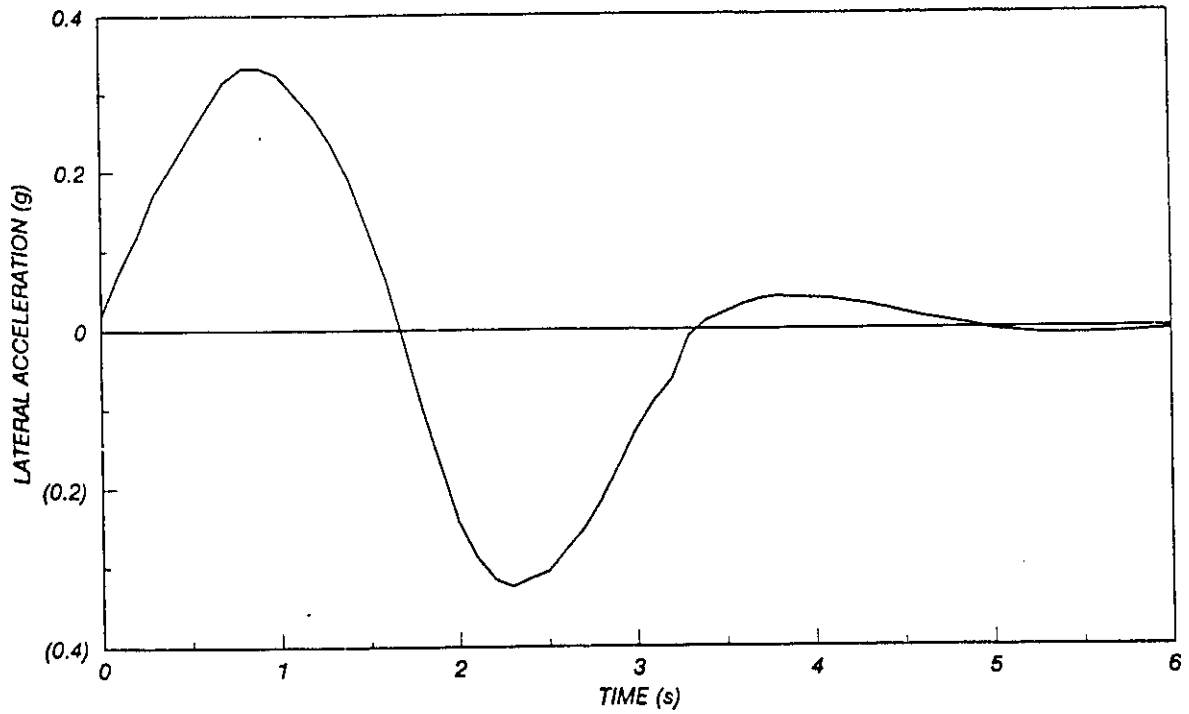

Figure 4.2 Transient lateral acceleration of an inter-city bus during a typical lane change maneuver

on a highway bus concluded that although a lateral acceleration as high as 0.5 *g* was measured on a skid-pad, the maximum level of lateral acceleration measured during a continuous lane change maneuver at maximum permissible speed is 0.3 *g* [73]. The oscillation frequency of such acceleration is of the order of 0.3 *Hz*. Figure 4.2 illustrates the transient lateral acceleration measured during a lane change maneuver at 110 *Km/h*. The magnitude of lateral acceleration excitation, however, decreases when the maneuvers are performed at reduced speeds. The lateral acceleration excitation, shown in Figure 4.2, may thus be considered to be realistic under severe maneuvers.

Since the lateral acceleration normally causes a roll motion of sprung mass around its roll center (it is assumed that roll center of unsprung mass and its c.g coincide), the overturning moment acting on a vehicle during steady steer or lane change maneuver can be expressed as

$$T_g(t) = T_g'(t) + T_g''(t) \tag{4.1}$$

where $T_g(t)$ is the total roll moment acting on the vehicle, as presented in equations (2.2), (2.27) and (2.31); T_g' is the primary overturning moment due to lateral acceleration and T_g'' is the roll moment due to the lateral displacement of the sprung mass as shown in Figure 4.3. Assuming small roll angles, roll moments caused by lateral acceleration and displacement of the sprung mass can be expressed as

$$T_g' = m_s a_y h_2 \tag{4.2}$$

$$T_g'' = m_s g \vartheta_s(t) h_2 \tag{4.3}$$

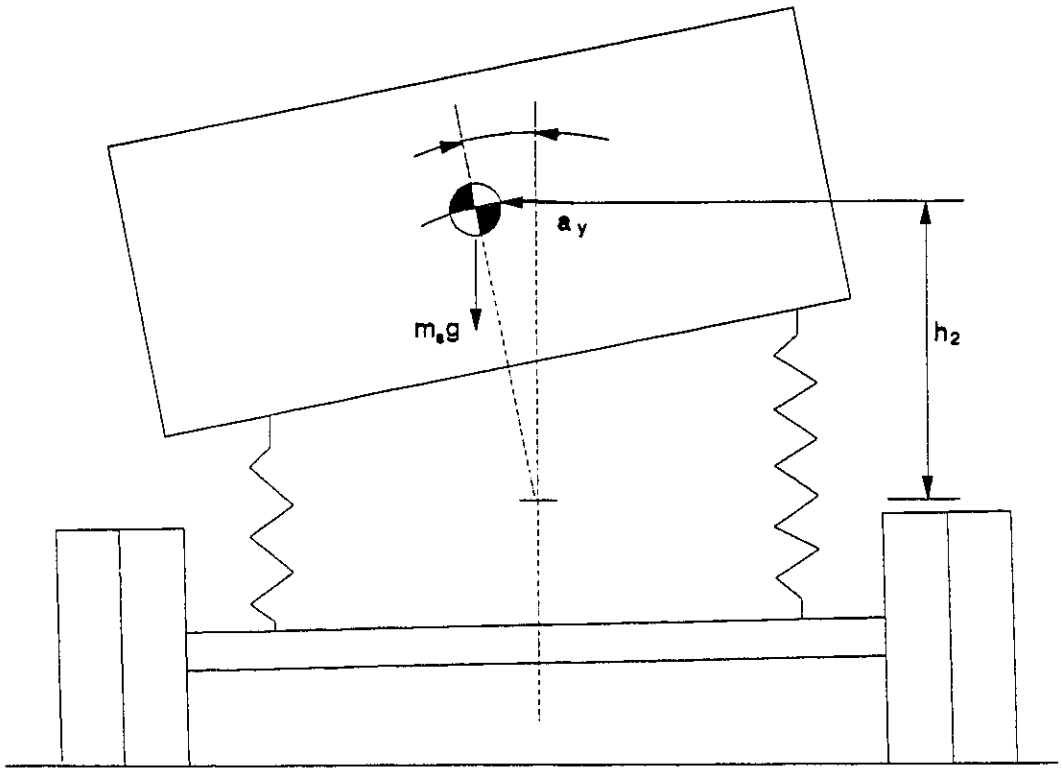

Figure 4.3 Lateral acceleration excitation of the roll plane model during steering maneuvers

where a_y is the lateral acceleration of the vehicle, encountered during steady steer or lane change maneuvers, and g is the acceleration due to gravity. Equation (4.1) reveals that a vehicle with smaller roll stiffness will experience a larger roll moment than that with larger roll stiffness, even though the magnitude of lateral acceleration and the roll center height are the same.

4.2.2 Excitations due to Tire-Terrain Interactions

Apart from on-board excitations, the main excitation source of road vehicles comes from tire-terrain interactions - the road roughness [76]. Road roughness is described by the elevation profile along the wheel tracks over which the vehicle passes. It has been reported that the amplitude of surface undulations on medium-quality roads is in the order of 0.013 m or less, while amplitudes of 0.005 m are characteristic of very good roads [74]. Road profiles fit the general category of "wide-band random signals" and, hence, can be described either by the profile or its statistical properties. One of the most useful presentations is the Power Spectral Density (PSD) function. The response characteristics of vehicles incorporating the interconnected suspension under stochastic inputs will be discussed in Chapter 5.

The relative ride performance of vehicle suspension, however, can be effectively evaluated using deterministic excitations representing the tire-terrain interactions [74]. Relative transient response characteristics of different suspension may be evaluated using a bump excitation characterized by a half-sine pulse displacement shown in Figure 4.4. Vertical shock attenuation performance characteristics can be evaluated using in-phase bump excitations at both wheels. Out-of-phase excitations at the two wheels can provide the coupled vertical and roll response characteristics. In this study half-sine pulse and rounded-step displacement (Figure 4.5) excitations are employed to

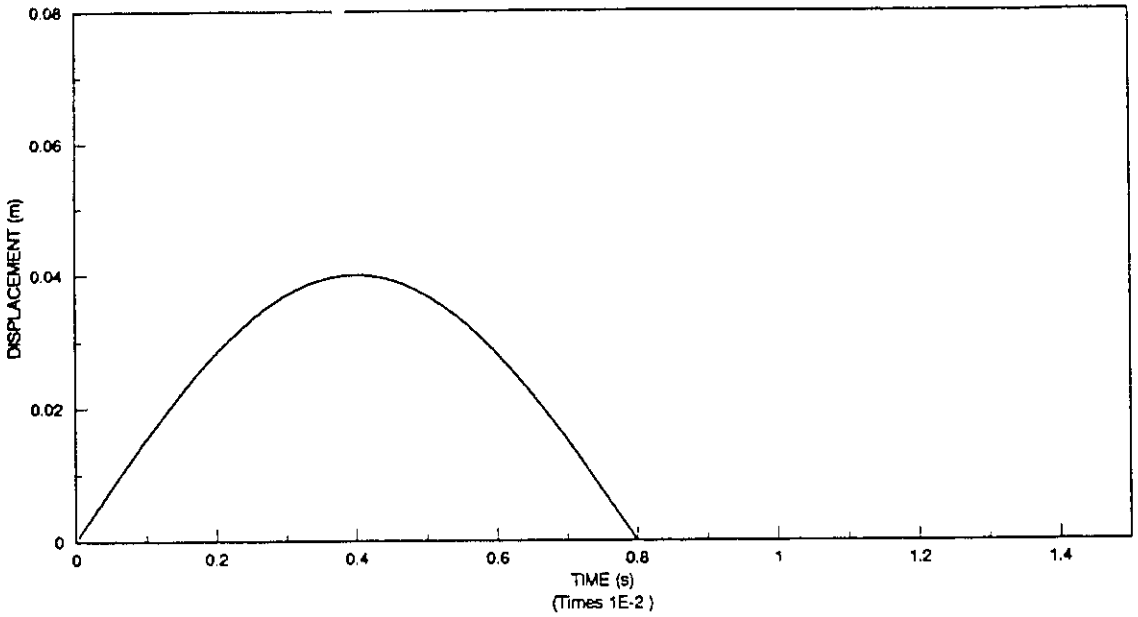

Figure 4.4 Half-sine displacement bump ocurring at tire-terrain interface

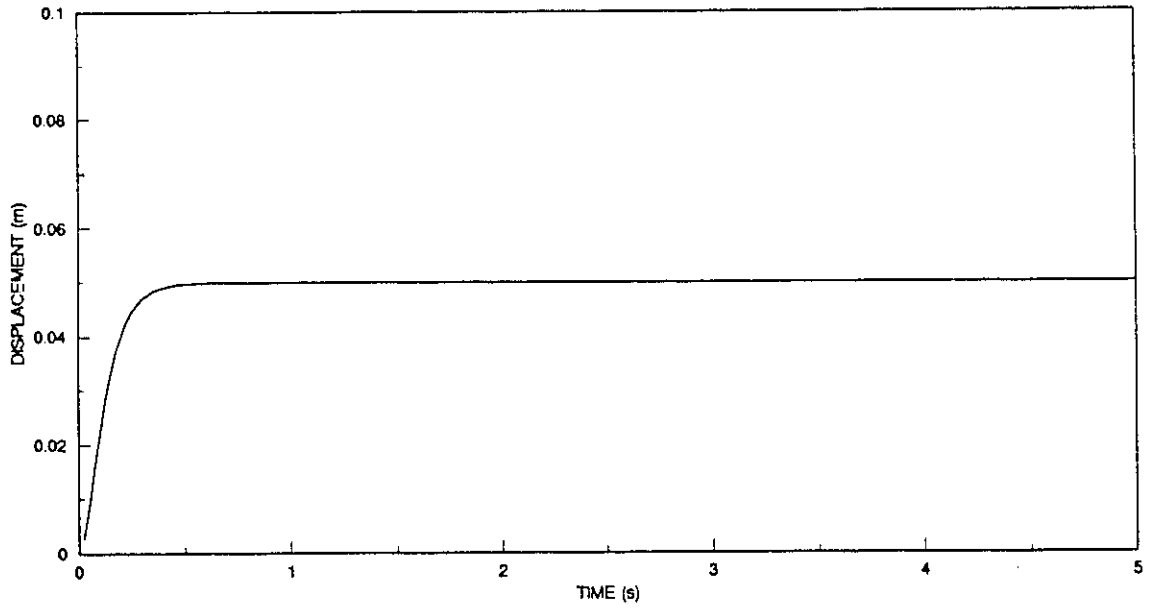

Figure 4.5 A rounded step displacement input occuring at tire-terrain interface

evaluate the relative shock attenuation performance characteristics of the suspension systems.

Two types of harmonic excitations are considered to evaluate relative vibration transmissibility characteristics of the suspension models: (i) in-phase harmonic excitation, right and left tires subjected to identical vertical sinusoidal excitations of 0.01 m amplitude; and (ii) out-of-phase excitation, right and left tires subjected to vertical sinusoidal excitations of identical amplitude but 180 degrees out-of-phase. The response to in-phase excitation will yield the vertical vibration transmission characteristics of the suspension systems, whereas the response to out-of-phase excitation will primarily provide roll vibration transmission characteristics of the suspension systems.

4.3 VEHICLE RESPONSE TO LATERAL ACCELERATION EXCITATIONS

The response characteristics of the vehicle with five different suspension configurations, described in Chapter 3, are evaluated for lateral acceleration excitations to assess the relative handling characteristics. The excitations considered here are the lateral accelerations encountered during steady turns and lane change maneuvers, as shown in Figures 4.1 and 4.2. The equations of motion for the vehicle models, derived in Chapter 2, are solved using numerical integration approach to determine roll response of the sprung and unsprung masses.

4.3.1 Response to a Rounded Step Lateral Acceleration

The roll angle response characteristics of the sprung mass of the vehicle employing different suspension systems, subjected to a rounded step lateral acceleration encountered during a steady turn, are shown in Figure 4.6. Unconnected suspension yields high amplitude roll response of the sprung mass

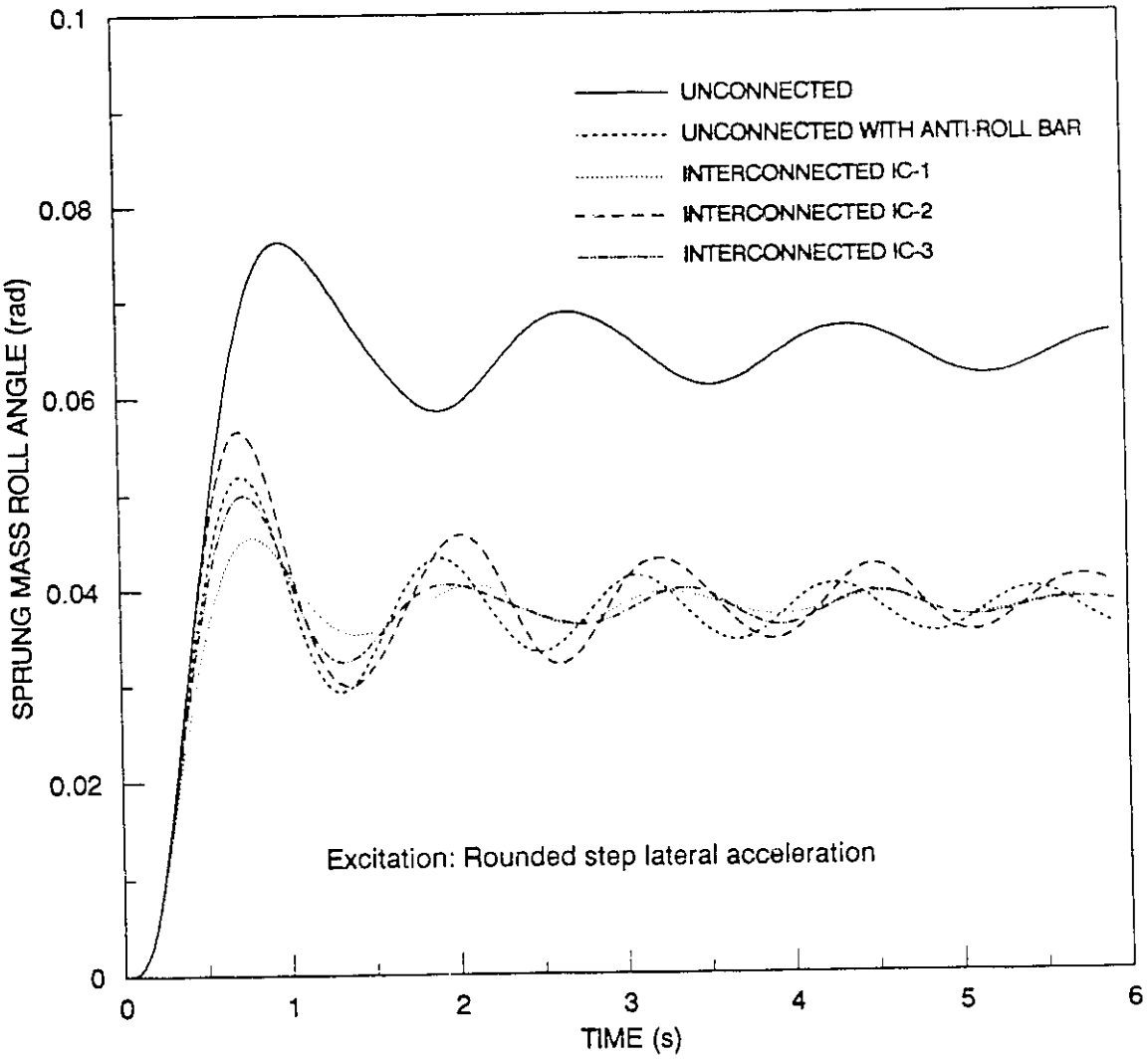

Figure 4.6 Roll angle response of the sprung mass of the vehicle employing different suspension systems subject to a rounded step lateral acceleration during steady turning meaneuver

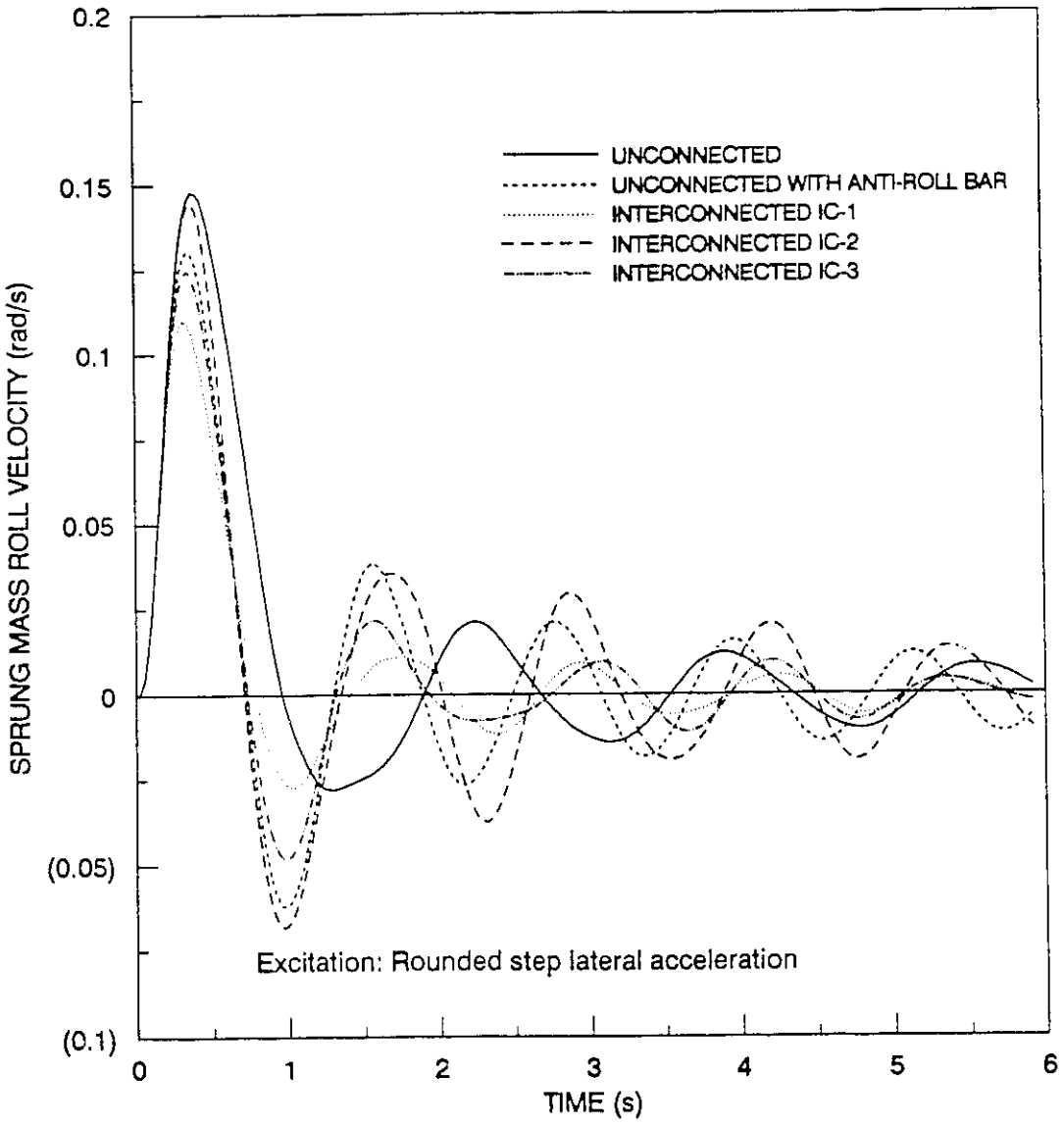

Figure 4.7 Roll velocity response of sprung mass of different suspensions subject to a rouned step lateral acceleration

as compared with those of the anti-roll bar and the interconnected suspensions. The magnitude of steady state of the sprung mass of the vehicle with unconnected suspension is quite large due to its low roll stiffness, with the value of 0.065 radians. The roll angle of sprung mass approaches a steady value of 0.038 radians when interconnected suspensions are employed. All the interconnected suspensions demonstrate the superior anti-roll capability due to their high roll stiffness rates. The anti-roll bar also limits the body roll in a highly effective manner. The roll angle of the sprung mass of the vehicle employing unconnected suspension with anti-roll bar also approaches a steady value similar to that of the vehicle employing interconnected suspensions. The roll response of the sprung mass of the vehicle with unconnected suspension exhibits an oscillation frequency of approximately 0.63 Hz. The oscillation frequency of the roll response of interconnected and anti-roll bar suspension are observed to quite similar, near 0.8 Hz. Although these suspensions are configured to yield identical static roll stiffness, the effective roll stiffness of different suspensions in the rolled position differs slightly as illustrated in Figure 3.6. The roll oscillation frequencies of the different suspension systems thus differ only slightly. The peak roll angle response and the rate of decay of different suspension systems, however, differ considerably, as shown in Figure 4.6. These differences are attributed to their damping characteristics in the roll mode as described earlier in Figure 3.8.

The peak roll angle response of the vehicle with IC-1 suspension is the lowest due to high roll mode damping of the suspension. The second lowest response is that of the IC-3 suspension, which provides the second largest damping force in roll model. Both the suspensions exhibit rapid decay of the roll response. The unconnected suspension with ant-roll bar yields the third lowest peak response with lower decay rate. Although the damping force of the IC-1

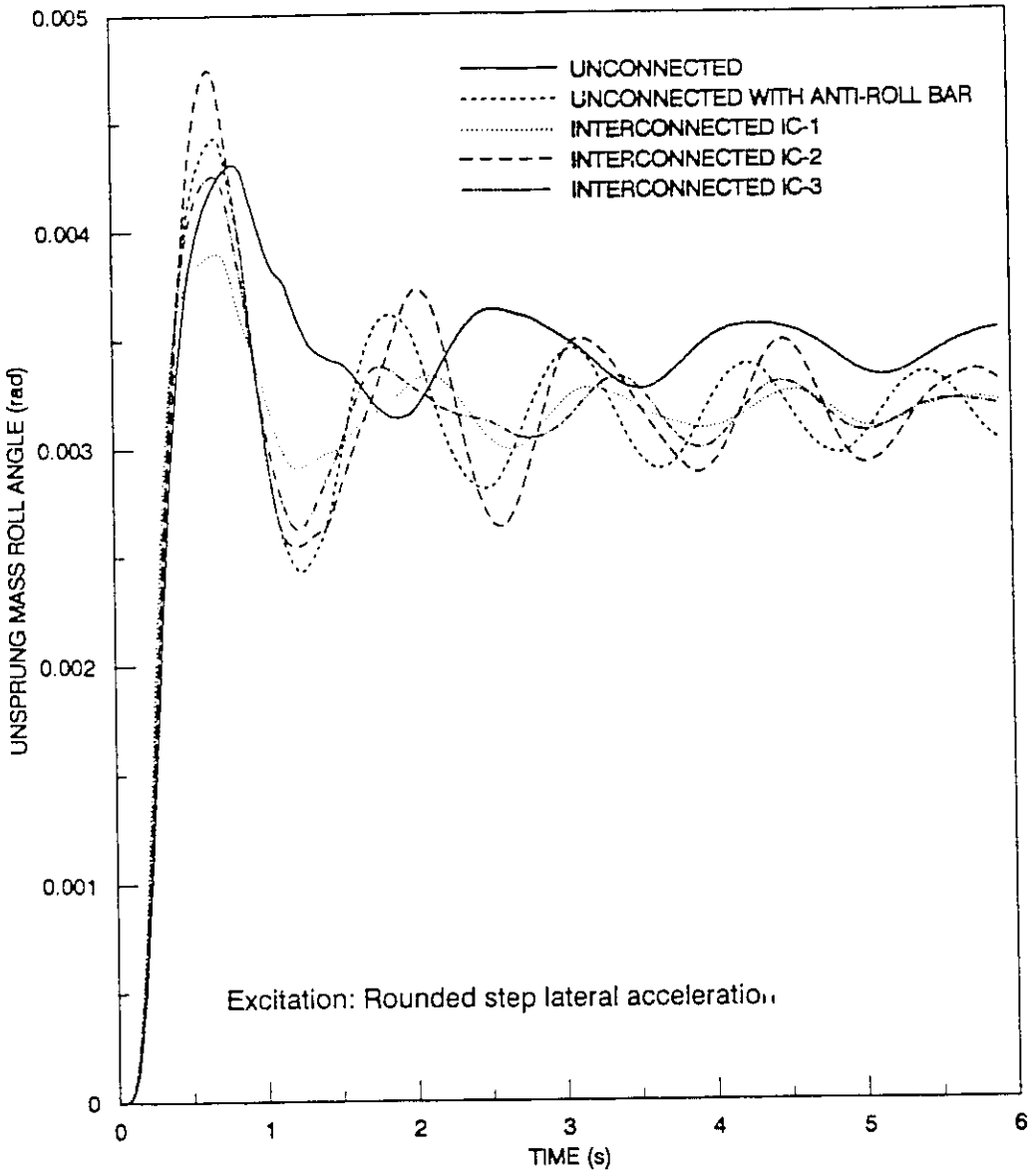

Figure 4.8 Roll angle response of the unsprung mass of the vehicle with different suspensions subjected to a rounded step lateral acceleration

suspension is the same as that of the unconnected in the bounce mode, the roll response of the IC-1 suspension decays faster due to its larger damping force in the roll mode. The IC-2 suspension exhibits the largest peak response of sprung mass among all the three interconnected suspensions due to its weakest damping in the roll mode, as shown in Figure 3.8.

Figure 4.7 illustrates the roll velocity response of sprung mass of the vehicle employing different suspensions. The unconnected suspension exhibits the largest peak roll velocity response, which decays rapidly due to its lower roll frequency. The velocity responses of other suspension configurations can be again ranked according to the magnitude of their damping forces in the roll mode. The IC-1 suspension yields the smallest response due to its largest damping force in the roll mode.

The roll angle response characteristics of the unsprung mass of the vehicle with five different suspensions are shown in Figure 4.8. A comparison of Figures 4.7 and 4.8 reveals that the roll angle response of the unsprung mass is considerably lower than that of the sprung mass due to high stiffness of the tires. Although the unconnected suspension yields larger steady response of unsprung mass, the peak roll angle response is lower than those of the anti-roll bar and IC-2 suspensions. The IC-2 suspension yields the largest peak roll response, while the peak response of the IC-1 suspension is the lowest. The peak roll angle response of the anti-roll suspension is slightly larger than that of the unconnected suspension. The figure further illustrates that the unsprung mass roll response of IC-1 and IC-3 suspension decays rapidly due to their high roll mode damping.

4.3.2 Response to a Transient Lateral Acceleration

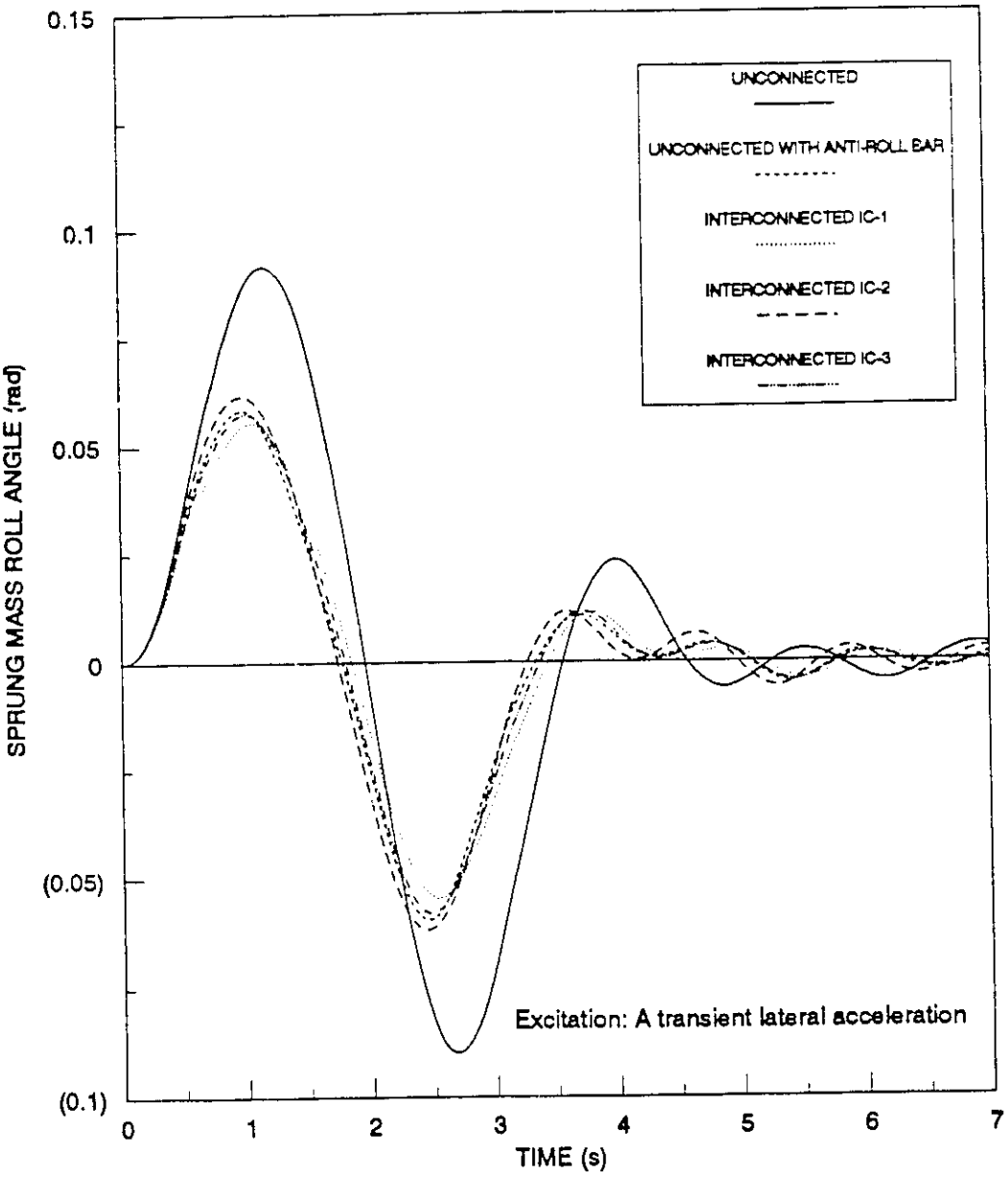

Figure 4.9 Roll angle response of sprung mass of the vehicle with different suspensions subject to a transient lateral acceleration

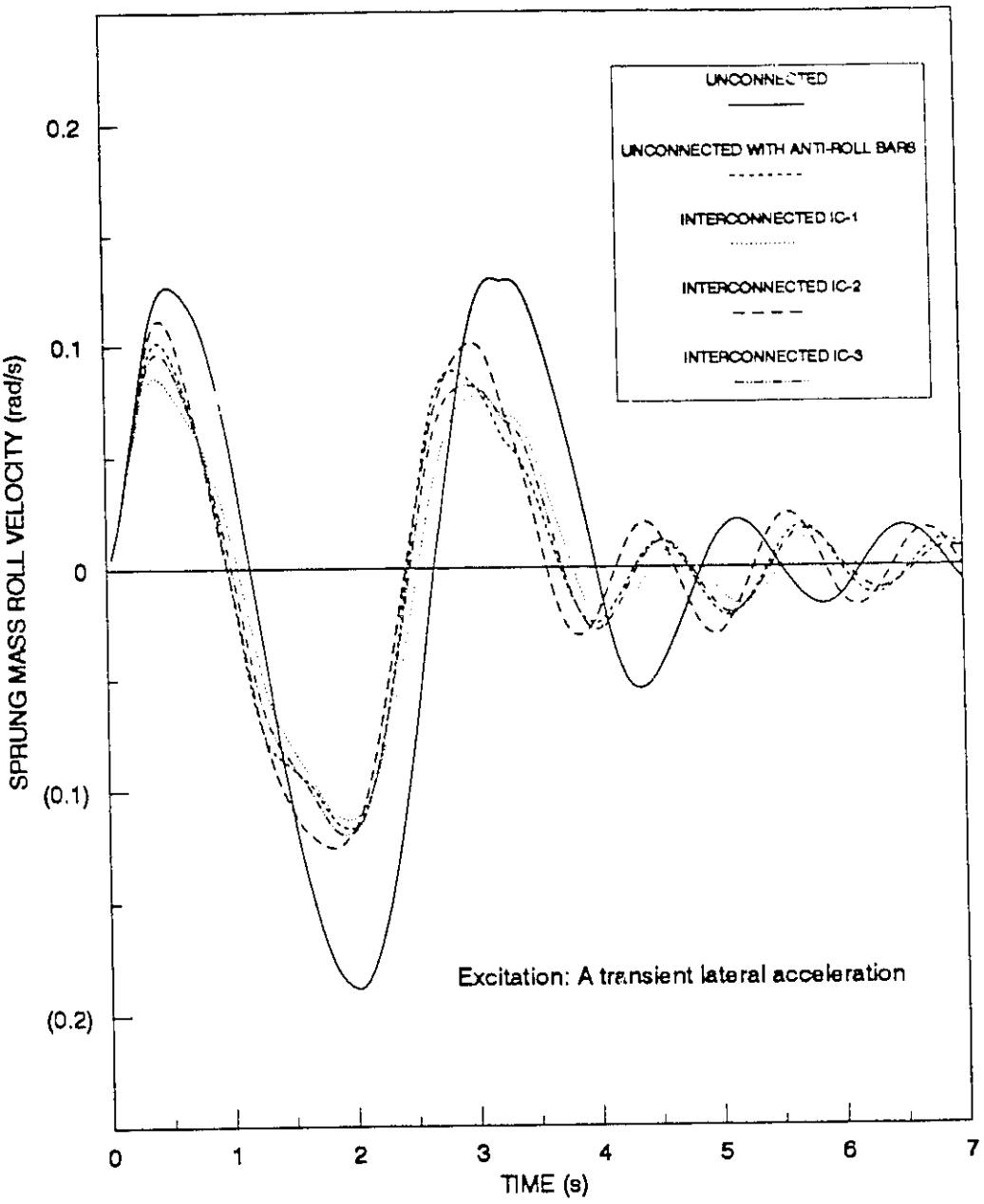

Figure 4.10 Roll velocity response of sprung mass of the vehicle with different suspensions subject to a transient lateral acceleration

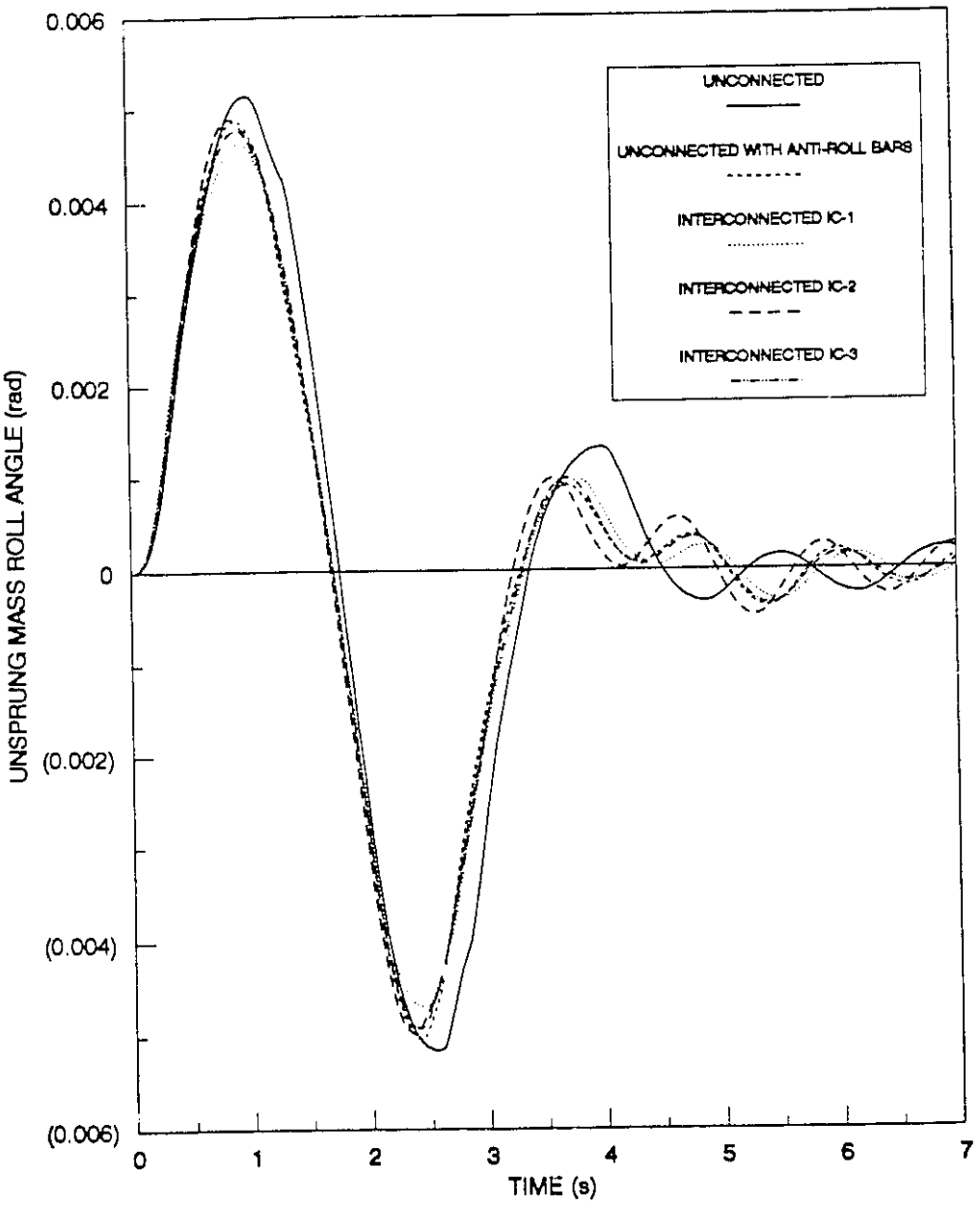

Figure 4.11 Roll angle response of unsprung mass of the vehicle with different suspensions subject to a transient lateral acceleration

The roll angle and roll velocity response characteristics of the sprung mass of the vehicle with different suspension systems, subjected to a transient lateral acceleration during a lane change maneuver, are shown in Figures 4.9 and 4.10. The results clearly reveal that the suspension system interconnected in the roll plane can effectively limit the body roll motion. The peak magnitude of roll angle response of the sprung mass with the unconnected suspension is observed to be 0.09 radians, whereas that of the sprung mass with interconnected suspensions is approximately 0.062 radians. The anti-roll bar suspension also demonstrates its superior anti-roll capability. A comparison of the peak response amplitudes of interconnected suspensions further reveals the influence of damping in the roll mode in reducing the body roll. The effect, however, is not as significant as that in Figure 4.6. An examination of the excitation and the roll response characteristics reveals significant phase delay when the unconnected suspension is employed. The phase angle between the excitation and response, however, is quite small with interconnected suspensions.

Figure 4.11 illustrates the roll angle response characteristics of the unsprung mass of the vehicle employing different suspension systems, subject to lateral acceleration excitation corresponding to a lane change maneuver. Comparison of Figures 4.9 with 4.11 reveals that the magnitude of roll response of the unsprung mass is considerably lower than that of the sprung mass, irrespective of suspension systems used. The unsprung mass of the vehicle with the unconnected suspension exhibits slightly larger roll angle response than that with other suspensions.

4.4 VEHICLE RESPONSE TO ROAD EXCITATIONS

Dynamic ride characteristics of the vehicle employing unconnected, unconnected with anti-roll bar and interconnected suspensions are analyzed in terms of transient vertical and roll response of the sprung mass, when subjected to excitations at the tire-terrain interface. The vertical shock attenuation characteristics are evaluated for an in-phase half-sine excitation, while the roll attenuation characteristics are evaluated for an out-of-phase half-sine bump excitation. A rounded step displacement excitation occurring only at the right tire-terrain interface is further used to evaluate the bounce and roll response characteristics of different suspension configurations.

The vertical displacement and acceleration response characteristics of the sprung mass of the vehicle employing different suspensions, subjected to an in-phase half-sine bump, are compared in Figures 4.12 and 4.13, respectively. The peak displacement response of the IC-1 suspension is similar to that of the unconnected suspension and considerably larger than those of the IC-2 and IC-3 suspensions. The large peak response of the unconnected and IC-1 suspensions is attributed to their high bounce mode damping. The displacement response of sprung mass with IC-3 suspension, however, decays at a faster rate than that with IC-2 suspension due to its low suspension rate. All the suspension configurations, except the IC-3, exhibit sprung mass bounce resonance near 1.2 Hz, while the corresponding frequency of the IC-3 suspension is near 1 Hz. The peak vertical acceleration response of the IC-2 and IC-3 suspensions is observed to be nearly 50% of the acceleration response of the unconnected and IC-1 suspensions, as shown in Figure 4.13.

The roll angle and acceleration response characteristics of the sprung mass of the vehicle employing different suspensions, subjected to an out-of-phase bump, are compared in Figures 4.14 and 4.15, respectively. The figures clearly reveal that the peak roll displacement and acceleration response of the

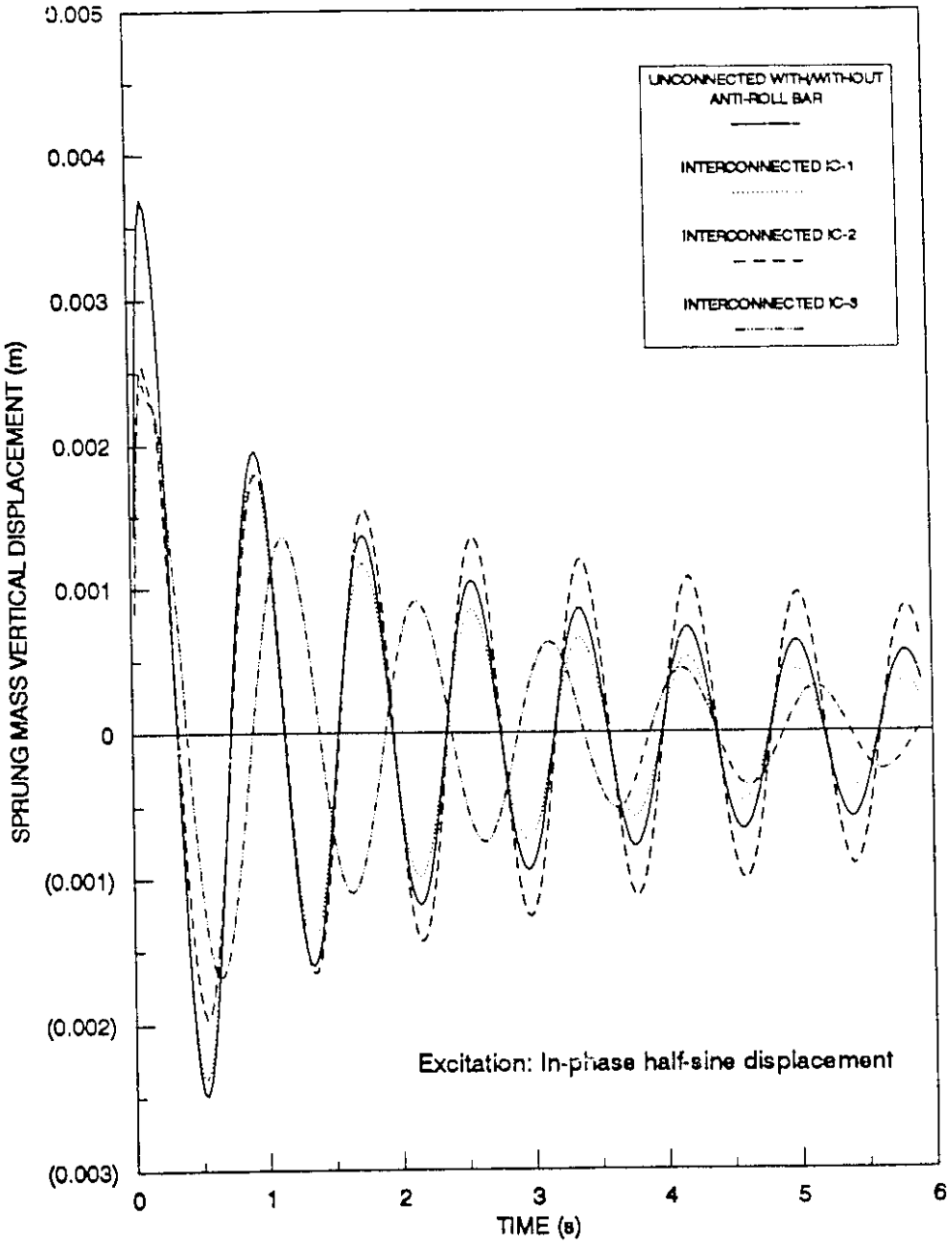

Figure 4.12 Displacement response of the sprung mass of the vehicle with different suspension systems subject to an in-phase half-sine displacement excitation

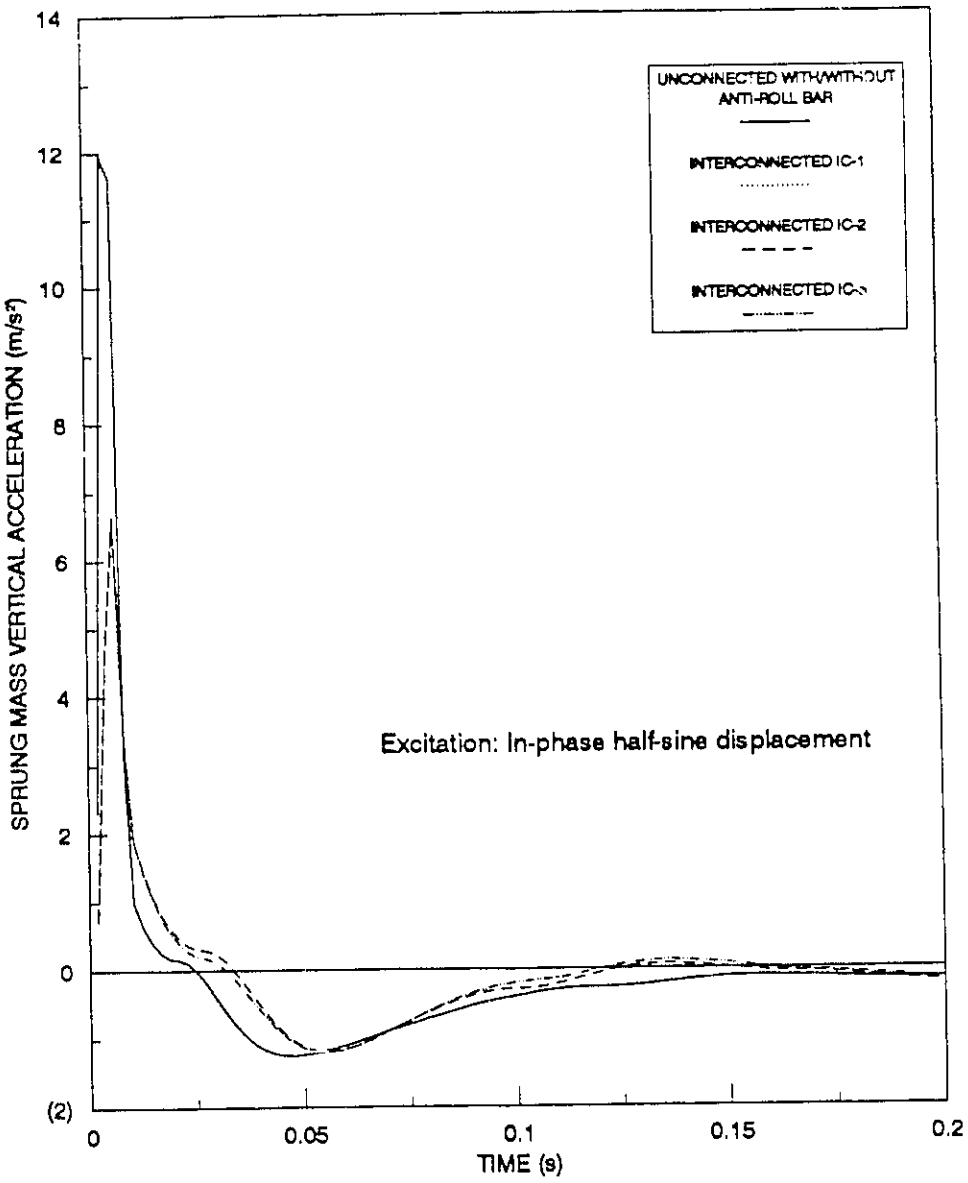

Figure 4.13 Vertical acceleration response of the sprung mass of the vehicle with different suspension systems subject to an in-phase half-sine displacement excitation

vehicle with IC-1 suspension is considerably larger due to its high suspension damping in the roll mode. The roll displacement response of the vehicle, however, decays rapidly. The vehicle with IC-2 suspension yields the lowest values of peak roll displacement and acceleration due to its low roll mode damping characteristics. The roll displacement response, however, decays at a slower rate than that of the IC-1 suspension. The results further demonstrate that the anti-roll bar has no significant influence on the roll ride response since the body roll angle is considerably small under such a excitation. The peak response of the IC-3 suspension is slightly larger than that of the anti-roll bar suspension. It should be noticed that the IC-1 suspension, which yields superior road holding performance, results in excessive roll acceleration of the sprung mass. It may thus be concluded that high suspension damping is desirable for good vehicle handling, while lower damping is preferred for enhancement of vehicle ride quality. Damping characteristics associated with fixed orifice can not satisfy these conflicting requirements.

The shock attenuation performance characteristics of the vehicle with different hydro-pneumatic suspension systems are further explored for a rounded step displacement excitation occurring only at the right tire-terrain interface. The vertical and roll acceleration response characteristics of the sprung mass of the vehicle equipped with different suspension are illustrated in Figures 4.16 and 4.17, respectively. Similar to the results presented earlier, the unconnected and IC-1 suspensions yield peak vertical accelerations considerably larger than those of the IC-2 and IC-3 suspensions. The vertical acceleration responses of the unconnected, IC-1, and IC-3 suspensions, however, decay faster than the IC-2 suspension, as shown in Figure 4.16. The peak roll acceleration response characteristics for a rounded step displacement excitation are also quite similar to those for out-of-phase half-sine displacement

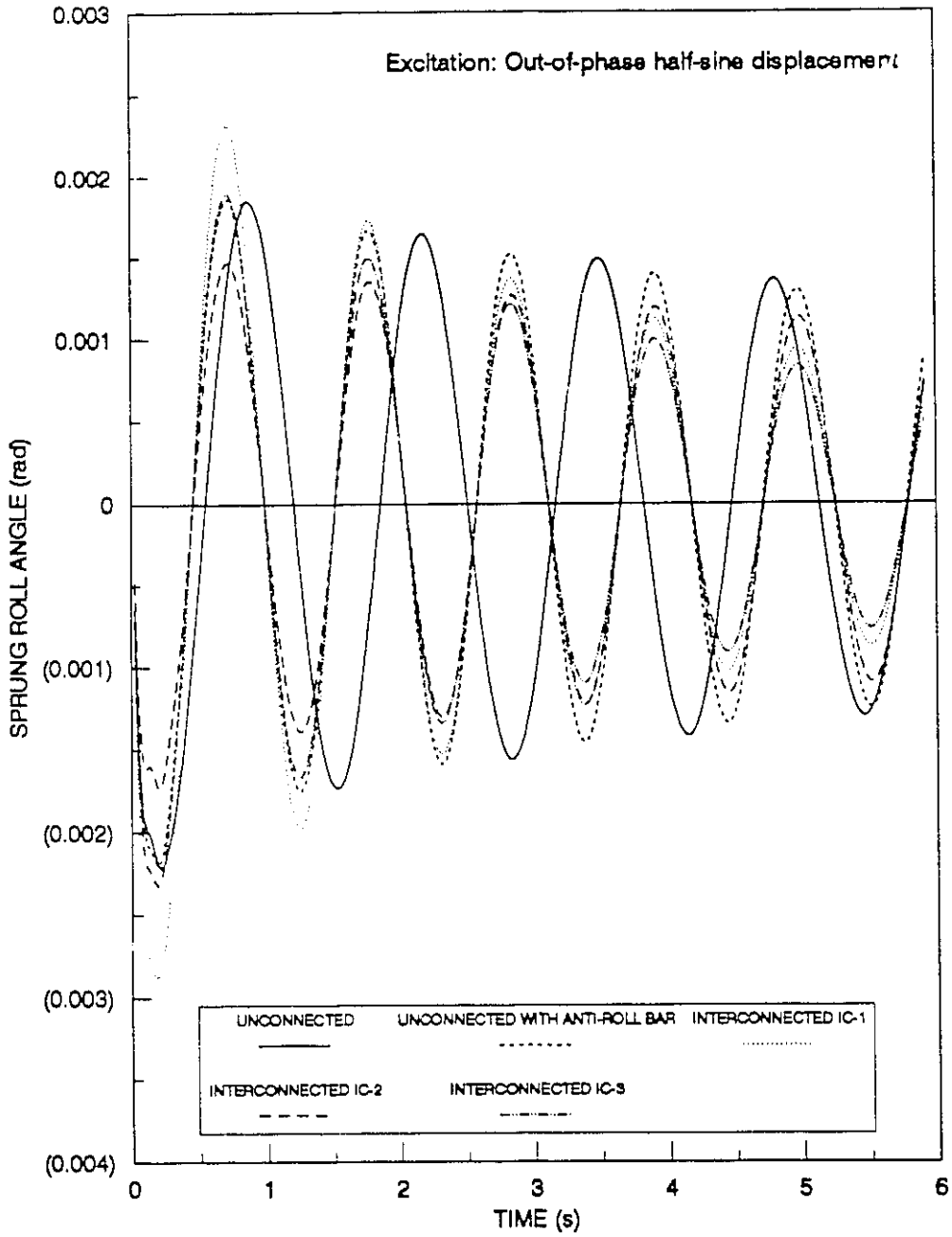

Figure 4.14 Roll angle response of the sprung mass of the vehicle with different suspensions subject to an out-of-phase half-sine displacement excitation

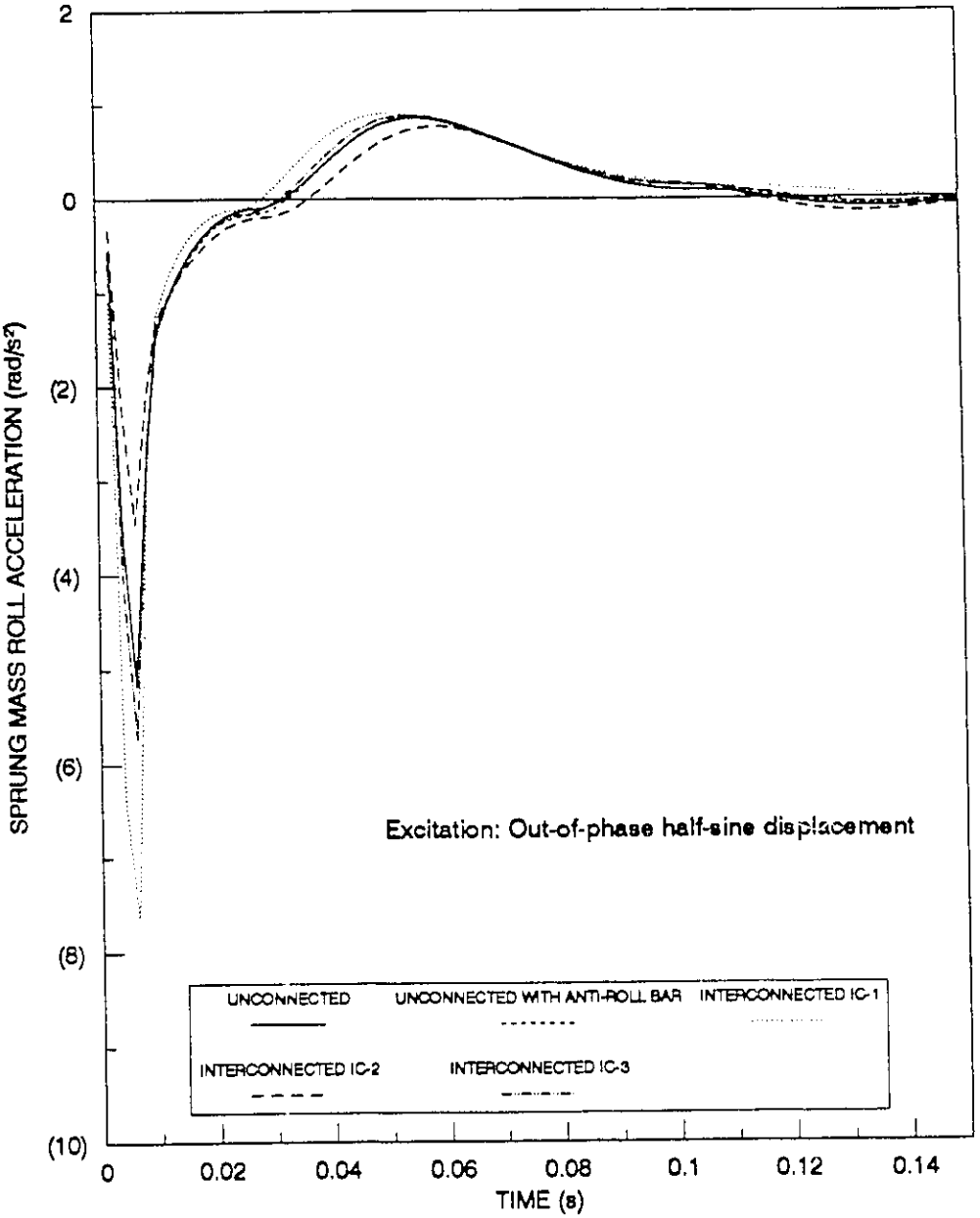

Figure 4.15 Roll acceleration response of the sprung mass of the vehicle with different suspensions subject to an out-of-phase half-sine displacement excitation

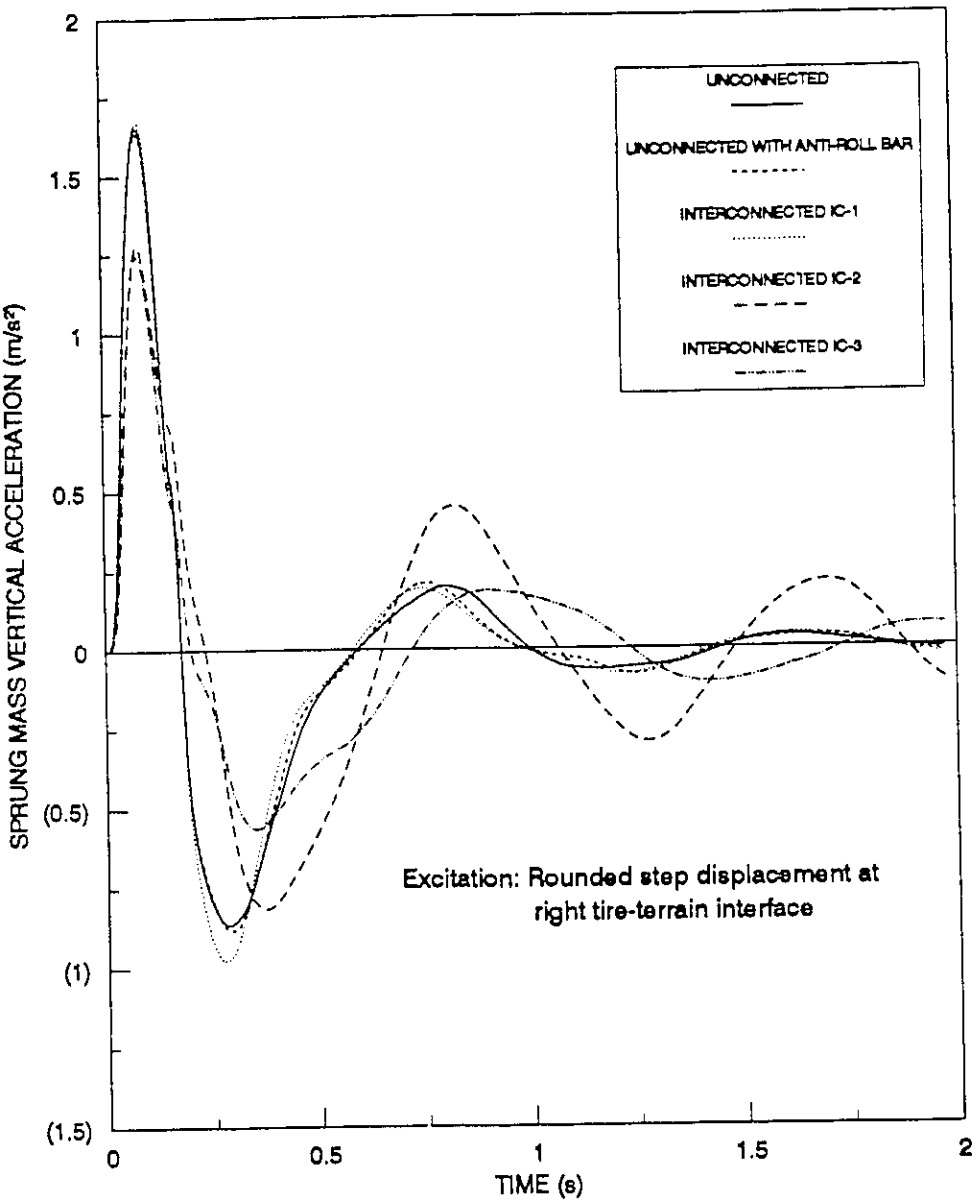

FIGURE 4.16 Vertical acceleration response of the sprung mass of the vehicle with different suspensions subject to a rounded step displacement excitation at right tire-terrain interface

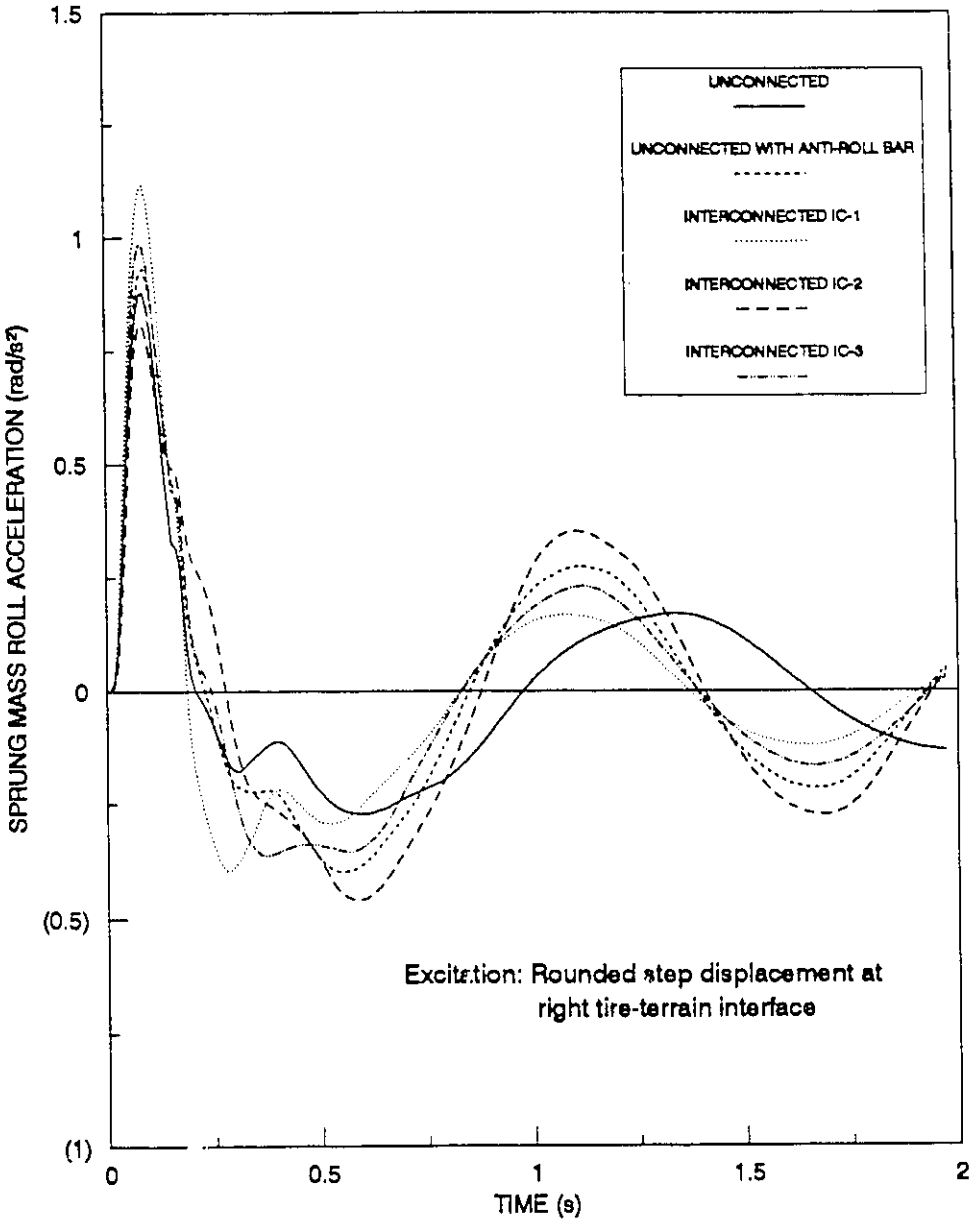

FIGURE 4.17 Roll acceleration response of the sprung mass of the vehicle with different suspensions subject to a rounded step displacement excitation at right tire-terrain interface

excitation. The anti-roll suspension, however, deteriorates the roll ride of the vehicle, as shown in Figure 4.17.

4.5 FREQUENCY RESPONSE CHARACTERISTICS

Frequency response characteristics of the vehicle employing different hydro-pneumatic suspension systems are evaluated in terms of displacement and roll angle transmissibility characteristics of the sprung and unsprung masses. The relative vertical displacement transmissibility characteristics are evaluated for 0.01 m in-phase harmonic excitations at the right and left tire-terrain interface. The roll transmissibility characteristics are evaluated for 0.01 m out-of-phase harmonic excitations. The frequency response characteristics are obtained by computing the ratio of steady state response amplitude to equivalent excitation amplitude in time-domain by sweeping the interested frequency range. Vibration isolation characteristics of different suspension systems are expressed by the following transmissibility ratios:

vertical displacement transmissibility of sprung mass, $T_{zs} = \frac{X_s}{X_e}$

vertical displacement transmissibility of unsprung mass, $T_{zu} = \frac{X_u}{X_e}$

roll angle transmissibility of sprung mass, $T_{\theta s} = \frac{\Theta_s}{\Theta_e}$

roll angle transmissibility of unsprung mass, $T_{\theta u} = \frac{\Theta_u}{\Theta_e}$

where X_s and X_u are the steady state amplitudes of displacement response of the sprung and unsprung masses, respectively; X_e is the amplitude of harmonic excitation; Θ_s and Θ_u are the amplitudes of roll angle response of the sprung and unsprung masses, respectively; and Θ_e is the amplitude of static roll angle of the vehicle under 0.01 m out-of-phase input.

Displacement transmissibility characteristics of the sprung and unsprung masses of the vehicle with different suspensions are present in Figures 4.18 and 4.19, respectively. The vehicle exhibits insignificant roll due to in-phase vertical excitations at both the tracks. The vertical displacement response characteristics of the sprung and unsprung masses exhibit peaks corresponding to their respective resonant frequencies. The bounce resonant frequencies of the vehicle employing different suspensions, under 0.01 m in-phase harmonic excitation, are illustrated in Table 4.1. Although all the suspensions, except the IC-3, are configured to yield identical bounce suspension rates, the frequencies corresponding to the peak responses tend to be lower than the undamped resonant frequencies. The damped sprung mass frequency of the unconnected and IC-1 suspensions is observed to be near 0.95 Hz, while the corresponding undamped frequency is 1.23 Hz. The undamped and damped resonant frequencies of the IC-2 suspension are 1.23 and 1.1 Hz, respectively. The relative small difference in the frequencies is attributed to its low damping. The IC-3 suspension, configured to yield lower vertical spring rate, exhibits the damped and undamped frequencies as 0.86 Hz and 1.0 Hz, respectively. The damped unsprung mass resonant frequencies of all the suspensions are observed to be considerably lower than those of undamped frequencies. The damped unsprung mass frequency of unconnected and IC-1 suspensions is reduced as low as 3.34 Hz due to the high damping developed by the struts, while the corresponding undamped frequency is 7.55 Hz. The damped unsprung mass resonant frequencies of IC-2 and IC-3 suspensions, however, are 4.5 and 4.3 Hz, respectively. The IC-2 suspension, due to its low damping, results in a large peak value around its resonant frequency, while the peak response around the unsprung mass resonant frequency is almost suppressed. Although the unconnected and IC-1 suspension systems give the lowest sprung mass

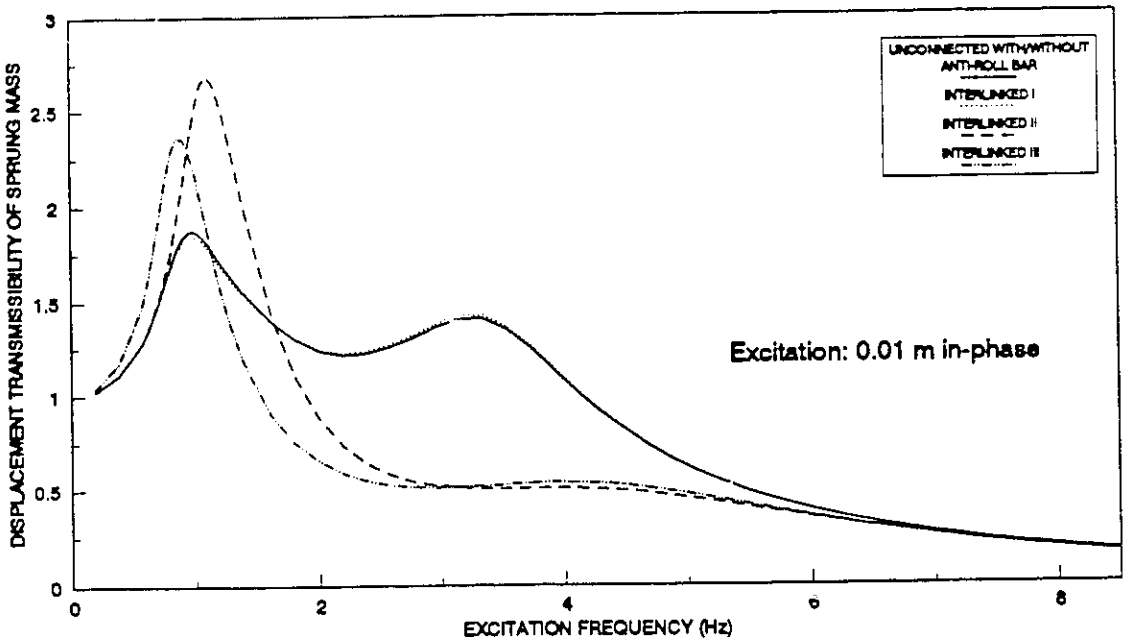

Figure 4.18 Displacement transmissibility of the sprung mass of the vehicle with different suspensions subject to 0.01 m in-phase harmonic excitation at tire-terrain interface

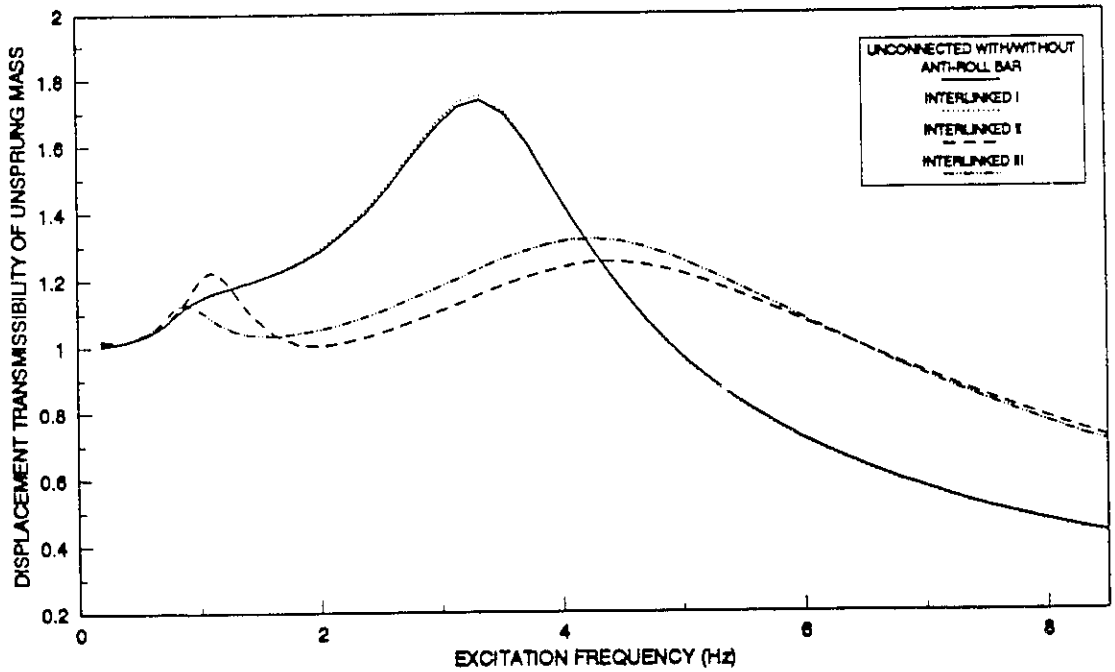

Figure 4.19 Displacement transmissibility of the unsprung mass of the vehicle with different suspensions subject to 0.01 m in-phase harmonic excitation at tire-terrain interface

displacement transmissibility around the resonant frequency of the sprung mass due to the high damping, the displacement transmissibility of the sprung mass around the wheel hop frequency is considerably large. The large response of the sprung mass at the resonant frequency of the unsprung mass implies that the vibration of the sprung mass is largely influenced by the movement of the unsprung mass. Since the ride quality of a vehicle is related to the vibration transmissibility of sprung mass in the frequency range of 4-8 Hz [7], these suspension systems with fixed orifice damping characteristics are unsuited to enhance vehicle ride quality. The lower spring rate of the IC-3 suspension yields peak sprung mass displacement transmissibility larger than the IC-1 suspension but smaller than that of the IC-2 suspension. The light damping properties of the IC-3 suspension, however, results in superior vibration attenuation at excitation frequencies beyond 1.5 HZ. Vibration attenuation of the IC-2 suspension is observed beyond 2 Hz, while those of the unconnected and IC-1 suspensions are obtained beyond 4 Hz. The unconnected and IC-1 suspensions also yield excessive peak vertical transmissibility of the unsprung mass corresponding to its resonant frequency, as shown in Figure 4.19.

Roll angle transmissibility characteristics of sprung and unsprung masses of the vehicle with different suspensions are present in Figures 4.20 and 4.21, respectively. The roll resonant frequencies of the vehicle employing different suspensions, under 0.01 m out-of-phase harmonic excitations, are illustrated in Table 4.2. The damped sprung mass resonant frequency of the unconnected suspension is 0.67 Hz due to its low roll stiffness, while the corresponding frequencies of other suspensions are observed in the range of 0.81-0.88 Hz. The IC-1 suspension yields the smallest roll transmissibility around its roll resonant frequency of the sprung mass due to its high damping in the roll mode, while the IC-2 suspension exhibits the largest peak response around the

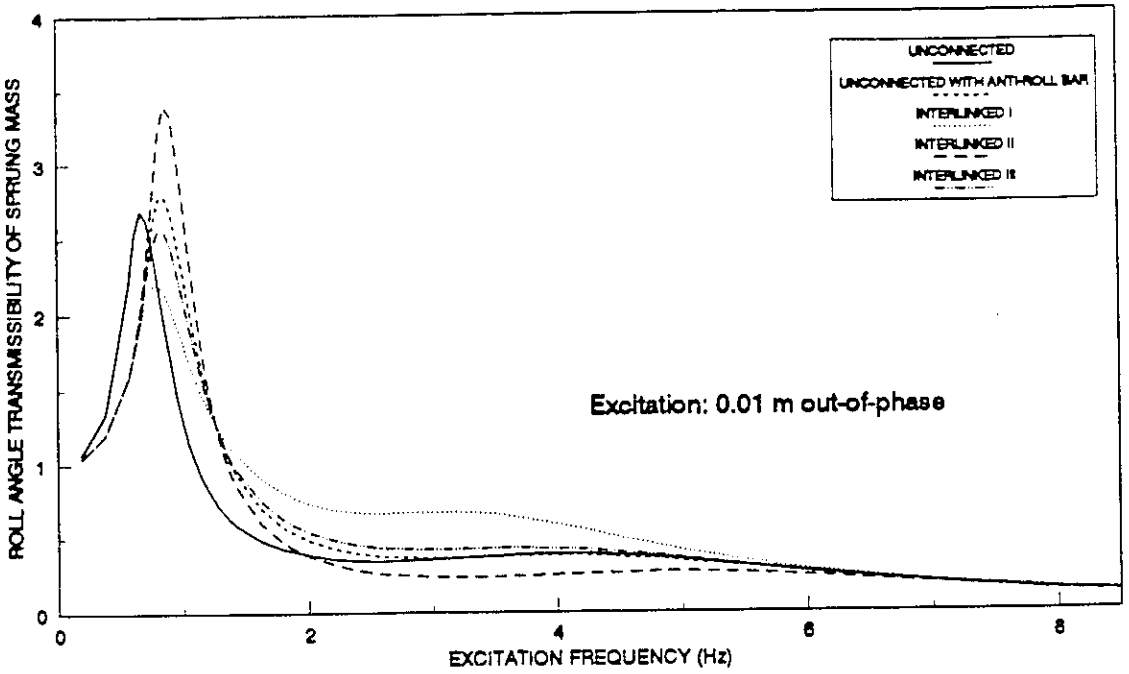

Figure 4.20 Roll angle transmissibility of the sprung mass of the vehicle with different suspensions subject to 0.01 m out-of-phase harmonic excitation at tire-terrain interface

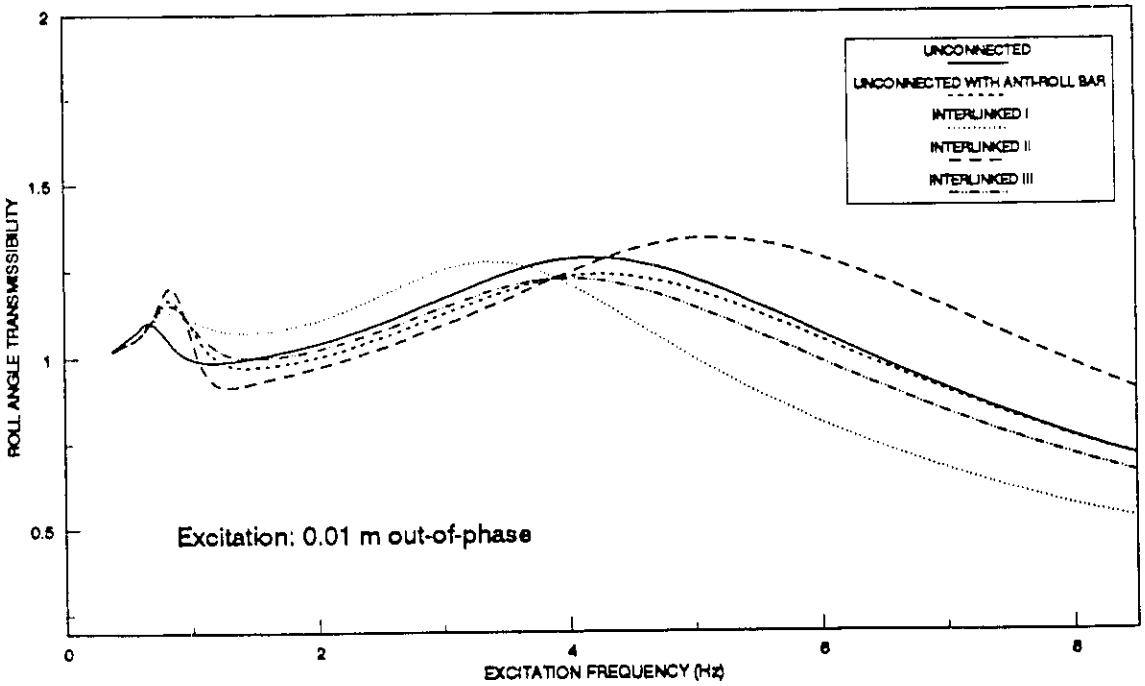

Figure 4.21 Roll angle transmissibility of the unsprung mass of the vehicle twith different suspensions subject to 0.01 m out-of-phase harmonic excitation at tire-terrain interface

Table 4.1

Bounce mode resonant frequencies of sprung and unsprung masses of the vehicle with different suspensions

Mass of Vibration	*Damped Resonant Frequency (Hz) [Undamped]*			
	Unconnected with/without Anti-roll Bar	*Interlinked IC-1*	*Interlinked IC-2*	*Interlinked IC-3*
Sprung Mass	*0.95 [1.23]*	*0.95 [1.23]*	*1.1 [1.23]*	*0.86 [1.0]*
Unsprung Mass	*3.34 [7.55]*	*3.34 [7.55]*	*4.5 [7.55]*	*4.3 [7.38]*

Table 4.2

Roll mode resonant frequencies of sprung and unsprung masses of the vehicle with different suspensions

Mass of Vibration	*Damped Resonant Frequency (Hz) [Undamped]*				
	Unconnected	*Unconnected with Anti-roll bar*	*Interlinked IC-1*	*Interlinked IC-2*	*Interlinked IC-3*
Sprung Mass	*0.67 [0.76]*	*0.86 [0.97]*	*0.81 [0.97]*	*0.88 [0.97]*	*0.84 [0.97]*
Unsprung Mass	*4.2 [7.31]*	*4.3 [7.43]*	*3.34 [7.43]*	*5.1 [7.43]*	*4.1 [7.43]*

resonant frequency of the sprung mass. The anti-roll bar suspension, however, deteriorates the ride performance of the vehicle by exhibiting larger roll response than the unconnected suspension in the frequency range of 0.8-4 Hz. A comparison of Figure 4.18 and 4.20 reveals that although the vertical transmissibility of sprung mass of the vehicle with IC-1 suspension is identical to that with unconnected suspensions, the peak roll response of sprung mass of the vchicle with IC-1 suspension is much smaller than that with unconnected suspensions. The sprung mass roll response of IC-1 suspension, however, exhibits poor vibration attenuation beyond 1.3 Hz. The roll response of sprung mass of the IC-3 suspension is observed to be smaller than that of anti-roll bar suspension around the sprung mass resonant frequency and slightly larger beyond 1.3 Hz.

Table 4.3

A comparison of the computed and measured natural frequencies of the unconnected suspension

Methods for natural frequencies	*Bounce mode (Hz)*		*Roll mode (Hz)*	
	sprung mass	*unsprung mass*	*sprung mass*	*unsprung mass*
Computed	*1.21*	*7.4*	*0.74*	*7.16*
Measured	*1.49*	*7.99-*	*-*	*9.99*

A comparison of the computed lightly damped (with equivalent damping ratio of 0.2) natural frequencies of the unconnected suspension with the measured ones is presented in Table 4.3. The comparison reveals that

computed natural frequencies correlate quite well with the measured dominant ride frequencies. The measured dominant frequency of the bounce motion of the sprung mass (1.49 Hz), however, is slightly higher than the computed resonant frequency (1.21). This discrepancy may be produced by the high stiffness of the rubber bushings employed in the torque rods of the suspension system. The dominant frequencies of the vertical and roll motion of the unsprung mass are also slightly higher than the computed ones. The roll mode resonant frequency of the unsprung mass is 7.16 Hz, and the corresponding measured one is 9.99 Hz. This discrepancy is mainly attributed to the auxiliary roll stiffness introduced by anti-roll stiffeners and Panhard rods.

4.6 SUMMARY

The ride and handling performance characteristics of five hydro-pneumatic suspension configurations are investigated for deterministic excitations using numerical integration technique. The deterministic excitations include lateral accelerations experienced by the sprung mass during steering maneuvers and vertical excitations arising from the tire-terrain interactions. Relative handling quality analyses are performed for rounded step and transient lateral acceleration excitations. The shock and vibration attenuation performance characteristics are evaluated for half-sine displacement bump, rounded step displacement excitation, and 0.01 m in-phase and out-of-phase harmonic excitations. The results clearly demonstrated that interconnecting the suspension in the roll plane effectively limits the body roll motion during steering maneuvers due to the enhanced roll stiffness of the suspension. The damping characteristics the suspension systems, on the other hand, play a very important role in ride quality and road holding abilities. While high damping is desirable for improved road holding, light damping is preferred for adequate shock and

vibration attenuation. Interconnected suspensions demonstrate larger damping rates in the roll mode than in the bounce mode. The interconnected suspensions thus offer a considerable potential to achieve a better compromise between handling performance and ride comfort. While the anti-roll bar suspension effectively limits the body roll during steering maneuvers, the vehicle ride quality is deteriorated. The comparison of vibration transmissibility characteristics of different suspensions also revealed that the interconnected suspension with reduced suspension rate can provide improved vibration isolation performance. The fixed orifice damping, however, is not suited to realize a better compromise between the handling and ride qualities of a vehicle. A variable orifice damping is vital for enhancement of these performance characteristics.

CHAPTER 5

DETERMINISTIC AND STOCHASTIC ANALYSES OF THE INTERCONNECTED SUSPENSION WITH VARIABLE DAMPING

5.1 INTRODUCTION

The results discussed in the previous chapter clearly demonstrate the inherent performance limitations of unconnected and interconnected suspensions with fixed orifice damping. High damping forces developed by fixed orifice suspension tend to suppress the roll oscillations caused by out-of-phase excitations at the tire-terrain interface and the lateral acceleration excitations. High damping forces further reduce the amplitude of vertical vibration around the bounce natural frequency of the vehicle. The vibration isolation performance of the heavily damped passive suspension, however, is deteriorated considerably in the higher frequency range. While a lightly damped suspension is desirable when the disturbance frequencies are beyond the natural frequency, light damping yields poor response corresponding to the vehicle resonance.

In order to overcome these inherent limitations, many passive, semi-active and active variable damping mechanisms have been proposed and investigated. Passive suspension dampers are designed to yield high damping at low velocities across the dampers due to bleed flows, and low damping at high velocities due to blow off valves. A tunable passive sequential hydraulic damper has been proposed and analyzed to achieve variable damping within a vehicle suspension [26]. A three-level adjustable shock absorber was developed by Nissan Motor Co. Ltd., which allows the drivers to select the damping force setting [28]. A number of semi-active dampers employing "on-off" or sequential damping have been proposed and investigated [31, 32, 33]. Semi-active shock

absorbers that provide soft ride under normal driving conditions and firm damping for improved handling, when required, have been developed [30]. Active vehicle suspensions with parameters that change with variations in excitation and response characteristics, have also been extensively investigated, [41-43].

Active vehicle suspensions, however, require an external energy source and sophisticated control system with large number of sensors, which limits the applications of active suspension to cases where performance benefits outweigh the disadvantages associated with costs and complexities [44, 45]. Although hardware implementation of a semi-active suspension is considerably simpler than an active suspension, the realization of semi-active damping still requires a comprehensive instrumentation package and control devices. In this chapter, a passive variable damping mechanism is implemented within the interconnected suspension to achieve improved vibration isolation as well as handling performance. The vibration isolation performance of the vehicle suspension employing the variable damping is further investigated under deterministic and random excitations via computer simulation.

5.2 VARIABLE SUSPENSION DAMPING

The simulation results discussed in Chapter 4 demonstrated that the vehicle ride comfort and handling performance impose conflicting requirements on vehicle suspension damping. High suspension damping is desirable to achieve good handling by controlling the roll response of the vehicle, while the attainment of good ride comfort necessitates variable damping. Fixed orifice high damping further deteriorates the shock isolation performance of the interconnected suspension. The damping requirements of a vehicle suspension under different driving conditions can be summarized as:

(1) High damping is preferable to suppress the sprung mass roll encountered during directional maneuvers.

(2) High suspension damping is desirable in the frequency band around the natural frequency of the sprung mass to control the resonant response.

(3) High suspension damping is desirable in the frequency band around the natural frequency of the unsprung mass to reduce the wheel hop response and dynamic wheel load transmitted to the road.

(4) Light damping is desirable in the frequency band between the natural frequencies of the sprung and unsprung masses to achieve good ride response. The vehicle ride comfort is directly related to magnitude of transmitted vibration in this frequency range, since human body is most sensitive to vibration in the 2-7 Hz frequency range.

(5) Light damping is desirable corresponding to excitations at frequencies beyond the natural frequency of the unsprung mass.

Although it is quite difficult to satisfy all the above requirements through the use of passive damping mechanisms, an adequately tuned variable damper can fulfill the requirements (1) to (4).

5.2.1 Variable Damping Mechanism

In a hydraulic damper the strut velocity, $\dot{z}$, is related to the pressure differential across the orifice, p_{23}, through the following nonlinear relation, derived in Chapter 2:

$$p_{23} = \frac{\rho A_2^2}{2C_d^2}\left(\dot{z}/a\right)^2 sgn(\dot{z}) \tag{5.1}$$

Damping force, f_d, due to the pressure differential across orifice restriction is expressed as:

$$f_d = p_{23} A_2 \tag{5.2}$$

Equations (5.1) and (5.2) reveal that the damping force is related to square of the relative velocity, $\dot{z}$, across the strut. Constant orifice dampers thus yield high damping forces corresponding to high frequency excitations and therefore poor vibration isolation. The magnitude of damping force at higher excitation frequencies or relative velocities can be effectively controlled by modulating the orifice area a.

The damping requirements (1) to (4), described in the previous subsection, can be satisfied by varying the damping force through variations in the orifice area. The orifice area may be varied with the pressure differential using pressure control valves. The damping valve is designed to yield constant area orifice when the pressure difference, p_{23}, is below certain pressure value, $(p_{23})_0$. The damper thus yields high damping corresponding to low pressure difference and thus low strut velocity. When the pressure differential across the damper, p_{23}, exceeds the preset value $(p_{23})_0$, a pressure control valve modulates the damping orifice area such that the pressure differential remains nearly constant in the modulation range. The pressure control valve, however, becomes fully opened beyond the modulation range. This damping force control scheme thus yields three stages of the damping force, as illustrated in Figure 5.1. The stage one is achieved by relatively small orifice area when the pressure control valve is not actuated. After the damping force reaches a certain value, which corresponds to the preset pressure differential value, the pressure control valve begins to modulate the fluid flow resulting in nearly constant damping force

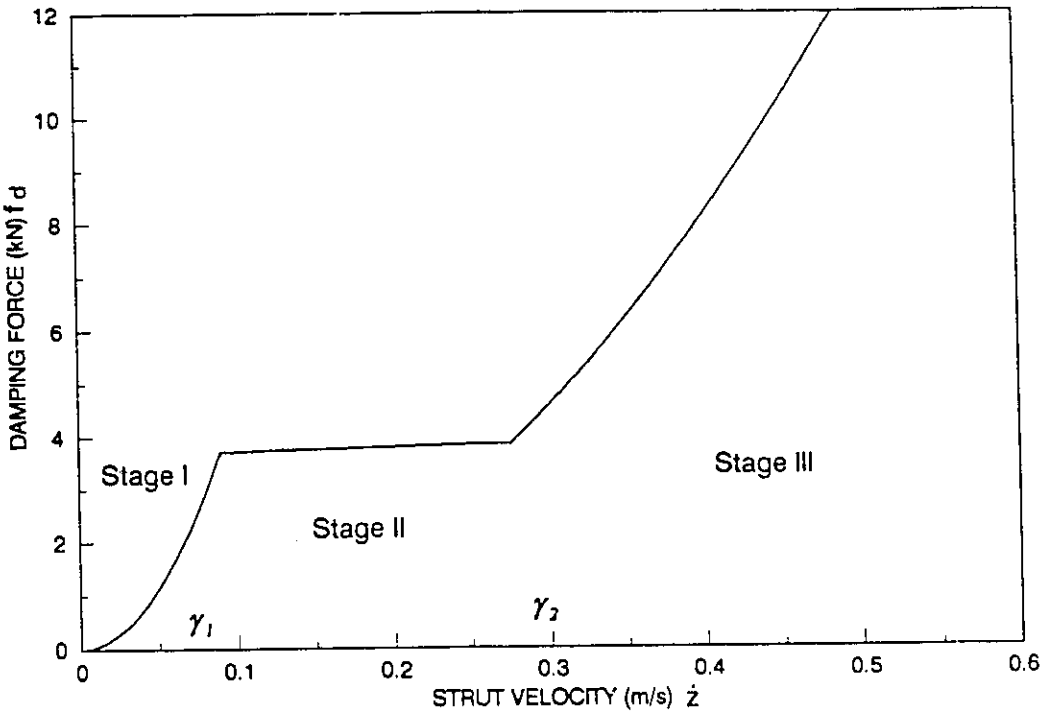

Figure 5.1 Damping force characteristic of the multi-stage damper

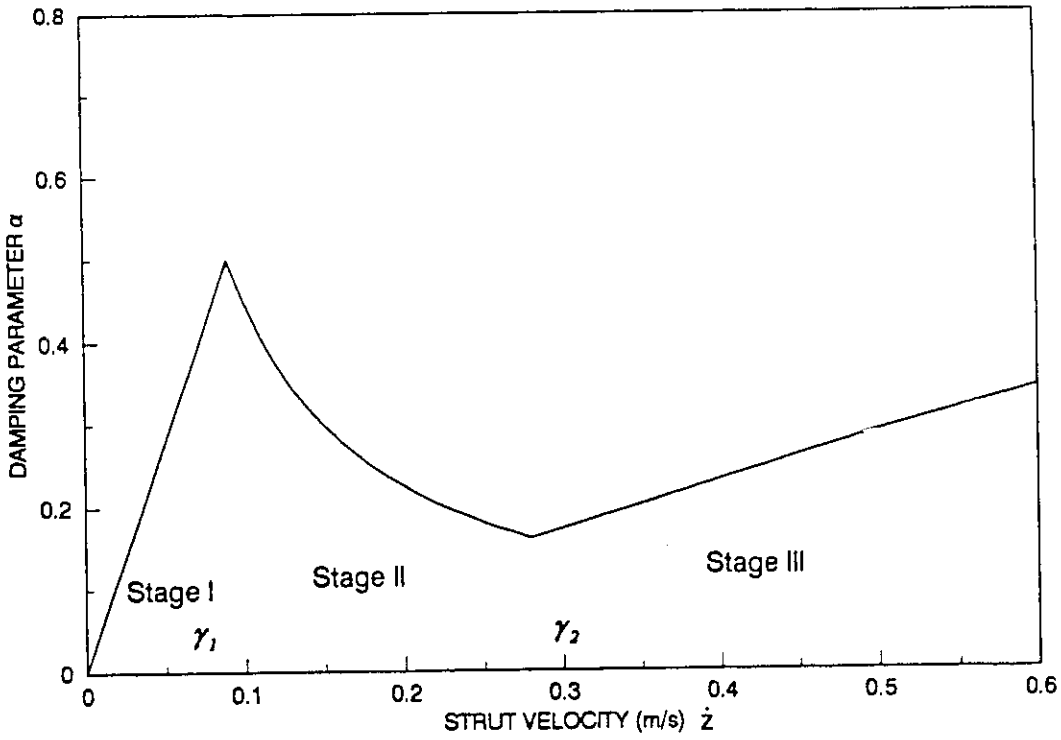

Figure 5.2 Damping parameter characteristic of the multi-stage damper

in the second stage. In the third stage, the pressure control valve approaches fully open position, and the corresponding pressure and damping force increase with the strut velocity. Assuming nearly constant damping force during stage II, the damping force may be expressed as:

$$f_d = \begin{cases} c_1 \dot{z}^2 sgn(\dot{z}); & \text{for } |\dot{z}| \le \gamma_1; \text{ for stage I} \\ c_1 \gamma_1^2 sgn(\dot{z}); & \text{for } \gamma_1 < |\dot{z}| \le \gamma_2; \text{ for stage II} \\ c_2 \dot{z}^2 sgn(\dot{z}); & \text{for } |\dot{z}| > \gamma_2; \text{ for stage III} \end{cases} \tag{5.3}$$

where $c_1 = \rho A_2^3 / 2C_d^2 a_1^2$ is the damping coefficient corresponding to the orifice area a_1 in the first stage; $c_2 = \rho A_2^3 / 2C_d^2 a_2^2$ is the damping coefficient corresponding to the orifice area a_2 in the third stage; γ_1 and γ_2 are the strut velocities representing the modulation range. For convenience of analysis, a damping parameter, α, is defined as the ratio of damping force to the corresponding linear critical damping force of the system:

$$\alpha = \frac{f_d}{c_c \dot{z}} \tag{5.4}$$

where c_c is the critical damping coefficient. Upon substituting Equation (5.3), the damping parameter corresponding to the three stages can be expressed as:

$$\alpha = \begin{cases} \dfrac{c_1}{c_c} \dot{z}; & \text{for stage I} \\ \dfrac{c_1 \gamma_1^2}{c_c \dot{z}}; & \text{for stage II} \\ \dfrac{c_2}{c_c} \dot{z}; & \text{for stage III} \end{cases} \tag{5.5}$$

Equation (5.5) reveals that damping parameter of the variable damper is proportional to the magnitude of relative velocity response in the first damping stage. However, as the relative velocity response increases, the corresponding

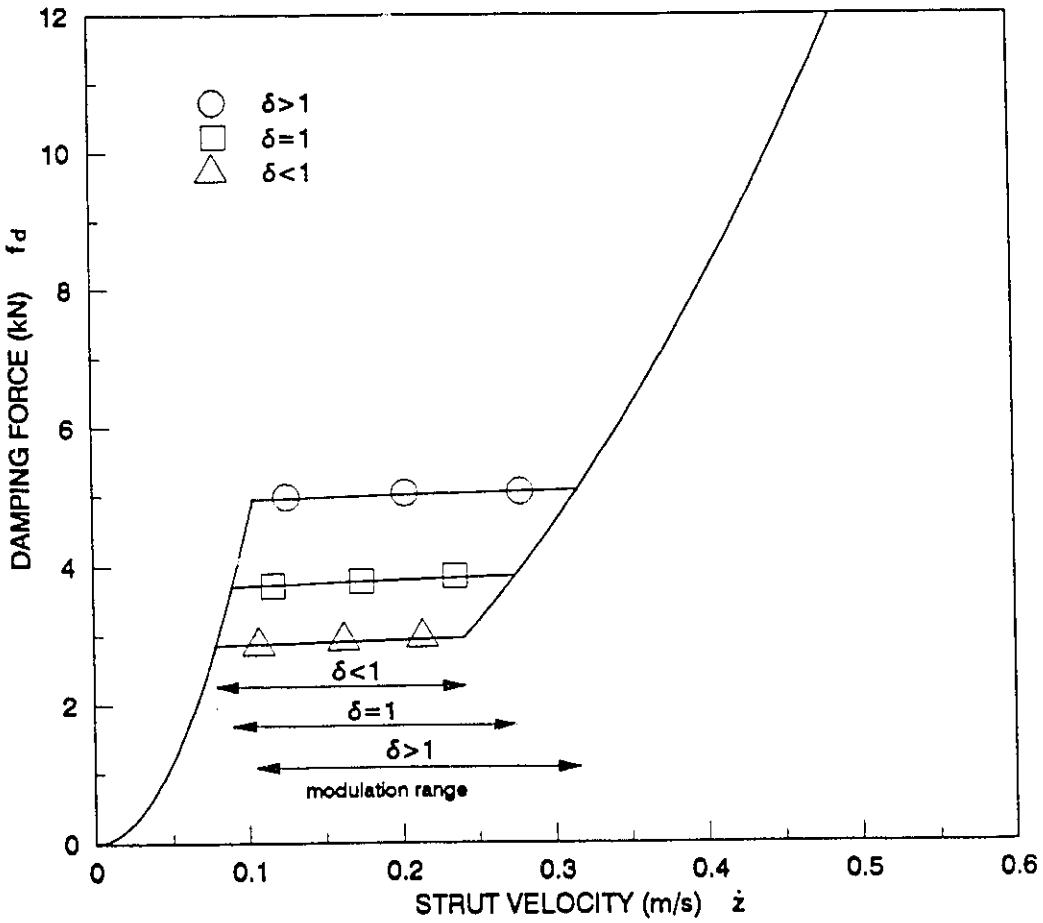

Figure 5.3 The influence of tuning factor on transition velocities

damping parameter is observed to be inversely proportional to magnitude of the relative velocity response. In the third stage, the damping parameter is again proportional to the magnitude of relative velocity response. Figure 5.2 illustrates the variations in damping parameter with the strut velocity. The damping parameter approaches its peak value at the velocity between stages one and two. The damping parameter then decreases with increase in the strut velocity during the second stage, and increases again in a moderate manner in the third stage. By selecting adequate modulation range and damper parameters, it is thus possible to achieve high damping around the natural frequency of the sprung mass (corresponding to the peak damping parameter in the transition range between stage I and II) to control the resonant response; light damping in the frequency band between the natural frequencies of the sprung and unsprung masses (stage II and III); and high damping around the natural frequency of unsprung mass (stage III). Different preset values of pressure differentials, however, need to be selected for different terrain profiles and applications. The preset pressure differential (p_{23}) may be related to a tuning factor, δ, in the following manner:

$$(p_{23}) = \delta(p_{23})_0 \tag{5.6}$$

Figure 5.3 illustrates the force-velocity characteristics of the damper for different values of the tuning factor. The results clearly show that the range of modulation (γ_1, γ_2) is directly related to the preset pressure or the tuning factor.

Figure 5.4 illustrates the schematic of a possible damper valve that may be used to realize the above damping characteristics. The damper comprises fixed orifices and pressure control valves with tapered pins. High damping rate is realized corresponding to low strut velocity since the pressure control valve remains closed due to low pressure differentials. As the strut velocity increases, the pressure control valve opens progressively. The modulation of the pressure

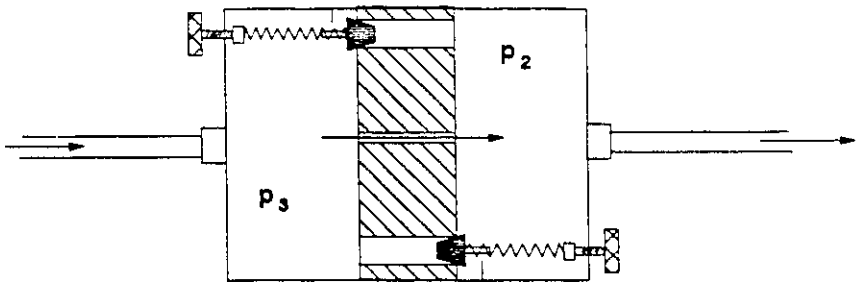

(a) Stage I

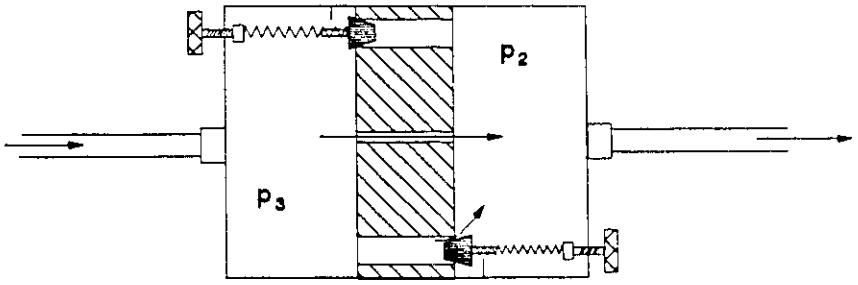

(b) Stage II

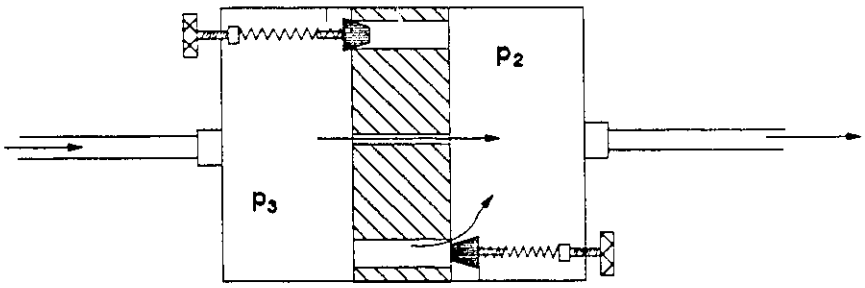

(c) Stage III

Figure 5.4 Schemtic of the multi-stage damper in extension

control valve results in nearly constant damping force with reduced damping parameter. With further increase in strut velocity, the valve approaches its fully open position and the damping force tends to increase as square of the relative velocity. The pressure control valves, shown in Figure 5.4, can be tuned to achieve different preset pressures and modulation ranges in compression and rebound strokes.

5.2.2 Damping Parameters

The ride and handling performance characteristics of a suspension system are strongly dependent upon the damping coefficients corresponding to low and high velocities, and the transition velocities. The enhancement of improved compromise between the ride and handling performance characteristics thus necessitates the selection of appropriate damping properties and the transition velocities. Different transition velocities can be obtained by adjusting the pre-load on the pressure control valve springs. The damping ratio of a highway bus suspension typically varies in the range of 0.2 to 0.4, which corresponds to bounce resonant vibration transmissibility in the 1.25-2.5 range. The fixed orifice area of the interconnected suspension is thus selected to achieve sprung mass bounce resonant transmissibility in the above range. The fixed area orifice, $a_1 = 2 \times 10^{-4}\ m^2$, is selected to achieve resonant transmissibility of 1.8. A transition velocity of approximately 0.1 m/s is recommended , such that high suspension damping is available to control roll oscillations and resonant vertical vibrations [29, 52]. The preset pressure differential of the pressure control valve $(p_{23})_{01}$ is selected as 150 kPa, which corresponds to strut velocity of 0.09 m/s. The total orifice area is assumed to vary linearly with the inflation pressure until the valve approaches its fully open position, as shown in Figure 5.5. The valve is assume to approach fully open position at a pressure

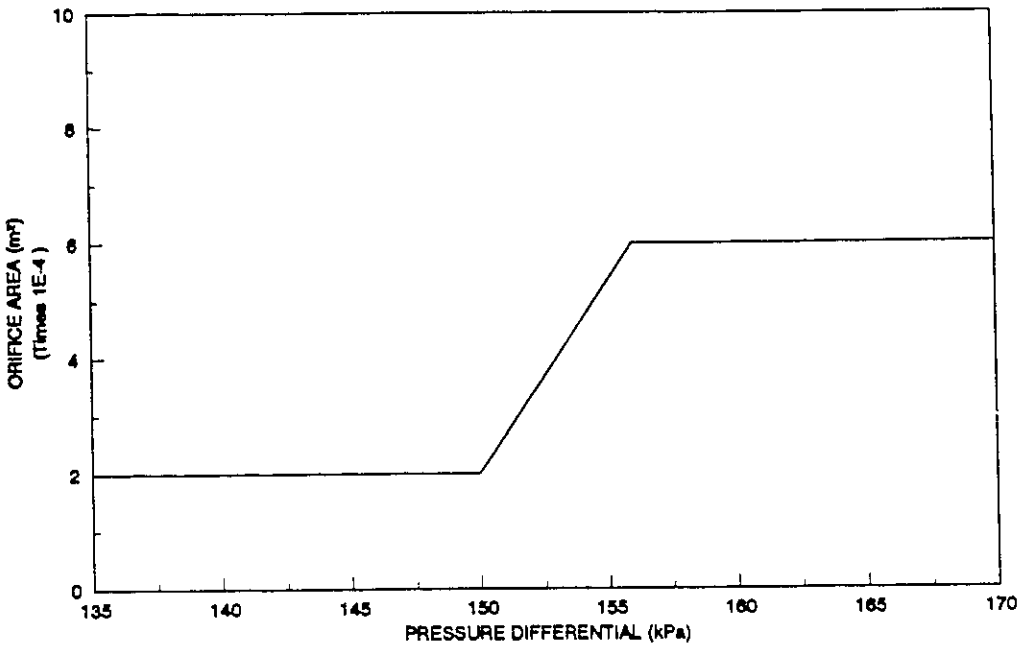

Figure 5.5 Variation of orifice area in the multi-stage damper

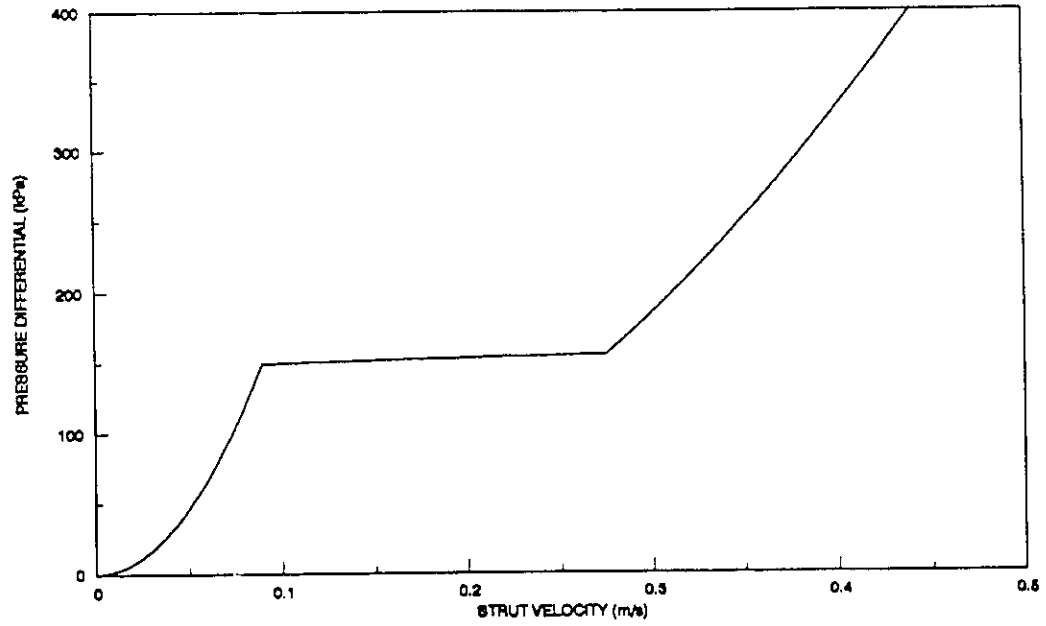

Figure 5.6 Variation of pressure differential across the multi-stage damper

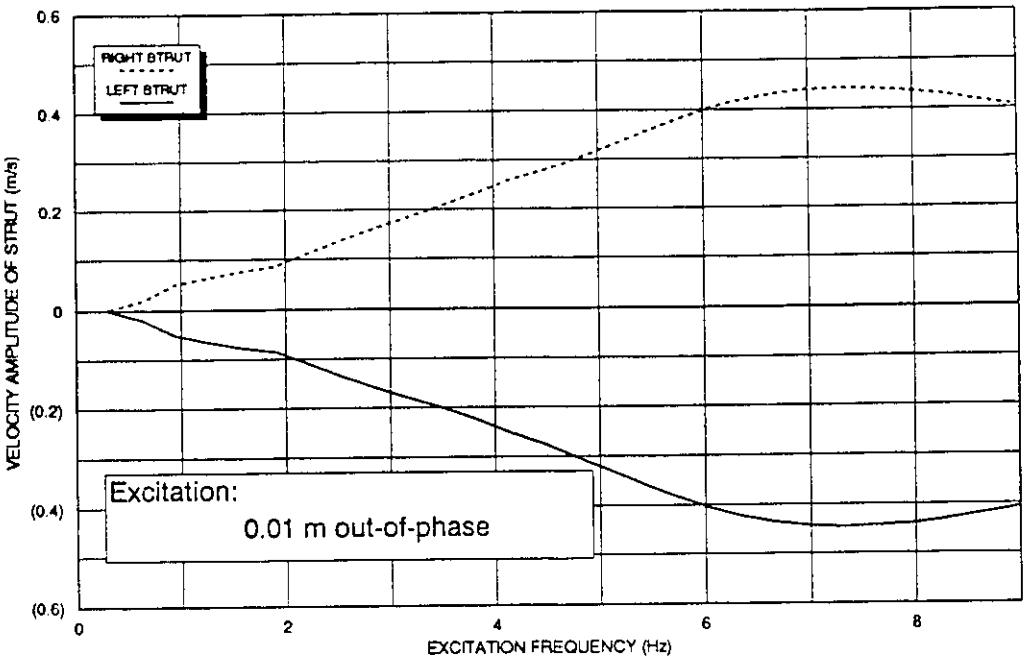

Figure 5.7 Suspension strut velocity of the vehicle employing the multi-stage damper subject to 0.01 m out-of-phase excitation at tire-terrain interface

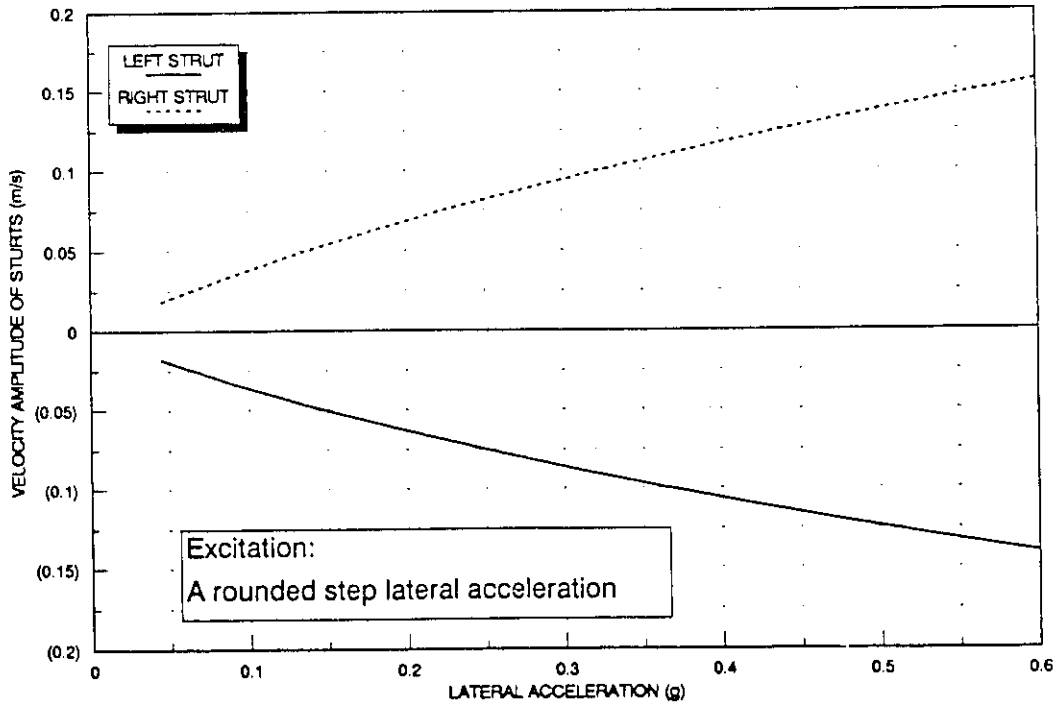

Figure 5.8 Suspension strut velocity of the vehicle with fixed orifice damper subject to a rounded step lateral acceleration

differential of 156 kPa $(p_{23})_{02}$, which corresponds to a strut velocity of approximately 0.28 m/s, as shown in Figure 5.6.

The damper yields high damping when the strut velocity is about 0.09 m/s, reduced damping in the wide strut velocity range of 0.09-0.28 m/s, and increased damping at strut velocity greater than 0.28 m/s. The transition velocities may be further derived from the strut velocity response to realistic excitations. The peak amplitude of undulations of medium-quality roads is known to be in the order of 0.013 m or less [74]. The strut velocity response is thus investigated for in-phase and out-of-phase 0.01 m harmonic excitations. The strut velocity is further investigated for typical lateral acceleration excitations arising from directional maneuvers. It has be established that peak lateral acceleration excitation caused by a steering maneuver of a high c.g. vehicle is less than 0.3g [73]. Figure 5.7 illustrates the amplitude of strut velocity when the vehicle employing variable damping suspension is subjected to 0.01 m out-of-phase harmonic excitation. Maximum strut velocity response of the vehicle employing the interconnected IC-3 suspension with fixed orifice damping a_1, subjected to different values of rounded step lateral acceleration, is shown in Figure 5.8. In the roll mode, the strut velocities of 0.09 and 0.28 m/s correspond to excitation frequencies of 1.9 Hz and 4.7 Hz, respectively, as shown in Figure 5.7. The frequency range, 1.9-4.7 Hz is beyond the sprung mass resonant frequency and corresponds to the desirable isolation region. At strut velocity great than 0.28 m/s, the damping tends to increase as the excitation frequency approaches the unsprung mass resonance. The peak strut velocity under 0.3g lateral acceleration is also observed to be below 0.09 m/s (Figure 5.8). The damping requirements (1) to (4), described in section 5.2, can be thus satisfied using the proposed variable damping mechanism.

5.3 DYNAMIC PROPERTIES OF THE INTERCONNECTED SUSPENSION WITH VARIABLE DAMPING

Dynamic ride performance characteristics of the interconnected suspension with the multi-stage dampers are evaluated in terms of transient vertical and roll velocities and accelerations and compared to those with fixed orifice dampers, to demonstrate the effectiveness of the variable damping. A rounded step displacement excitation occurring at the right tire-terrain interface is used for this investigation.

Vertical and roll velocity response characteristics of the sprung mass of the vehicle employing IC-3 suspension with multi-stage and fixed orifice dampers are presented in Figures 5.9 and 5.10, respectively. The peak vertical velocity response of sprung mass with fixed orifice damping is 0.14 m/s, while that of sprung mass with multi-stage damping is 0.12 m/s. The peak roll velocity of sprung mass with fixed orifice damping is 0.12 rad/s, while that of sprung mass with multi-stage damping is about 0.1 rad/s. The multi-stage damper improves the shock attenuation performance of the interconnected suspension due to its variable damping. The rates of decay of vertical and roll velocity responses of the sprung mass with both dampers are quite similar, since the multi-stage dampers continue to behave as the constant orifice dampers at low strut velocities.

Vertical and roll acceleration response characteristics of sprung mass of the vehicle employing multi-stage and fixed orifice dampers, subject to a rounded step displacement excitation at the right tire-terrain interface, are presented in Figures 5.11 and 5.12. The peak vertical accelerations of sprung mass with fixed orifice and multi-stage dampers are 1.5 m/s^2 and 1.25 m/s^2, respectively. The peak amplitudes of roll acceleration of the sprung mass with fixed and variable orifice damping are observed as 1.24 rad/s^2 and 1.0 rad/s^2,

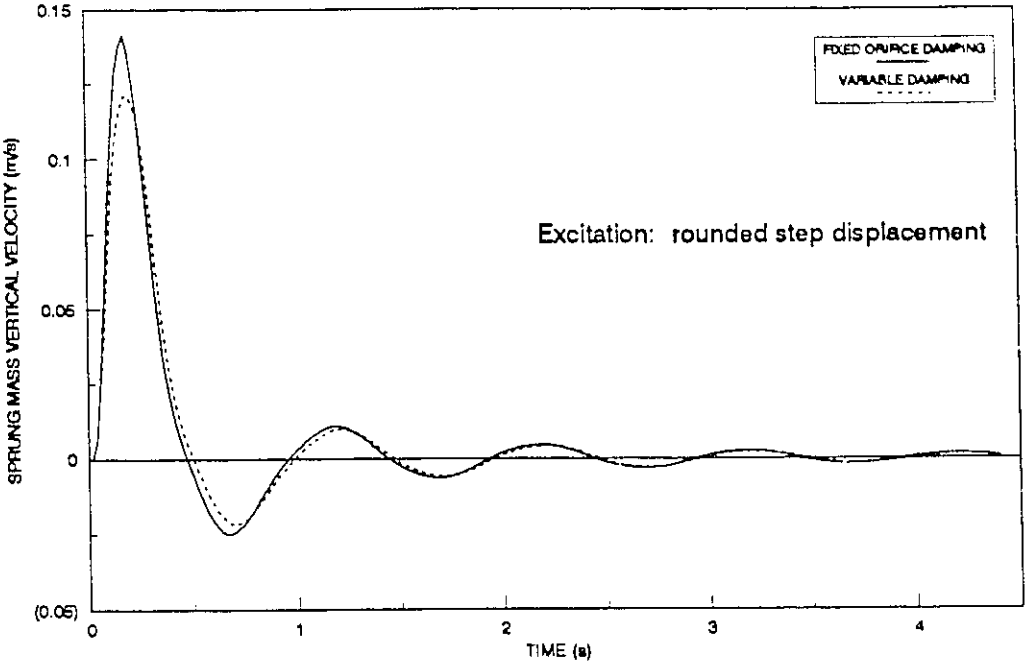

Figure 5.9 Vertical velocity response of the sprung mass of an interconnected suspension with fixed and variable orifice damping subject to a rounded step displacement excitation at tire-terrain interface

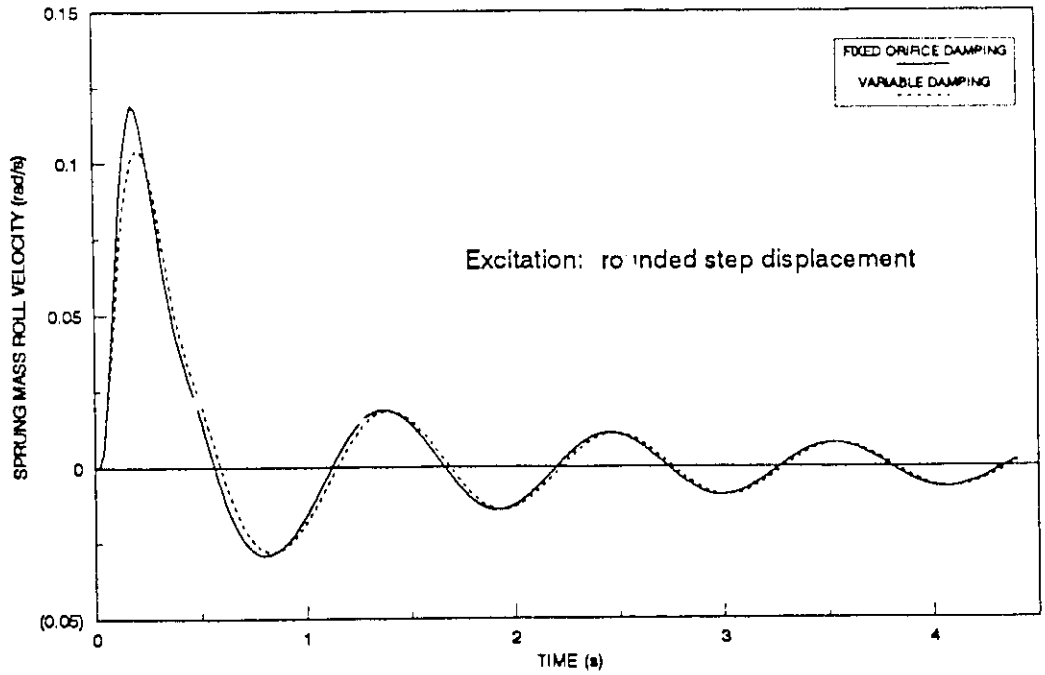

Figure 5.10 Roll velocity response of the sprung mass of an interconnected suspension with fixed and variable orifice damping subject to a rounded step displacement excitation at tire-terrain interface

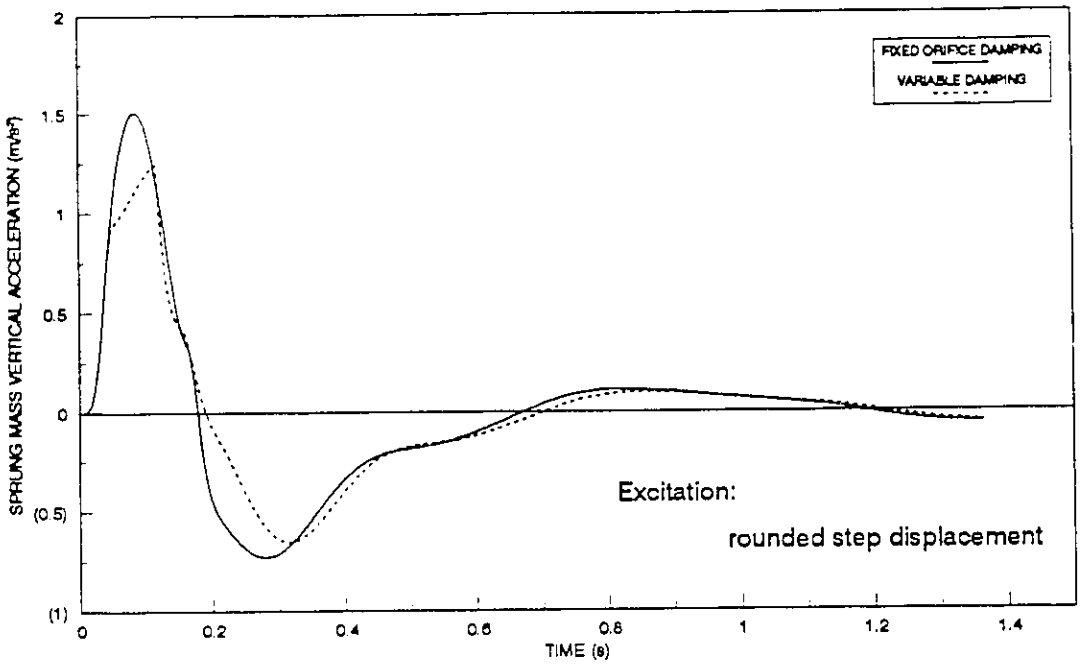

Figure 5.11 Vertical acceleration response of the sprung mass of an interlinkted suspension with fixed and variable orifice damping subject to a rounded step displacement excitation at tire-terrain interface

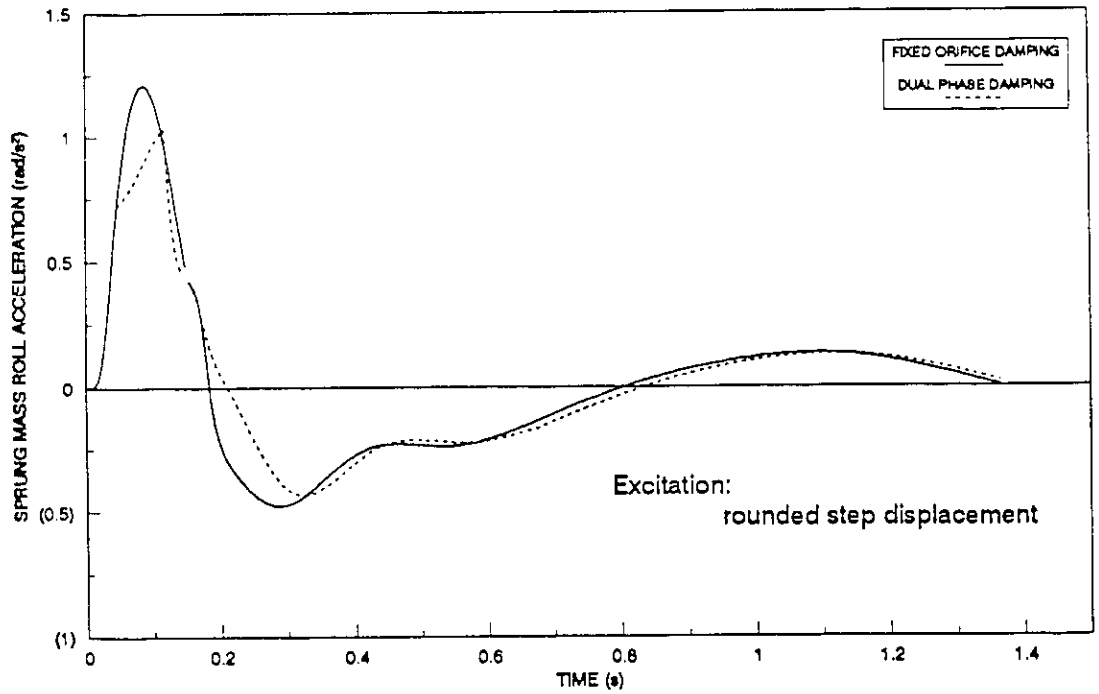

Figure 5.12 Roll acceleration response of the sprung mass of an interconnected suspension with fixed and variable orifice damping subject to a rounded step displacement excitation at tire-terrain interface

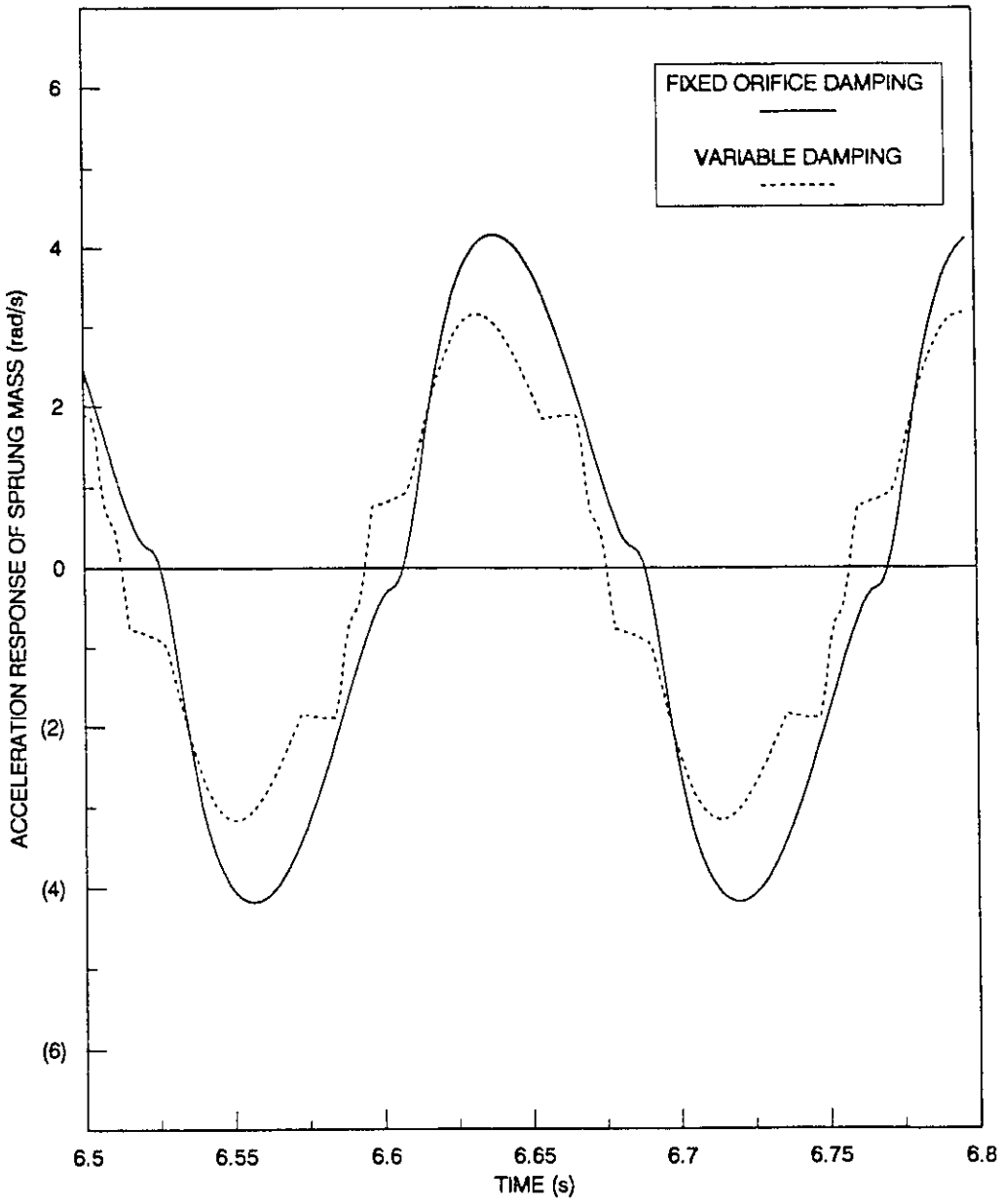

Figure 5.13 Comparison of steady state acceleration response

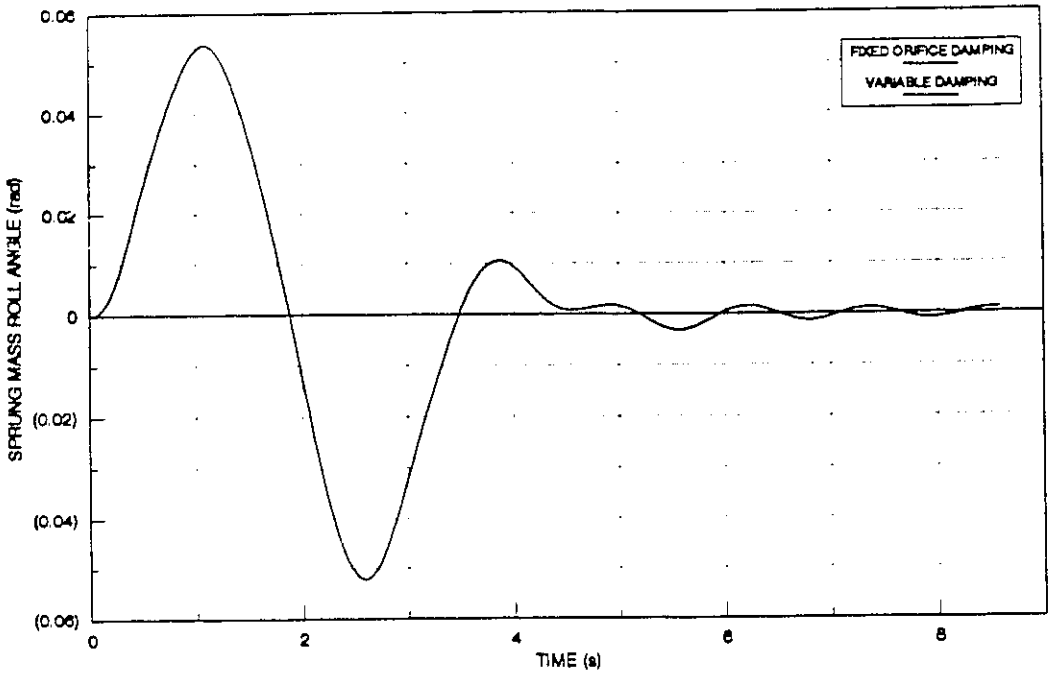

Figure 5.14 Roll angle response of the sprung mass of the vehicle employing IC-3 suspension with fixed and variable orifice damping subject to a transient lateral excitation during a lane change maneuver

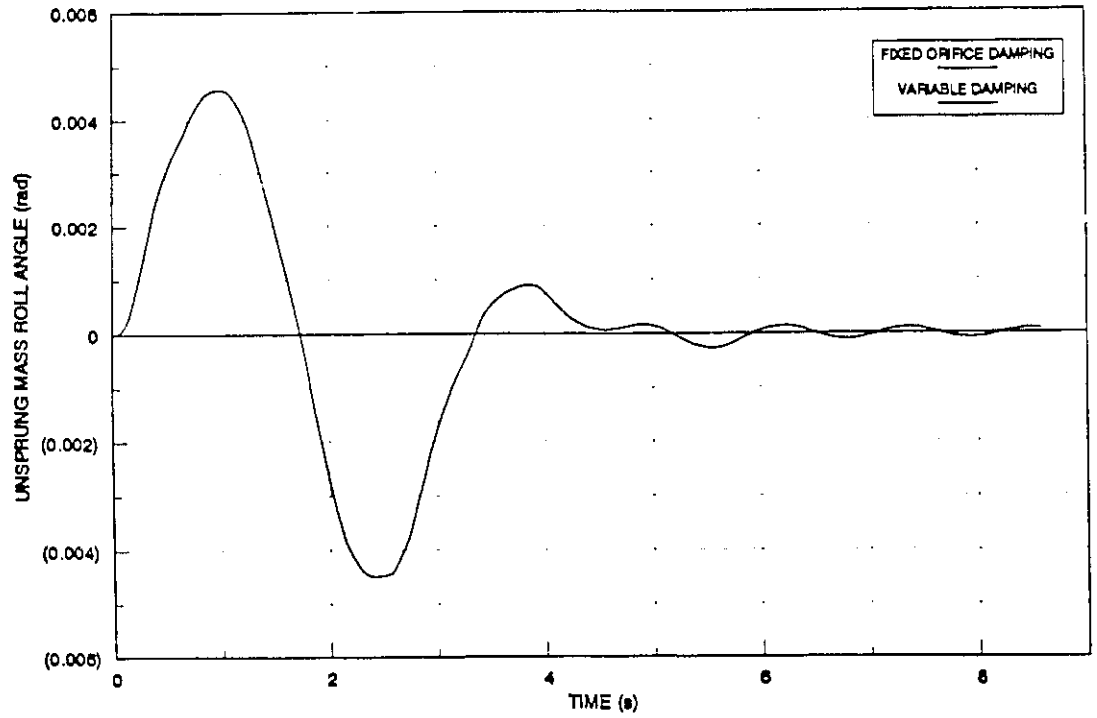

Figure 5.15 Roll angle response of the unsprung mass of the vehicle employing IC-3 suspension with fixed and variable orifice damping subject to a transient lateral excitation during a lane change maneuver

respectively. The reduction in peak vertical and roll acceleration responses of the variable damping suspension are attributed to the relatively low damping force developed by the multi-stage dampers.

While variable passive damping mechanism offer simple and reliable means to improve ride and handling performance characteristics, they tend to reduce the jerk associated with switching of the semi-active variable dampers [4]. Figure 5.13 illustrates the steady state roll acceleration response of sprung mass of the vehicle employing fixed and multi-stage orifice dampers, subjected to 0.01 m out-of-phase harmonic excitation at a frequency near 6 Hz. While the discontinuities in the acceleration response of the sprung mass with multi-stage dampers are evident, the associated jerk is negligible. The discontinuities in the response are attributed to sharp transitions of the damping parameter, shown in Figure 5.2. It should be noted that sharp transitions in the damping parameter occur due to assumptions made in the simple analysis. Such sharp transitions, however, do not exist in practice and the corresponding acceleration response can thus be expected to be relatively smooth.

The roll response characteristics of sprung and unsprung masses of the vehicle employing the interconnected suspension with fixed and multi-stage dampers are presented in Figures 5.14 and 5.15, for excitations arising from a typical lane change maneuver. The roll response of the interconnected suspension with multi-stage dampers is identical to that with fixed orifice dampers due to low velocities across the struts. The results clearly demonstrate that the multi-stage damping does not deteriorate the handling response of the vehicle.

5.4 FREQUENCY RESPONSE CHARACTERISTICS

The vibration attenuation characteristics of the interconnected suspension with fixed and multi-stage orifice dampers are evaluated in terms of vertical displacement and roll angle transmissibility of sprung and unsprung masses. The vertical and roll response characteristics are evaluated for 0.01 m in-phase and out-of-phase displacement excitations, respectively. The transmissibility characteristics are computed as the ratio of steady state response amplitude to the constant excitation amplitude at each excitation frequency, as described in Section 4.5. Displacement transmissibility characteristics of the sprung and unsprung masses of the vehicle with fixed and multi-stage orifice dampers are illustrated in Figures 5.16 and 5.17, respectively. The transmissibility characteristics exhibit two peaks corresponding to vertical mode natural frequencies of the sprung and unsprung masses. The vertical displacement response of the sprung mass with multi-stage dampers is identical to that with the fixed orifice dampers when excitation frequencies are less than 2.2 Hz. The vertical displacement response of the sprung mass with multi-stage dampers, however, is considerably reduced for higher excitation frequencies due to its reduced damping. The displacement transmissibility of the sprung mass is as high as 1.05 near the natural frequency of the unsprung mass with fixed orifice damping, while the corresponding transmissibility with the variable damper is approximately 0.27. The displacement response of the unsprung mass corresponding to its natural frequency, however, increases slightly when variable damping is used, as shown in Figure 5.17. The natural frequencies of the unsprung masses are also quite different in two cases. The high damping rate of the fixed orifice damper at higher excitation frequencies tends to reduce the unsprung mass natural frequency to 3.5 Hz. The natural frequency of the unsprung mass of the vehicle with variable damping is observed to be near 6.3

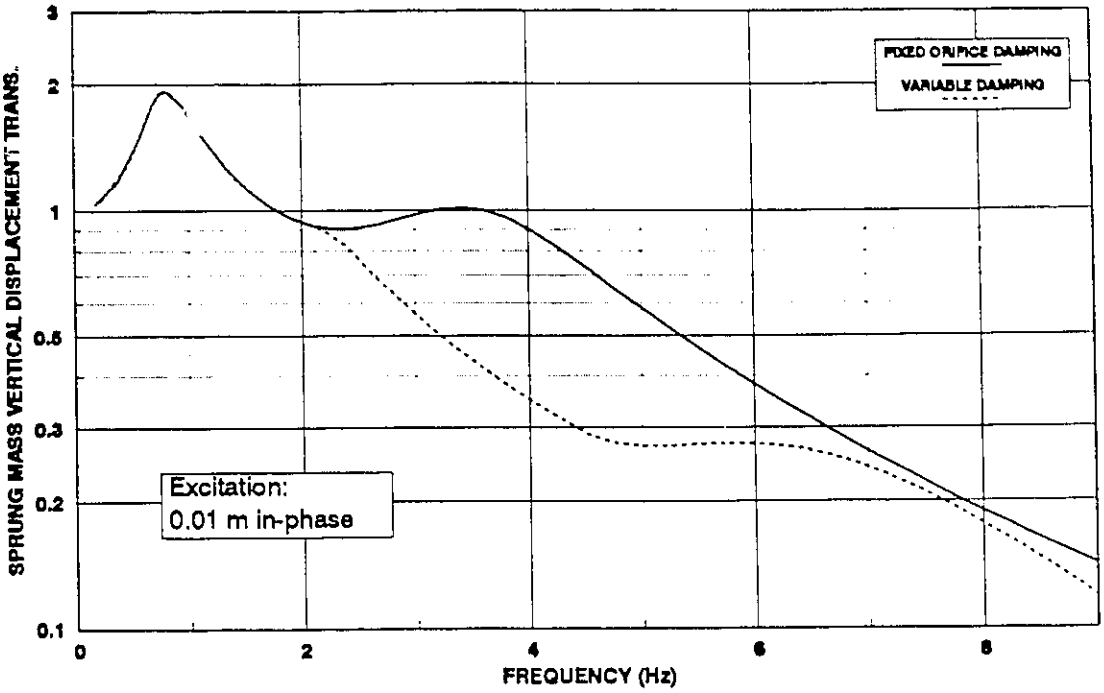

Figure 5.16 Vertical displacement transmissibility of the sprung mass of the vehicle with fixed and variable orifice damping for 0.01 m in-phase excitation

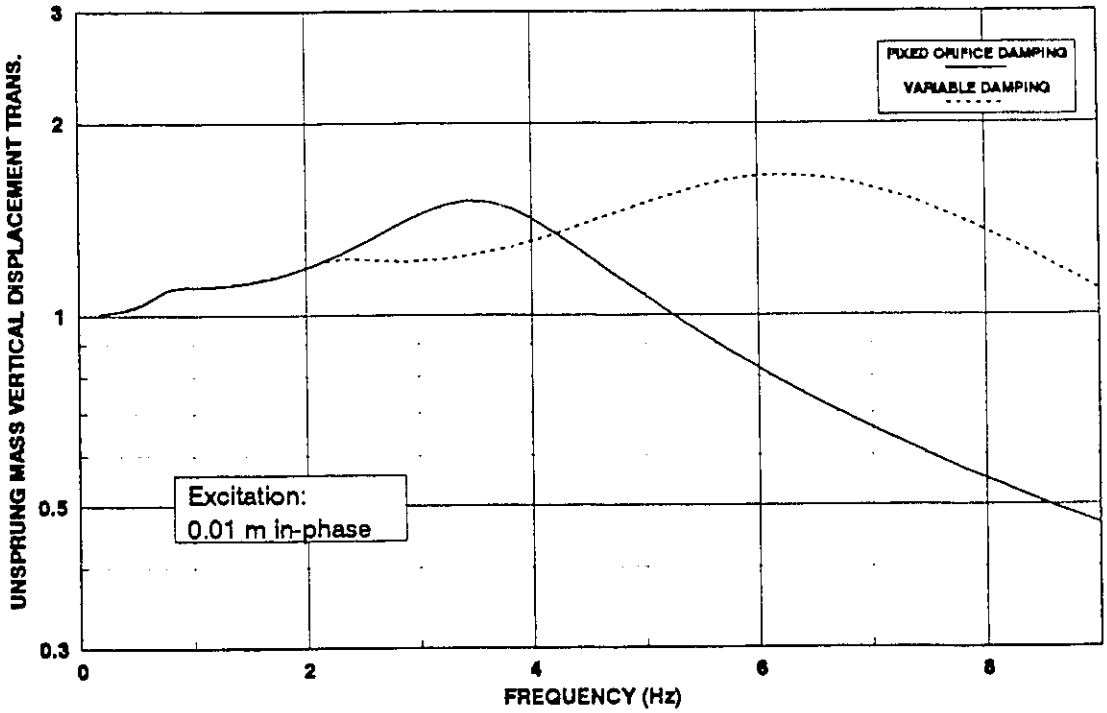

Figure 5.17 Vertical displacement transmissibility of the unsprung mass of the vehicle with fixed and variable orifice damping for 0.01 m in-phase excitation

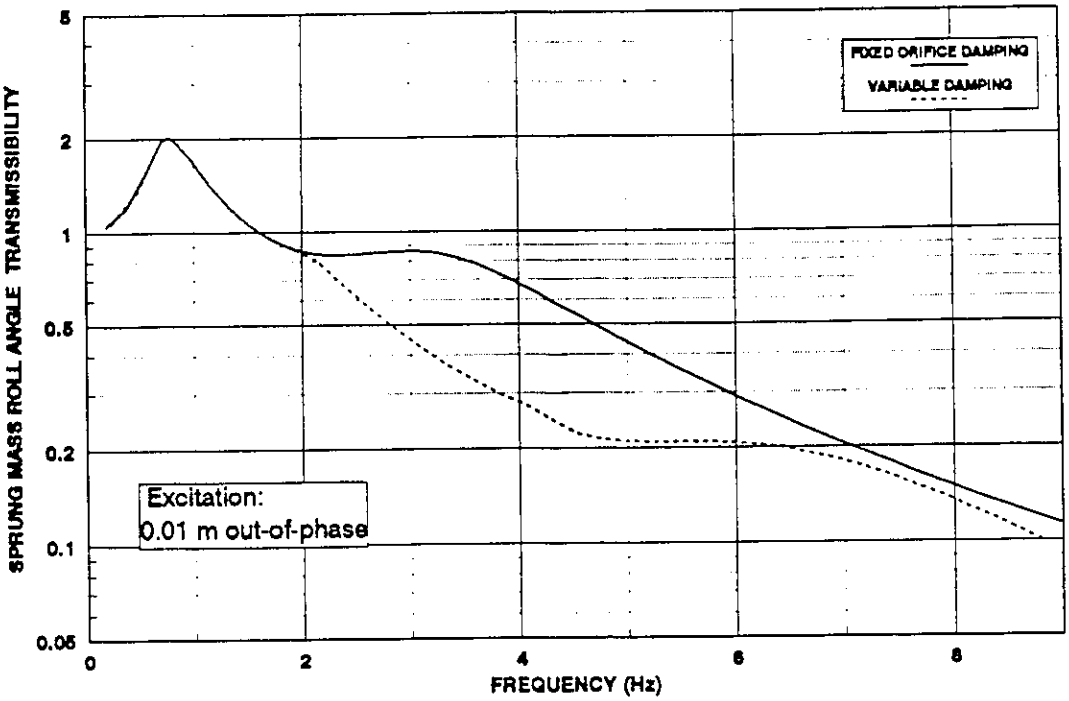

Figure 5.18 Roll angle transmissibility of the sprung mass of the vehicle with fixed and variable orifice damping for 0.01 m out-of-phase excitation

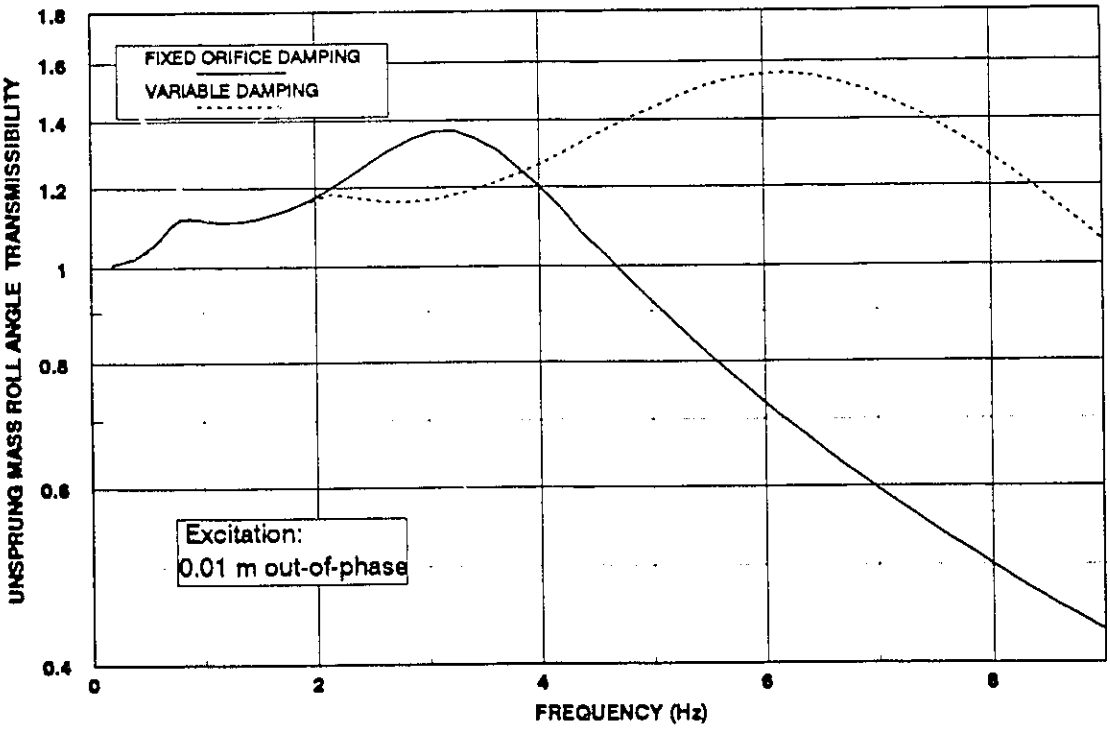

Figure 5.19 Roll angle transmissibility of the unsprung mass of the vehicle with fixed and variable orifice damping for 0.01 m out-of-phase excitation

Hz. Figure 5.16 clearly demonstrates that vibration isolation performance of interconnected suspension can be significantly improved by using multi-stage dampers.

Roll angle transmissibility characteristics of sprung and unsprung masses of interconnected suspension with fixed and multi-stage orifice dampers are presented in Figures 5.18 and 5.19. The roll displacement transmissibility response characteristics are quite similar to those described in Figures 5.16 and 5.17. The roll angle response of the sprung mass with multi-stage dampers is identical to that with the fixed orifice dampers, when excitation frequencies are less than 1.9 Hz. At excitation frequencies beyond 1.9 Hz, the pressure control valves in the multi-stage dampers offer light damping by modulating the damping area. The corresponding roll response of the sprung mass is thus considerably lower than that due to fixed orifice damping. The resonant frequency of the unsprung mass of the vehicle with variable damping is near 6.1 Hz. The corresponding frequency of the unsprung mass with high constant orifice damping is about 3.2 Hz. The light damping due to variable dampers results in unsprung mass roll angle response considerably larger than that of the unsprung mass with fixed orifice damping, as shown in Figure 5.19.

5.5 STOCHASTIC RESPONSE ANALYSIS OF THE INTERCONNECTED SUSPENSION

While deterministic excitations are effectively used to carry out relative performance characteristics of different suspension designs, the ride performance of a vehicle suspension needs to be assessed for realistic random road excitations. It has been established that the road surface irregularities are approximately Gaussian distributed [53, 54]. The road roughness can thus be described either by its profile or by its statistical properties, such as power

spectral density (PSD) function. The stochastic response analysis of nonlinear systems, in general, involves various complexities. Since exact solutions of nonlinear systems subject to random excitations are limited to only few classes of nonlinearities, many approximate or numerical techniques have been developed to predict the response behavior of nonlinear systems subjected to random excitations [55-58]. These method can be classified as: (1) Markov methods; (2) perturbation method; (3) equivalent linearization methods; and (4) simulation methods.

When the future state of a system response process only depends on the most recently known state, the process is called Markov process. A Markov random process is completely described in terms of the first and transition probability densities [58]. The response characteristics of a system with Markov process properties can be explored using Fokker-Planck equation. The exact solutions of Fokker-Planck equation, however, have been limited to a special class of nonlinear functions [57]. Although a number of techniques have been developed to obtain approximate solutions of the Fokker-Planck equation, the Fokker-Planck equation of dynamic systems with nonlinearities involving velocities, or inertial or damping coupling between the general coordinates, still remain to be solved [59, 60].

The perturbation method is an effective technique to analyze dynamic systems with weak nonlinearities. In this approach, the magnitude of non linearity is assumed to be controlled by a small perturbation parameter ε. The solution of the nonlinear equation of motion is expressed by a power series of the perturbation parameter ε. Substituting the power series solution into the original equation of motion and equating the coefficients of like powers of ε, a hierarchy of linear differential equations are obtained and solved sequentially using linear theory [57].

The equivalent linearization techniques, invariably, approximate the nonlinear system by an equivalent linear system, such that the linearized response behavior does not deviate significantly from that of the nonlinear system. Thomson [61] developed a deterministic linearization method based on energy similarity, where equivalent linear damping coefficient is evaluated by equating the energy dissipated per cycle of the linear damping element to that of the nonlinear damper. This simple approach has also been used to approximate random response of nonlinear systems [62]. Statistical linearization technique, where the nonlinear stiffness and damping elements are replaced by optimal linear elements, have been extensively used for stochastic response analysis. The linear elements are selected by minimizing the mean square errors between the nonlinear and linear response [57]. Rakheja et al. [63, 64] proposed a local equivalent linearization method, based on principle of energy similarity, to characterizes the nonlinear damping by an array of local damping constants as function of local excitation and amplitude, response and type of nonlinearity. Su [4] extended the local equivalent method to deal with nonlinear elastic elements.

The simulation techniques can be generally applied to almost all types of nonlinear systems. The technique, in general, involves: (i) generation of sample functions of the excitation process; (ii) computation of the corresponding sample functions of the response process; and (iii) determination of the desired response characteristics through statistical analyses. For stationary, ergodic processes, the method is simplified due to the fact that temporal averaging needs only one input/output realization of sufficient duration. The vehicle model with interconnected suspension exhibits strong nonlinearities associated with orifice flows, gas springs, damping valves and the coupling effects between the left and right struts. The methods based on Fokker-Planck equation, perturbation analysis, and equivalent linearization can not be applied. The simulation method

is, therefore, used to evaluate the vibration isolation performance of interconnected suspension under random excitations.

The first step in the simulation method is to generate an excitation process representing road surface irregularities. Roadway surface profiles have been extensively measured and expressed in terms of their PSD by various researchers [1, 65, 66, 67]. Although the PSD of every road section is known to be unique, majority of the roads exhibit a characteristic drop in the amplitude with wave number or frequency. Since offside and nearside wheels do not traverse identical profiles, the idea that road surfaces are isotropic are proposed to derive a coherence function describing the relationship between parallel tracks on a surface at a specific separation [65, 68]. Redfield [66] developed a method to create random road input for parallel tracks with desired statistics of track variance and parallel track covariance. The description of road surface using the spectral density of a single profile, however, has been accepted for predictions of vehicle ride response [65]. In this investigation, a single-profile model is thus used to assess the stochastic ride response of the vehicle model employing the interconnected suspension.

5.5.1 Road Excitation Process

The power spectral density of different road surfaces has been related to the vehicle speed in the following manner [69, 70]:

$$S(\omega)=\left(\frac{\sigma_1^2}{\pi}\right)\left[\frac{\lambda_1 v}{\omega^2+\lambda_1^2 v^2}\right]+\left(\frac{\sigma_2^2}{\pi}\right)\left[\frac{\lambda_2 v(\omega^2+\lambda_2^2 v^2+\tau^2 v^2)}{(\omega^2+\lambda_2^2 v^2-\tau^2 v^2)^2+4\lambda_2^2\tau^2 v^4}\right] \qquad (5.7)$$

where $S(\omega)$ is the PSD of road roughness; ω denotes the angular frequency; v is the vehicle velocity; $\lambda_1, \lambda_2, \tau, \sigma_1^2$ and σ_2^2 are coefficients depending on the type of road or terrain and are presented in Table 5.1. Figure 5.20 illustrates the PSD

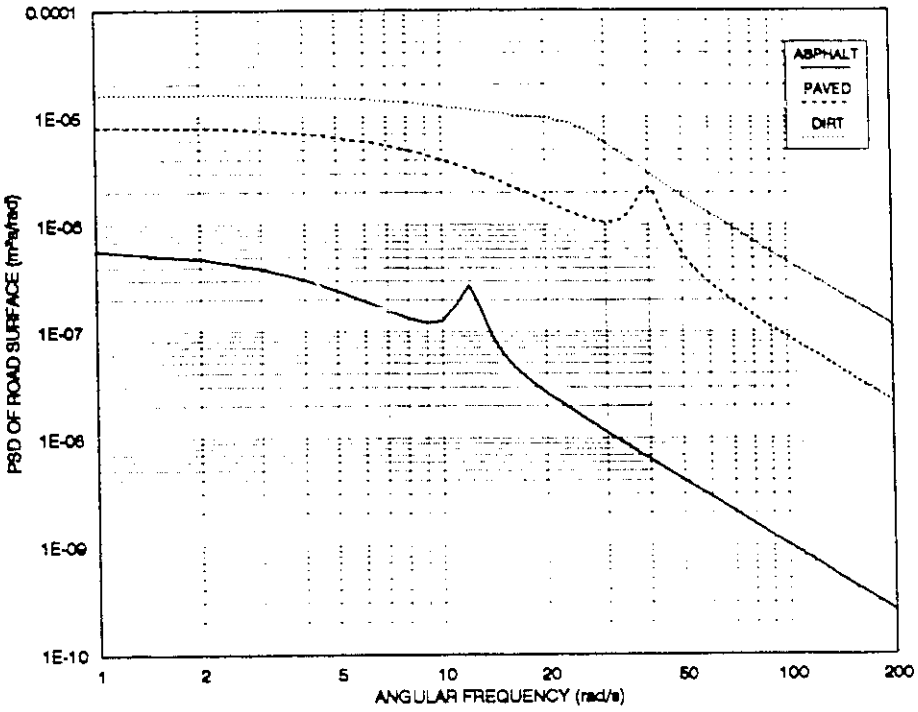

Figure 5.20 Power spectral densities for different types of roads

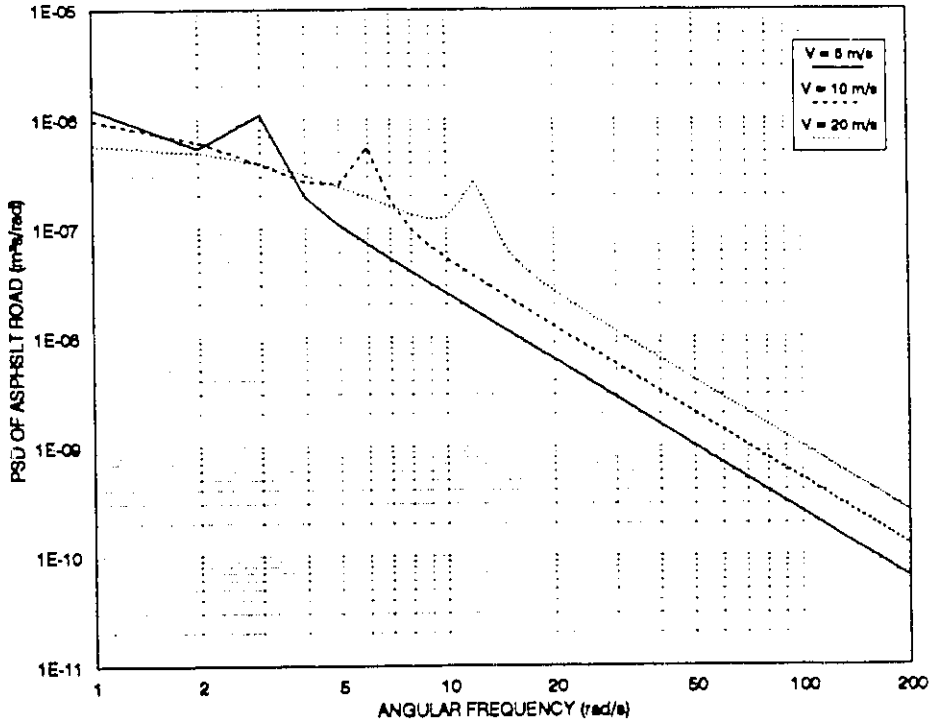

Figure 5.21 Power spectral densities for an asphalt road at different vehicle velocities

of different road surfaces, and the PSD of an asphalt road is presented in Figure 5.21, as a function of the vehicle forward speed v. From Figure 5.21, it is evident that the PSD of road excitation and the frequency corresponding to peak PSD increase with an increase in the vehicle speed.

Table 5.1

Values of parameters describing road surface spectrum

Type of road	$\lambda_1[rad/m]$	$\lambda_2[rad/m]$	$\tau[rad/m]$	$\sigma_1^2[m^2]$	$\sigma_2^2[m^2]$
asphalt	0.2	0.05	0.6	7.65×10^{-6}	1.35×10^{-6}
paved	0.5	0.2	2.0	2.55×10^{-4}	4.5×10^{-5}
dirt	0.8	0.5	1.1	7.5×10^{-4}	2.5×10^{-4}

Equation (5.7) can be rewritten as

$$S(\omega)=\frac{b_1\omega^4+b_2\omega^2+b_3}{\omega^6+b_4\omega^4+b_5\omega^2+b_6} \tag{5.8}$$

where

$$b_1=\frac{v}{\pi}(\sigma_1^2\lambda_1+\sigma_2^2\lambda_2)$$

$$b_2=\frac{v^3}{\pi}[2\sigma_1^2\lambda_1(\lambda_1^2-\tau^2)+\sigma_2^2\lambda_2\lambda_1^2+\sigma_2^2\lambda_2(\lambda_2^2+\tau^2)]$$

$$b_3=\frac{v^5}{\pi}\lambda_1(\lambda_2^2+\tau^2)[\sigma_1^2(\lambda_2^2+\tau^2)+\sigma_2^2\lambda_1\lambda_2]$$

$$b_4=v^2(\lambda_1^2+2\lambda_2^2-2\tau^2)$$

$$b_5=v^4\{(\lambda_2^2-\tau^2)[2\lambda_1^2+(\lambda_2^2-\tau^2)]+4\lambda_2^2\tau^2\}$$

$$b_6=v^6\lambda_1^2(\lambda_2^2+\tau^2)^2$$

The stochastic excitations of a given road and vehicle speed can be generated through derivation of a linear filter subject to band-limited white noise

excitation. The filter transfer function, $H(\omega)$, is selected such that its output is equal to the PSD defined in Equation (5.7) or (5.8). Let S_0 denote the power spectral density of the band-limited white noise, the desired road PSD can then be related to the frequency response function of the filter in the following manner:

$$S(\omega) = |H(\omega)|^2 S_0 \tag{5.9}$$

The linear filter is characterized by the third order differential equation of the form:

$$\eta_0 \dddot{x} + \eta_1 \ddot{x} + \eta_2 \dot{x} + \eta_3 x = \eta_4 \ddot{\varsigma} + \eta_5 \dot{\varsigma} + \eta_6 \varsigma \tag{5.10}$$

where $\eta_0, \cdots, \eta_6$ denote the coefficients; ς is the amplitude of white noise input, and $\dot{\varsigma}$ and $\ddot{\varsigma}$ are the first and second derivatives, respectively; x denotes the desired random road excitation. The transfer function of the linear filter defined in Equation (5.10) is derived as:

$$H(\omega) = \frac{\eta_6 - \eta_4 \omega^2 + \eta_5 \omega i}{\eta_3 - \eta_1 \omega^2 + (\eta_2 \omega - \eta_0 \omega^3) i} \tag{5.11}$$

Equation (5.9) can thus be rewritten as

$$S(\omega) = \frac{\eta_4^2 \omega^4 + (\eta_5^2 - 2\eta_6 \eta_4)\omega^2 + \eta_6^2}{\eta_0^2 \omega^6 + (\eta_1^2 - 2\eta_2 \eta_0)\omega^4 + (\eta_2^2 - 2\eta_3 \eta_1)\omega^2 + \eta_3^2} S_0 \tag{5.12}$$

The filter coefficients $\eta_0, \cdots, \eta_6$ are then obtained from Equations (5.8) and (5.12):

$$\eta_0 = 1$$

$$\begin{cases} \eta_1^2 - 2\eta_2 = b_4 \\ \eta_2^2 - 2\sqrt{b_6}\,\eta_1 = b_5 \end{cases}$$

$$\eta_3 = \sqrt{b_6}$$

$$\eta_4 = \sqrt{b_1 / S_0}$$

$$\eta_5 = \sqrt{(b_2 + 2\sqrt{b_1 b_3}) / S_0}$$

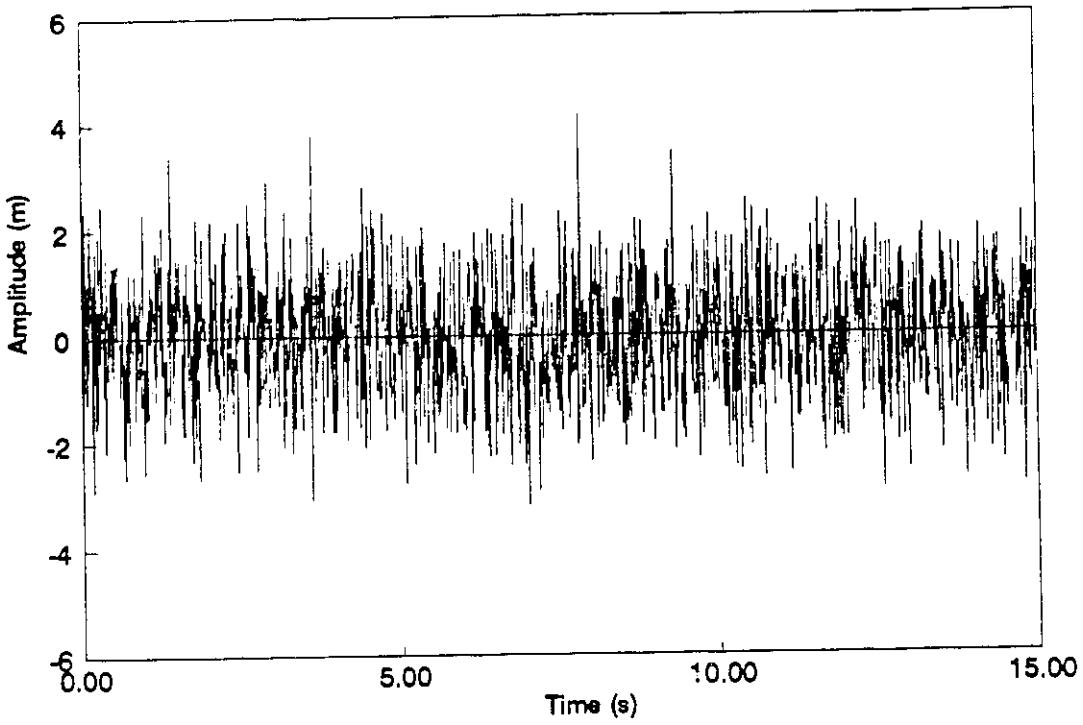

Figure 5.22 Band-limited white noise input

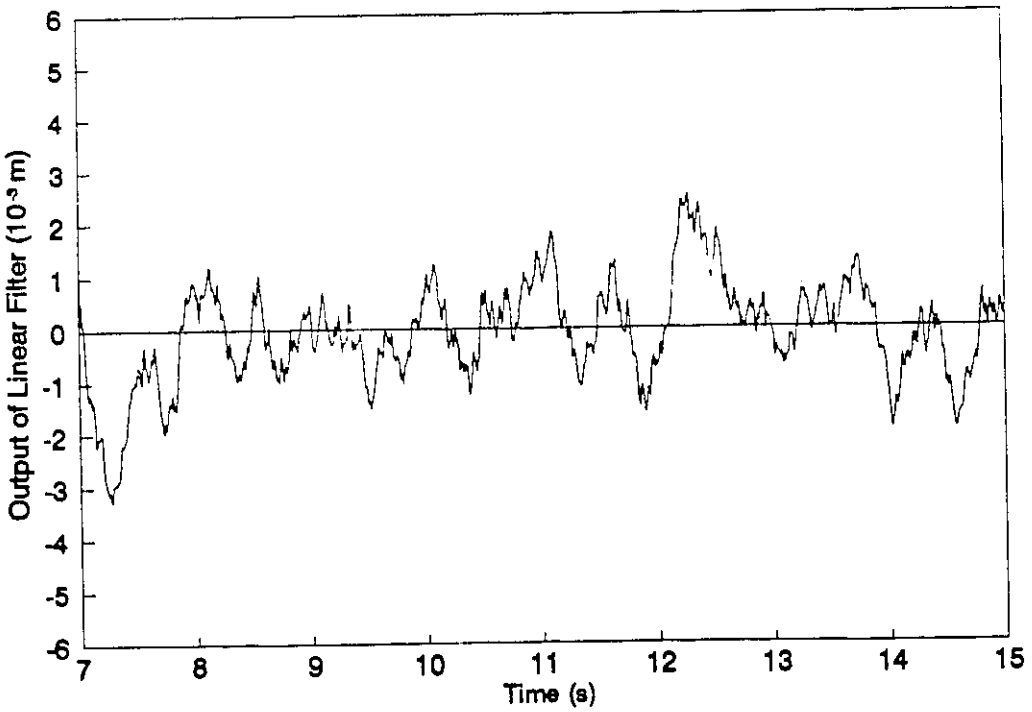

Figure 5.23 Output of linear filter

$$\eta_6 = \sqrt{b_3 / S_0} \tag{5.13}$$

The output of the above filter, subjected to a sample function of band-limited white noise, represents the random excitation of the specified road surface corresponding to vehicle speed v in the time domain. The random response of the interconnected suspension system can then be evaluated using numerical integration. The random response in the time domain can be expressed by its PSD using a Fast Fourier Transform (FFT) algorithm.

The proposed filter design is used to generate the random excitation due to asphalt and dirt roads. The PSDs of road excitations are compared to those derived from Equation (5.7) in order to validate the filter design. A Gaussian distributed white noise with zero mean value and 64 Hz cut-off frequency is generated using a random signal generator, as shown in Figure 5.22. The filter coefficients corresponding to $v = 20$ m/s are computed using Equation (5.13), and the filter output is obtained from direct integration of Equation (5.10). Figure 5.23 illustrates the linear filter response that represents the displacement excitations due to an asphalt road for $v = 20$ m/s. Figure 5.24 presents a comparison of the PSD estimation of the filter output and the PSD derived from Equation (5.7) for asphalt and dirt roads. The comparison clearly illustrates that the random road roughness can be accurately estimated from the linear filter design.

5.5.2 Random Ride Response

Ride response characteristics of the vehicle model employing the interconnected suspension, subjected to random road excitations, are evaluated in terms of PSD of vertical acceleration of the sprung mass. The equations of motion of the vehicle model, derived in Chapter 2, are solved for random road excitations generated from the linear filter shown in Figure 5.23. The PSD of the

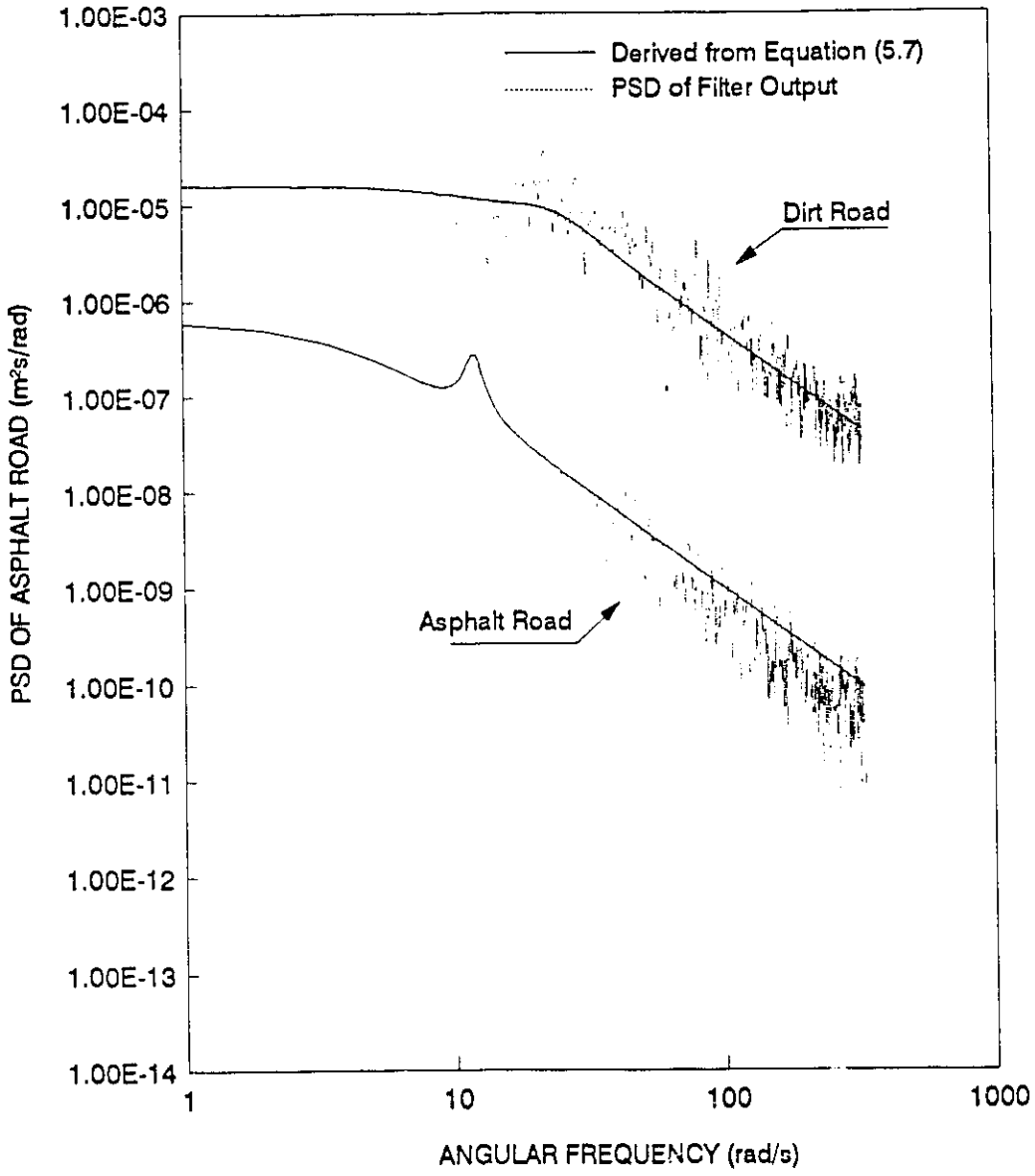

Figure 5.24 Comparison of road PSD derived from equation 5.7 and PSD of filter output

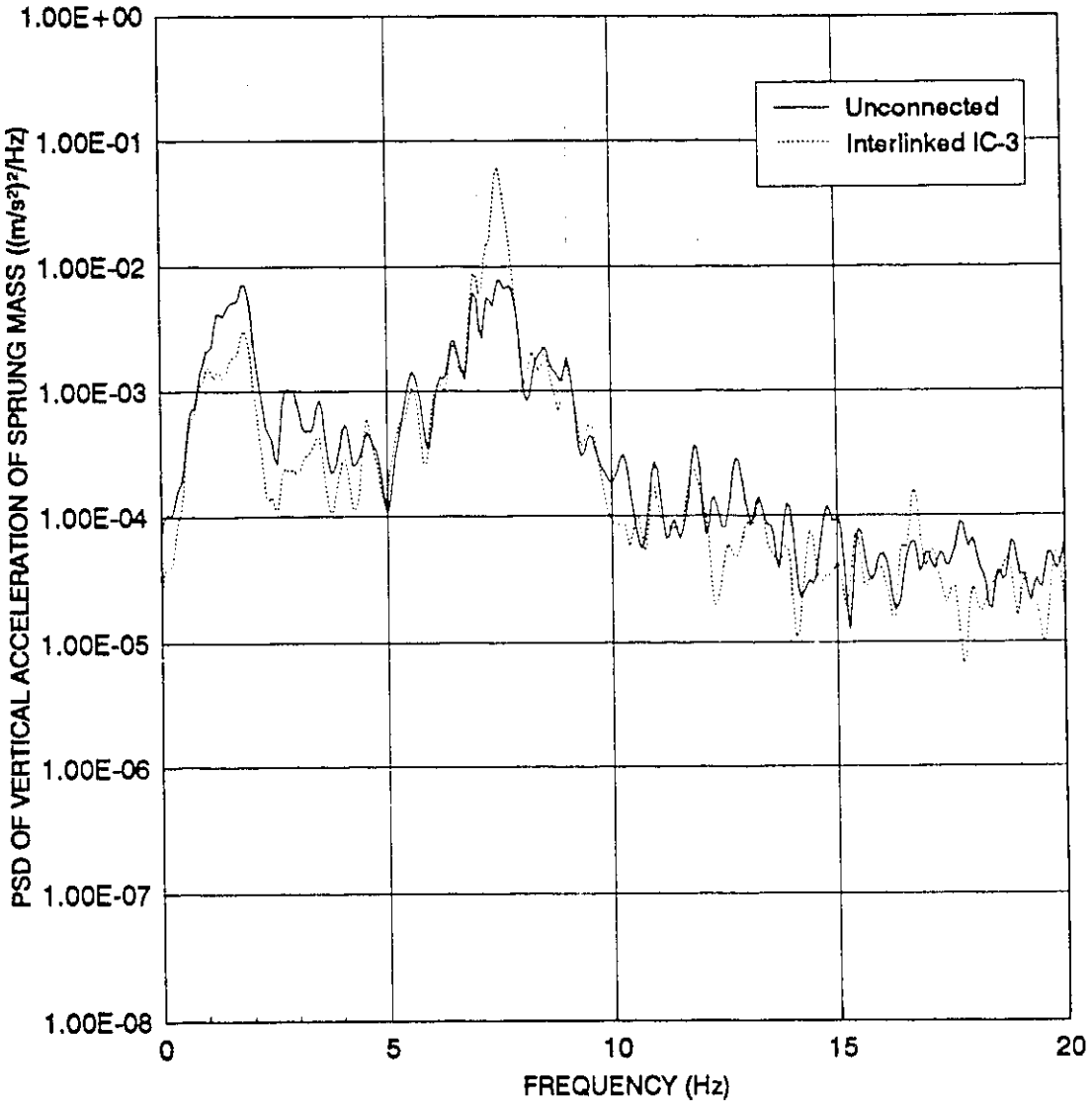

Figure 5.25 PSD of vertical acceleration response of the sprung mass of the vehicle with different suspensions subject to asphalt road excitation with v=20 m/s

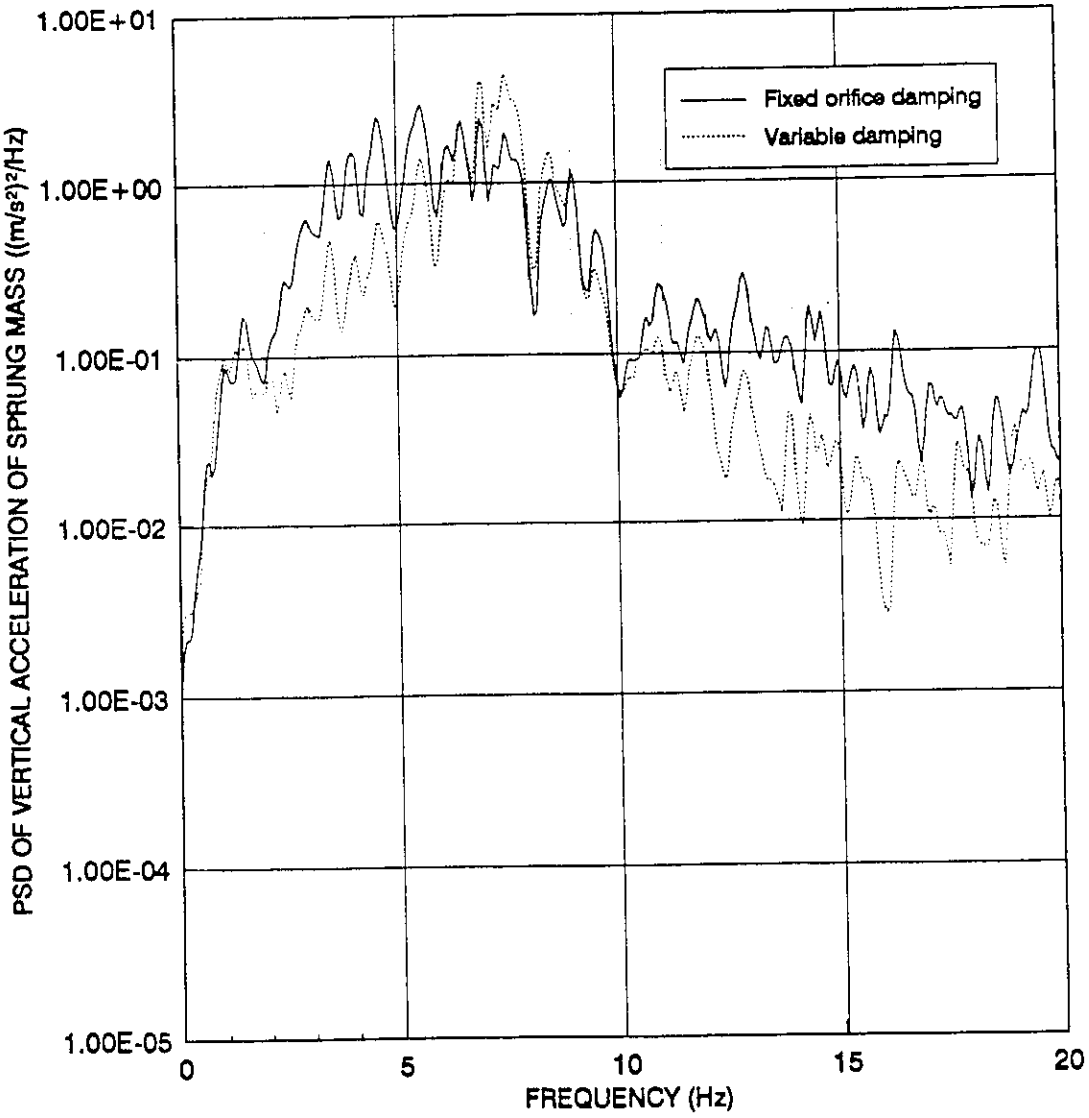

Figure 5.26 PSD of vertical acceleration response of the sprung mass of the vehicle with different dampers subject to dirt road excitation with v=20 m/s

sprung mass acceleration response is then estimated using an FFT algorithm. It should be pointed out that the random excitation data, derived from the output of the third order linear filter, demonstrates a peak value around 1.8 Hz for asphalt road with v=20 m/s (Figure 5.24). The vehicle response, therefore, also exhibits this characteristic with peak value around 1.8 Hz.

PSDs of vertical acceleration of the sprung mass of the vehicle employing interconnected IC-3 and unconnected suspensions with fixed orifice dampers, traveling on an asphalt road at a forward speed of 20 m/s, are illustrated in Figure 5.25. The response PSDs are presented in the 0-20 Hz frequency range, such that the ride performance of the suspension can be assessed. The acceleration PSD response of the interconnected suspension is lower than that of the unconnected suspension in the 1 to 5 Hz frequency range. The acceleration response of the interconnected suspension, however, exceeds the acceleration PSD response of the unconnected suspension near the natural frequency of unsprung mass 7.55 Hz. The interconnected suspension then yields slightly better vibration isolation performance beyond the natural frequency of unsprung mass. It should be noted that only bounce mode is excited for the single profile excitation considered in this study. In the pure bounce mode, the flows through interconnecting pipes are relatively insignificant. The interconnected suspension thus behaves similar to the unconnected suspension. The IC-3 suspension under pure bounce motion is equivalent to the unconnected suspension with lower suspension rate and light damping, as described earlier in Chapter 3. The ride performance benefits of the IC-3 suspension, however, are evident.

. Vertical acceleration PSD of sprung mass of the vehicle employing interconnected IC-3 with fixed and multi-stage damping characteristics, traveling on a dirt road with a forward speed of 20 m/s, are shown in Figure 5.26. The first

stage orifice area of the variable damper is selected to be identical to that of fixed orifice damper in order to demonstrate the effectiveness of the multi-stage damper. The bounce acceleration response of the vehicle with variable dampers is identical to that of the vehicle with fixed orifice damper at low excitation frequencies. Since the relative velocity response and thus the pressure differential across the damper is small at low frequencies, the damping characteristics of the variable dampers are similar to those of the fixed orifice dampers due to closed control valves. However, as the excitation frequency increases, the control valves begin to modulate the damping rate. The multi-stage dampers thus yield lower acceleration response in the 1.5 to 6.5 Hz range due to reduced damping. Although the acceleration response of the variable damping suspension is slightly larger around the natural frequency of the unsprung mass, the response is considerably reduced beyond the unsprung mass natural frequency. It can be therefore concluded that the bounce acceleration PSD of the vehicle can be significantly improved by using the multi-stage dampers.

5.6 SUMMARY

Based on damping requirements of ride comfort and handling, a tunable multi-stage damper is proposed to achieve improved overall performance of a interconnected suspension. Upon selecting suitable damping parameters and the tuning factor, a multi-stage damper can provide high damping around natural frequency of the sprung mass, light damping in the middle range of excitation frequencies, and high damping around and beyond the natural frequency of the unsprung mass. Moreover, it is possible to maintain high damping during turning and lane change maneuvers to achieve good handling performance. Vibration isolation performance characteristics of an interconnected suspension

incorporating multi-stage damper are investigated using computer simulation for deterministic and random excitations. The simulation results clearly reveal that vibration isolation performance of the vehicle can be improved by using the multi-stage dampers.

CHAPTER 6

CONCLUSIONS AND RECOMMENDATIONS FOR FUTURE WORK

6.1 GENERAL

The passenger ride comfort and vehicle handling performance pose conflicting requirements on the suspension design, which often results in a compromise between the two design goals. The handling and directional control characteristics constitute the primary design considerations for heavy vehicle suspensions, while the ride quality receives the secondary consideration. The heavy vehicle suspensions are thus designed to yield high roll stiffness to enhance highway safety through improved handling and control performance. Such suspension designs, however, yield poor ride performance. In this dissertation, a concept of hydro-pneumatic suspension interconnected in the roll plane is thoroughly investigated to achieve an improved compromise between the ride and handling performance characteristics of a heavy vehicle.

The primary objectives of this study included: (i) development of a model of the proposed interconnected suspension system in the roll plane; (ii) development of methodologies to evaluate the static and dynamic properties of the interconnected suspension; (iii) evaluation of roll and ride dynamic potentials of the proposed suspension by comparing its properties to those of conventional suspensions; and (iv) analysis of the proposed suspension with multi-stage orifice damping to further improve its ride performance. The major highlights of the study and the conclusion drawn are discussed in the following sections.

6.2 MAJOR HIGHLIGHTS OF THIS INVESTIGATION

The major highlights of this investigation are summarized below:

(1) The concept of a hydro-pneumatic suspension, interconnected in the roll plane, is discussed in view of its ride and roll performance potentials. Three different hydro-pneumatic beam-axle suspension systems, namely, unconnected, unconnected with anti-roll bars, and interconnected, are described and analytically modeled in the roll plane of the vehicle. The mechanics of anti-roll bars is described and expressed analytically. The roll plane dynamics of a heavy vehicle with three suspension systems are represented by a four-degrees-of-freedom model subject to excitations arising from road irregularities and directional maneuvers. The dynamic suspension forces are derived assuming incompressible fluid in hydraulic struts, turbulent flows through the orifice restrictions, polytropic process of gas in accumulators, and laminar flows through the interconnecting pipes.

(2) The static and dynamic properties of the three suspension systems are derived analytically and compared in terms of load-carrying capacities, suspension rates, roll stiffness rates and damping forces. The roll stiffness amplification factor of the interconnected suspension is proposed and derived.

(3) Five different suspension configurations, including an unconnected, unconnected with anti-roll bar, and three interconnected (IC-1, IC-2, and IC-3) suspensions, are proposed based on the same load-carrying capacity and suspension rate (IC-3). The fundamental properties of these five suspension systems are evaluated, compared and discussed.

(4) The ride and handling performance characteristics of five hydro-pneumatic suspensions are investigated using numerical integration approach for deterministic excitations. The natures of excitations arising from tire-terrain interactions and steering inputs are described. The roll performances of the suspension systems are evaluated in terms of the

transient and steady state roll response of the sprung and unsprung masses during constant radius turning and lane changing maneuvers. The dynamic ride performance characteristics are established in terms of both heave and roll shock isolation response of the suspensions subjected to road excitations. Transmissibility characteristics of different suspensions are investigated using harmonic excitations arising from tire-terrain interactions.

(5) A variable damping mechanism is integrated to achieve improved vibration isolation performance of the interconnected hydro-pneumatic suspension system. Dynamic ride performance characteristics of the interconnected suspension with variable dampers are evaluated in terms of transient vertical and roll velocities and accelerations. Frequency response characteristics of the interconnected suspension with variable and fixed orifice dampers are further investigated in terms of displacement and roll angle transmissibility characteristics of sprung and unsprung masses in order to demonstrate the effectiveness of the variable dampers.

(6) Various approaches to analyze stochastic response of nonlinear dynamic systems are briefly reviewed. The spectrum of road surface irregularities is approximately modeled by a rational function and a linear filter is designed to generate random road excitations in the time domain. The random response characteristics of the interconnected suspension are evaluated using numerical integration and discrete FFT algorithm in terms of bounce acceleration PSD of the sprung mass.

6.3 CONCLUSIONS

Based on the studies carried out in this thesis work, the following conclusions can be drawn:

- The vibration isolation and handling performance characteristics of the interconnected hydro-pneumatic suspension can be effectively investigated from the roll plane model of the vehicle.
- An anti-roll bar can be modeled as a torsion spring, which introduces an auxiliary roll stiffness when sprung mass experiences a relative roll motion with respect to unsprung mass.
- The interconnected struts generate coupling or feedback effects, which influence both static and dynamic properties of the interconnected suspension.
- Suspension rate of the interconnected hydro-pneumatic suspension is proportional to the square of the piston rod area, whereas that of the unconnected suspension is proportional to the square of the piston head area.
- The interconnected suspension exhibits an inherent anti-roll capability, which can be expressed by a roll stiffness amplification factor determined from the strut configurations.
- Unlike unconnected suspensions, interconnected suspensions yield higher damping in the roll mode than that in the bounce mode.
- High suspension damping tends to improve vehicle handling performance, while light suspension damping yields improved shock attenuation performance.
- A vehicle suspension with softer bounce rate and enhanced roll stiffness can be achieved from the interconnected struts.
- The interconnected suspension can thus provide a better compromise between handling performance and ride comfort.

- The interconnection technique has significant effect on restricting body roll motion due to the enhanced roll stiffness of the interconnected suspension.
- While anti-roll bars effectively restrict the body roll moment, they tend to increase the roll response of the vehicle subject to a single-wheel bump.
- The fixed orifice suspension damping yields unsatisfactory ride performance of the vehicle. Multi-stage damping can be achieved via modulating the pressure differential across the damper using pressure control valves.
- By selecting suitable preset pressure differential values, the multi-stage damper can provide firm damping around natural frequency of sprung mass, low damping in the frequency range between the resonance of the sprung and unsprung masses, and firm damping around and beyond the natural frequency of unsprung mass. The variable dampers further provide firm damping during vehicle directional maneuvers for good road holding performance.
- The multi-stage damping offers an improved shock and vibration isolation performance.
- Unlike semi-active on-off dampers, the multi-stage dampers can be realized passively without using sensors and signal processors. The jerk associated with 'on' and 'off' states of the on-off damper can be also eliminated by the passive damping mechanism.
- The simulation method used in this investigation is found to be effective to analyze the nonlinear dynamic system with displacement and velocity coupling under stochastic excitations.

– The random ride response of the interconnected suspension system clearly reveals that vibration isolation performance can be significantly improved by using the multi-stage damper.

6.4 RECOMMENDATIONS FOR FUTURE WORK

The thesis research is carried out to evaluate the roll and ride dynamic performance of an interconnected hydro-pneumatic suspension system. In view of the significant potentials demonstrated in this study, it is recommended tc undertake the following future works to further explore its performance potentials, and facilitate its realization and implementation.

❶ The analytical model of the interconnected suspension needs to be validated through fabrication and testing of a prototype. Efforts are needed to incorporate fluid compressibility, inlet and outlet flow losses of interconnecting pipes, and unsteady state flows in the roll plane vehicle model.

❷ A more elaborate three-dimensional vehicle model, incorporating fluid flow interconnections in the roll and pitch planes, should be developed and analyzed to assess the ride, anti-roll and anti-pitch characteristics of the vehicle suspension.

❸ The dynamic properties of the proposed multi-stage damper should be investigated, and a physical validation must be carried out for realization and application of such a damper.

❹ Stochastic excitations to the roll plane vehicle model should be generated by using more elaborate models describing the relationship between parallel tracks. Stochastic analysis of the roll plane vehicle model under such inputs should be carried out to evaluate the ride performance of the interconnected suspension with multi-stage dampers.

- An optimal design of interconnected hydro-pneumatic system should be carried out to achieve the best vibration isolation performance without deteriorating the handling performance.
- Efforts should be made to incorporate self-leveling ability of interconnected hydro-pneumatic suspension to achieve even better ride comfort and handling performance of the vehicle.

REFERENCES

1. Sharp, R. S, and Crolla, D. A, "Road Vehicle Suspension System Design - a review", Vehicle System Dynamics, 16, 1987, pp. 167-192.
2. Sharp, R. S, and Hassan, S. A. "An Evaluation of Passive Automotive Suspension Systems With Variable Stiffness and Damping Parameters," Vehicle Systems Dynamics, 15, 1986, pp. 335-350.
3. Sutton, H. B., "The Potential for Active Suspension Systems", IMechE 1979, pp. 21-23.
4. Su, H. "An Investigation of Vibration Isolation Systems Using Active, Semi-active and Tunable Passive Mechanisms with Applications to Vehicle Suspensions", Ph. D. Thesis, Concordia University, 1990.
5. Rakheja, S., Liu, P.J., Ahemed, A.K.W., and Su, H., "Analysis of an Interlinked Hydro-pneumatic Suspension", Proceedings of the ASME Winter Annual Meeting, New Orleans, LA, Nov. 28 - Dec. 3, 1993.
6. Pevsner, J.M., "Equalizing Types of Suspension", Automobile Engineer, January, 1957.
7. Bastow, B., "Car Suspension and Handling", 2nd Edition, Pentech Press Limited, London, 1987.
8. Moulton, A. E. and Best, A., "Rubber Springs and Inter-connected Suspension Systems", Engineering Design Show Conference, Paper No. 15a, 1970.
9. Moulton, A. E., and Best, A., "Hydragas Suspension", SAE Paper No. 790374.
10. Hartley, J., "Design Evaluation of the Moulton Hydragas Suspension", Engineering Materials and Design, June 1973, pp. 23-26.

11. Newton, K., "The Motor Vehicle", ISBN 0408010827, London; Boston: Butterworths, 1989.

12. Meller, T., "Self-Energizing Hydro-pneumatic Leveling Systems," SAE Paper No. 780052.

13. Felez, J., and Vera, C., "Bond Graph Assisted Models for Hydro-pneumatic Suspensions in Crane Vehicles," Vehicle System Dynamics, Vol. 16, 1987, pp. 313-332.

14. Tanahashi, H., Shindo, K., Nogami, T. and Onuma, T., "Toyota Electronic Modulated Air Suspension for the 1986 SOARER," SAE Paper 870541.

15. Horton, D.N.L., and Crolla, D.A., "Theoretical Analysis of a Semi-Active Suspension Fitted to an Off-Road Vehicle", Vehicle System Dynamics, Vol. 15, 1986, pp. 351-372.

16. Pitcher, R.H., "Technology Showcase Active Ride Control System", Journal of Terra mechanics, Vol. 22, No. 4, 1986, pp. 237-243.

17. Cotterell, M., "Theoretical Analysis of an Active Suspension Fitted to a London Transport Bus"

18. Crolla, D. A., and D. N. L. Horton, "Active Suspension Control for an Off-road Vehicle", Proc Instn Mech Engrs Vol. 201 No. D1, 1987.

19. Howard, A. B., "A Study of Control Algorithms for Active Suspension Systems", Technical Report, Royal Military College of Science, England, Nov., 1985.

20. Hedrick, J. k., "Invariant Properties of Automotive Suspensions", Proceedings of the Institution of Mechanical Engineers, Advanced Suspensions, C423/88, IMech E 1988-9, pp. 35-42.

21. Morman, K. N., and Giannopoulos, Jr. and F., "Recent Advances in the Analytical and Computational Aspects of Modeling Active and Passive

Vehicle Suspensions", Computational Methods in Ground Transportation Vehicles, AMD Vol. 50, 1982, pp. 75-115.

22. Sharp, R. S., and Hassan, S. A., "The relative performance Capabilities of Passive, Active and Semi-Active Car Suspension Systems", Proc Instn Engrs Vol. 200, No. D3, 1986, pp. 219-228.

23. Van Vliet, M., "Computer Aided Analysis and Design of Off-Road Motorcycle Suspensions, Ph.D. Thesis, Mechanical Engineering Department, Concordia University, 1983.

24. Asami, T., Sekiguchi, H., and Taniguchi, S., "Study on an Oil Damper with Variable Damping Mechanism", Bulletin of JSME, Vol. 28, No. 246, 1985, pp. 2978-2985.

25. Hundal, M. S., "Impact Absorber With Two-Stage Variable Area Orifice Hydraulic Damper", Journal of Sound and Vibration, 50(2), 1977, pp. 195-202.

26. Rakheja, S., Su, H., and Sankar, T., S., "Analysis of a Passive Sequential Hydraulic Damper for Vehicle Suspension", Vehicle System Dynamics, 19(1990), pp. 288-312.

27. Meller, T., and Fruhauf, F., "Variable Damping - Philosophy and Experiences of a Preferred System", Proceedings of the Institution of Mechanical Engineers (International Conference) Advanced Suspensions, C432/88, IMechE 1988-9, pp. 113-118.

28. Lijima, Y., "The Development of a High-Performance Suspension of the New Nissan 300ZX", SAE 841189.

29. Yokoya, Y., et at., "Toyota Electronic Modulated Suspension (TEMS) System for the 1993 Soarer", SAE 840341.

30. Soltis, M. W., "1987 Thunderbird Turbo Coupe Programmed Ride Control (PRC) Suspension", SAE 870540.

31. Rakheja, S., and Sankar, S., "Vibration and Shock Isolation Performance of a Semi-Active "on-off" Damper", ASME J. of Vibration, Acoustics, Stress and Reliability in Design 107, pp. 384-403, 1985.

32. Sireteanu, T., "The Effect of Sequential Damping on Ride Comfort Improvement", Vehicle Noise and Vibration, C145/84, I MECH E Conference Publications 1984-5.

33. Alanoly, J., and Sankar, S., "Vibration Isolation Performance of a Dual-Phase Shock Absorber/Damper", Int. J. of Vehicle Design, IAVD Congress on Vehicle Design and Components, 1987.

34. Decker, H., Schramm, W., and Kallenbach, R., "A Practical Approach towards Advanced Semi-Active Suspension Systems", Proceedings of the Institution of Mechanical Engineers (International Conference) Advanced Suspensions, C430/88, IMechE 1988-9, pp. 93-99.

35. Lizell, M., "Semi-Active Damping", Proceedings of the Institution of Mechanical Engineers (International Conference) Advanced Suspensions, C429/88, IMechE 1988-9, pp. 83-91

36. Paker, G. A., and Lau, K. S., "A Novel Valve for Semi-Active Vehicle Suspension Systems", Proceedings of the Institution of Mechanical Engineers (International Conference) Advanced Suspensions, C427/88, IMechE 1988-9, pp. 69-73.

37. Duchnowski, L. J., and Hann, S. A., "Modeling and Analysis of an Automobile Semi-Active Suspension", Advanced Automotive Technologies, DSC Vol. 13, ASME, 1989, pp. 321-334.

38. Hennecke, D., and Zieglmeier, F. J., "Frequency Dependent Variable Suspension Damping - Theoretical Background and Practical Success", Proceedings of the Institution of Mechanical Engineers (International

Conference) Advanced Suspensions, C431/88, IMechE 1988-9, pp. 101-111.

39. Margolis, D. L., and Goshtasbpour, M., "The Chatter of Semi-Active On-Off Suspension and its Cure", Vehicle System Dynamics 13, pp. 129-144, 1984.

40. Alanoly, J., "Vibration Isolation Characteristics of a Class of Semi-Active Suspensions", M. Thesis, Mechanical Engineering Department, Concordia University, 1985.

41. Crolla, D. A., "Active Suspension Control for an Off-Road Vehicle", Proceedings of the Institution of Mechanical Engineers, Vol. 201, 1987.

42. Thompson, A. G. et al., "Active Suspensions with Vibration Absorbers and Optimal Output Feedback Control", SAE 841253

43. Pollard, M. G., "Passenger Comfort - the Role of Active Suspensions", Pro. Instn. Mech. Engrs., Vol. 198D, No. 11, 1984

44. Karnopp, D. C., "Are Active Suspension Really Necessary?" ASME Paper No. 78-WA/DE-12, 1978.

45. Deminy, J., and Bulman, D. N., "An Active Suspension for a Formula One Grand Prix Racing Car", J. of Dyn. Sys. Meas. and Control., 107, 73-78, 1985.

46. Margolis, D. L., "The Response of Active and Semi-Active Suspension to Realistic Feedback Signals, Veh. Sys. Dyn. 11, 267-282, 1982.

47. Karnopp, D. C., Crosby, M.I., and Harwood, R.A., "Vibration Control Using Semi-Active Force Generators", Transactions of ASME, Journal of Engineering for Industry, Series B, Vol. 96, No. 2, pp. 619-626, May 1974.

48. Healey, A. J., "Digital Processing of Measure Vibration Data for Automobile Ride Evaluation", The Design Engineering Technical Conference, Chicago, Illinois, September 26-28, 1977.

49. "Measurement and Presentation of Truck Ride Vibrations", SAE J1490, Jan. 1987.

50. Rao, S. S., "Mechanical Vibrations", Addison-Wesley Publishing Company, 2nd Edition 1990.

51. Kevin B, Todd and Bohdan T. Kulakowski, "Handling Performance of Road Vehicles with Different Active Suspensions", Transportation Systems, AMD-Vol. 108, ASME, 1990, pp. 19-26.

52. Dixon, J. C., "Tires, Suspension and Handling", Cambridge University Press, 1991.

53. Roa, B. K. N., Jones, B., and Ashley, C., "Laboratory Simulation of Vibratory Road Surface Inputs", Journal of Sound and Vibration , Vol. 31, No. 2, 1973, 175-183

54. Robson, J. D., "Road Surface Description and Vehicle Response", International Journal of Vehicle Design, 1, 1979, 25-35

55. Roberts, J. B., "Response of Nonlinear Mechanical Systems to Random Excitation, Part I: Markov Methods", The Shock and Vibration Digest, Vol. 13, No. 4, 1981, 17-28.

56. Roberts, J. B., "Response of Nonlinear Mechanical Systems to Random Excitation, Part II: Equivalent Linearization and other Methods", The Shock and Vibration Digest, Vol. 13, No. 5, 1981, 15-28.

57. Nigam, N. C., "Introduction to Random Vibration", The MIT Press, 1983.

58. Sankar, T. S., "Random Vibrations", Class Notes for the Course of ENGR 733, Concordia University, Summer, 1992.

59. Ihrahim, R. A., and Robert, J. W., "Parameter Vibration- Part V: Stochastic Problems", Shock and Vibration Digest, Vol. 10, N0. 5 1978 17-38.

60. Caughey, T. K., "Equivalent Linearization Techniques", The Journal of the Acoustical Society of America, Vol. , No. 11, 1963, 1706-1711.

61. Thompson, W. T., "Theory of Vibration with Applications", Prentice-Hall, Englewood Cliffs, N. J., 1965.

62. Hu, Y. S., "Random Vibration and Spectrum Analysis", Shanghai Institute of Railway Technology, Shanghai, P. R. China, 1990.

63. Rakheja, S., and Ahmed, A. K. W., "Simulation of Non-linear Variable Dampers Using Energy Similarity", Engineering Computations, Vol. 3, 1991, 333-343.

64. Rakheja, S., and Sankar, S., "Local equivalent Constant Representation of Non-linear Damping Mechanisms", Engineering Computations, Vol. 3, 1986.

65. Robson, J. D., "Road Surface Description and Vehicle Response", International Journal of Vehicle Design, 1, 1979, 25-35

66. Redfield, R. C., and Karnopp, D. C., "Roadway Elevation Profile Generation for Vehicle Simulation", Vehicle System Dynamics, 17(1988) 267-280.

67. Peter, T., and Bellay, A., "Integral Transformations of Road Profile Excitation Spectra for Variable Vehicle Speeds", Vehicle System Dynamics, 15(1986) 19-40.

68. Ruf, G., "The calculation of the Vibration of a Four-Wheeled Vehicle, Induced by Random Road Roughness of the Left and Right Track", Vehicle System Dynamics, 7(1978), 1-23.

69. Hac, A., "Adaptive Control of Vehicle Suspension", Vehicle System Dynamics, 16(1987), 57-74

70. Dukkipati, R.V., Osman, M.O.M., and Vallurupalli, S. S., "Real Time Adaptive Control Compared with Stochastic Optimal Control of Active

Suspension", Proceedings of CSME Forum, Montreal, Canada, 1992, Vol. 1, pp. 192-198.

71. Su, H., Rakheja, S. and Sankar, T. S., "Response of a Nonlinear Vehicle Suspension with Tunable Shock Absorber to Random Road Excitations", ASME Diagnostics, Vehicle Dynamics and Special Topics, The 12th ASME Vibration and Noise Conference, Montreal, Quebec, Sept., 1989, pp. 185-193.

72. Vehicle Dynamics Terminology - SAE J670e, SAE Handbook, 34.215-34.224, 1988.

73. Dulac, A., "An Investigation of Ride and Handling Performance of Passive and Combined Active-Passive-Bus-Suspension", M. Thesis, Mechanical Engineering Department, Concordia University, 1992.

74. Wong, J.Y., "The Theory of Ground Vehicles", John Wiley & Sons, Inc., 1978.

75. Whitehead J., "The Handling Characteristics of European Intercity Buses", SAE Paper 912678

76. Thomas D. Gillespie, "Fundamentals of Vehicle Dynamics", Society of Automotive Engineers, Inc. 1992